Acoustically Induced Vibration of, and Sound Radiation from, Slender Beams

by

James Ronald Bailey

of the

Institute of Sound and Vibration Research
Faculty of Engineering and Applied Science
University of Southampton

A thesis submitted for the degree

of

Doctor of Philosophy

December, 1970

ACKNOWLEDGEMENTS

The author wishes to thank Dr. F.J. Fahy for his advice and encouragement in supervising this research and the Atomic Energy Department of Babcock & Wilcox (Operations) Ltd. for financial support.

ABSTRACT

FACULTY OF ENGINEERING AND APPLIED SCIENCE

Doctor of Philosophy

ACOUSTICALLY INDUCED VIBRATION OF, AND SOUND RADIATION FROM, SLENDER BEAMS

by James Ronald Bailey

This thesis deals with the acoustic coupling between slender beam structures and a surrounding fluid medium. The sound radiated from an unbaffled slender cylindrical beam vibrating transversely at resonance is calculated by solution of the classical wave equation subject to the boundary conditions imposed by the motion of the beam. The relationship between sound radiation and acoustically induced vibration is then demonstrated by using a theory based upon the principle of reciprocity to predict the resonant response of a cylindrical beam to acoustic excitation. The results show that radiation and response are highly dependent on frequency and the ratio of structural to acoustic wavelengths.

An idealized acoustic source model for a transversely vibrating beam is established by calculating the sound pressure radiated to the far-field. The results show that a vibrating beam can be represented as a line of coupled dipole sources.

For periodically supported beams an exact solution of the wave equation is seen to be extremely difficult with the boundary conditions imposed by the complex mode shapes. Approximate solutions are obtained by defining an effective structural wavelength for sound radiation. These approximations are sufficiently accurate for use in design.

Experimental measurements of sound radiation and response have involved consideration of the statistical parameters which control sound and vibration measurements in a reverberant room. It has been shown

that reliable measurements of the radiation resistance of an extended source such as a vibrating beam can be made at a single point if the length of the source is longer than an acoustic wavelength, and if many microphone positions are used to determine the mean sound pressure level. This result has been utilized in an extensive experimental programme. The radiation resistance and pure-tone acoustic response of three freely-suspended and three periodically supported beams have been measured in a large reverberant room. The experimental results agree well with theoretical predictions.

An experimental programme has also been conducted in a large anechoic room. Measurements have been made of polar directivity and the wavelength coincidence effect which occurs when a plane wave impinges on a structure at an angle such that the acoustic trace wavelength is equal to the bending wavelength of the structural mode.

List of Contents

	Page
CHAPTER I Introduction	1
1.1 Definition of the Problem	1
1.2 The Objectives of the Investigation	2
1.3 The General Approach to the Problem	4
1.3.1 Review of the Literature	4
1.3.2 An Outline of the Presentation	6
1.3.2.1 Theory	6
1.3.2.2 Experimental	7
Figure (1.1)	
CHAPTER II Response of Structures to Acoustic Excitation	8
2.1 Theory	8
2.2 The Concept of Radiation Resistance	10
2.3 Response to Diffuse Sound Fields	12
2.3.1 Pure-Tone Acoustic Excitation	12
2.3.2 Broad-Band Acoustic Excitation	12
2.3.3 Application to Slender Beams	13
2.4 Summary	14
Figure (2.1)	
CHAPTER III An Introduction to the Radiation of Sound by Cylindrical Bodies	15
3.1 Introduction	15
3.2 The General Equations in Cylindrical Co-ordinates	16
3.3 An Example : The Pulsating Cylinder	20
3.4 Summary	22
CHAPTER IV Theory of Sound Radiation from Transversely Vibrating Cylindrical Beams	24
4.1 Introduction	24

Page

4.2 An Infinitely Long, Rigid Cylinder Vibrating in a Plane 25

4.3 An Infinitely Long Cylinder Vibrating in a Standing Wave 28

4.4 An Infinitely Long Cylinder Held Motionless Except for a Finite Section which Vibrates in a Standing Wave 32

4.4.1 Near-Field Calculations 33

4.4.2 Far-Field Calculations 37

4.4.3 Equivalent Acoustic Sources 39

4.5 Periodically Supported Beams 42

4.5.1 Natural Frequencies 42

4.5.2 Mode Shapes with Simply Supported Ends 43

4.5.3 Effective Wavelengths for Sound Radiation 43

4.5.4 Radiation Resistance 44

4.5.5 Comments on Clamped Beams 46

4.6 Summary 47

Figures (4.1) through (4.16)

CHAPTER V Notes on Computation 50

5.1 The MASTER PROGRAM 50

5.2 Typical Calculations 50

Figures (5.1) and (5.2)

CHAPTER VI Introduction to the Problems of Sound Measurements in Reverberant Rooms 53

6.1 Comments on Diffusivity 53

6.2 Fluctuations of Sound Pressure 54

6.2.1 General Theory 54

6.2.2 Measurements of the Standard Deviation of Pure-Tone Sound Pressure Levels 55

6.3 Spatial Variation of Room Impedance 56

6.3.1 Theory 56

6.3.2 Experimental Investigation 57

6.3.3 Near Wall Effect 59

Page

6.4 Summary 59

Figures (6.1) through (6.7)

CHAPTER VII Experimental Programme for Measuring Radiation Loss Factors of Slender Beams 61

7.1 Investigations with Three Freely-Suspended Beams 61

7.1.1 Description of the Apparatus 61

7.1.2 Measured Results 62

7.2 Investigations with Periodically Supported Beams 64

7.2.1 Description of the Apparatus 64

7.2.2 Natural Frequencies and Mode Shapes 65

7.2.3 Measured Radiation Loss Factors 66

7.3 Discussion of Results 67

Figures (7.1) through (7.13)

CHAPTER VIII Experimental Programme for Measuring the Resonant Response of Cylindrical Beams to Acoustic Excitation 69

8.1 Anechoic Room Experiments 69

8.1.1 Wavelength Coincidence Effects 69

8.1.2 Polar Directivity 71

8.2 Reverberant Room Experiments 71

8.2.1 Three Freely-Suspended Beams 71

8.2.2 Periodically Supported Beams 73

8.2.3 A Freely-Suspended Circular Ring 74

8.3 Summary 75

Figures (8.1) through (8.16)

CHAPTER IX Conclusions 76

9.1 General Conclusions 76

9.2 Design Criteria 79

9.3 Summary 80

References 81

Appendix I - Acoustic Point Sources A.1

Appendix II - The Hankel Function A.6

LIST OF SYMBOLS

A	cross sectional area; surface area
A_m	Fourier coefficient
a	radius of sphere or cylinder; distance between simple sources in a multipole
c	speed of sound in the acoustic medium
D	directivity factor for sound radiation
E	Young's Modulus
E_m	amplitude of the Hankel function of order m
F	generalised force
f	frequency; centre frequency of band
g	gravitational constant
H_m	Hankel function of order m
I	acoustic intensity, expression for an integral in Chapter 4.
i	$\sqrt{-1}$
J_m	Bessel function of order m
K	wavenumber
K_s	structural wavenumber
k_o	acoustic wavenumber equal to ω/c.
k	radial wavenumber equal to $\sqrt{k_o^2 - K_s^2}$
ℓ	typical linear dimension
M	total mass of a structure; modal overlap
m	subscript indicating order of a function, the order of a multipole
N_m	Neumann function of order m
n	mode number; modal density
o	subscript referring to the acoustic medium
p	acoustic pressure
Q, q	wavenumbers

R	spherical co-ordinate
R_{rad}	radiation resistance
R_{mech}	mechanical resistance
R_{TOT}	total resistance equal to $R_{rad} + R_{mech}$
r	cylindrical co-ordinate
$S(\omega)$	spectral density
S	spring constant, surface area
T	reverberation time
t	time
V	velocity amplitude; room volume
v	modal velocity
W	sound power
Z	impedance
z	spatial co-ordinate
Γ	coupling parameter
γ	mass per unit length
γ_m	phase of Hankel function of order m
Δ	frequency bandwidth
δ	Dirac delta function
η	loss factor equal to $R/\omega M$
θ	polar co-ordinate
λ	wavelength
μ	resistance ratio
ρ	mass density
σ_N^2	normalised variance
σ_N	normalised standard deviation
ϕ	polar co-ordinate
ψ	velocity potential

Ω angular co-ordinate

ω circular frequency equal to $2\pi f$

∇^2 Laplacian operator (equal to the divergence of the gradiant)

$\langle\ \rangle$ time average

$-$ spatial average

$'$ differentiation with respect to the argument of a function

LIST OF FIGURES

Chapter I

1.1 Schematic of a nuclear power station

Chapter II

2.1 Single degree of freedom system with radiation damping

Chapter IV

4.1 Top - An infinitely long standing wave

Bottom - A finite standing wave

4.2 Contours of integration for equation (4.49)

4.3 Contours of integration for equation (4.60)

4.4 Radiation loss factor of a steel cylinder vibrating in air

4.5 Normalized η_{rad} for a cylindrical beam

4.6 Directivity patterns - fundamental mode

4.7 Directivity patterns - second mode

4.8 Directivity patterns - third mode

4.9 Directivity patterns - fourth mode

4.10 Directivity patterns - fifth mode

4.11 Directivity patterns - ninth mode

4.12 Directivity patterns - tenth mode

4.13 Acoustic source model

4.14 Effective wavelengths for first group of modes - beam 4 with five supports

4.15 Effective wavelengths for second group of modes - beam 4 with five supports

4.16 η_{rad} - first two groups of modes of a beam with five supports

Chapter V

5.1 Flow diagram for MASTER PROGRAM

5.2 Variations of response with number of supports

Chapter VI

6.1 Microphone traverse at 172 Hz.

6.2 Microphone traverse at 1600 Hz.

6.3 Microphone traverse at 3700 Hz.

6.4 Standard deviation of sound pressure level

6.5 Normalised standard deviation of radiation resistance

6.6 Arrangement for measuring spatial variation of room impedance

6.7 Near Wall Effect

Chapter VII

7.1 The experimental apparatus

7.2 Reverberation time decay trace

7.3 Frequency response of Beam III measured at bottom end opposite the coil

7.4 Frequency response of Beam III measured at top end in plane of coil

7.5 Measured η_{rad}

7.6 Full scale drawing of simple support

7.7 Experimental arrangement for periodically supported beam

7.8 Ratio of experimental to theoretical natural frequency with two supports

7.9 Ratio of experimental to theoretical natural frequency with three supports

7.10 Ratio of experimental to theoretical natural frequency with five supports

7.11 Typical accelerometer outputs in each span

7.12 Radiation loss factor - 2 supports

7.13 Radiation loss factor - 3 supports

7.14 Radiation loss factor - 5 supports

Chapter VIII

8.1 Experimental arrangement for measuring dual coincidence effects

8.2 Beam response to sound at grazing incidence

8.3 Beam response to sound incident at 35°

8.4 Subcritical directivity - 6th mode

8.5 Supercritical directivity - 7th mode

8.6 Supercritical directivity - 9th mode

8.7 Supercritical directivity - 10th mode

8.8 Polar directivity

8.9 Acoustic frequency response of Beam III measured at bottom opposite coil

8.10 Acoustic frequency response of Beam III measured at top in plane of coil

8.11 Typical damping decay trace

8.12 Normalized Acoustic Response

8.13 Pure-Tone Response - 2 supports

8.14 Pure-Tone Response - 3 supports

8.15 Pure-Tone Response - 5 supports

8.16 Frequency response of circular ring in plane of curvature

8.17 Frequency response of circular ring at 90° to plane of curvature

CHAPTER 1

INTRODUCTION

1.1 Definition of the Problem

Acoustically induced vibration of slender beam-like structures has recently become a major design problem in certain power generation systems, particularly in the heat exchangers of gas-cooled nuclear reactors where sound pressure levels of up to 180 dB may be generated by the gas circulators. Hydrodynamic excitation of heat exchanger elements has been recognised as a serious fatigue problem for a considerable time (cf. 1, 2, 3, 4). This new acoustic problem has been added because of the high efficiency and low volume required in nuclear systems. A schematic of a gas cooled reactor is shown in Figure (1.1). Designers must be able to predict the response of multi-supported beam-type components such as heat exchanger (boiler) tubes and control rods to the acoustic excitation generated by the gas blower. In the aerospace industry considerable effort has been directed towards predicting the response of plates and shells to the high intensity sound generated by rocket and jet engines. The response of unbaffled beam-type structures has been neglected in general, although the rather unrealistic problem of baffled beam response has been briefly considered by Lyon and Maidanik (5).

An associated problem arising from the coupling of a surrounding fluid with a vibrating beam is that of sound radiation. Sound waves are generated by the vibration of a rigid body in contact with a fluid medium. Often it is desirable to control the amount of vibratory energy transferred to the fluid from the body. This is particularly important when the vibratory energy is unwanted sound. Sound radiation from train rails is a typical example of this problem.

Another question of interest is closely related to the above problem. The energy dissipated by the motion of a body in a fluid is essentially a form of velocity dependent damping. Acoustic radiation can be an important damping mechanism, especially if the total damping of the structure is small. An understanding of this acoustic damping is therefore needed for the analysis of many types of structural vibration, e.g., the vibration of a wire in uniform normal flow when the Strouhal frequency of vortex shedding is coincident with a resonant frequency of the wire (Leehey and Hanson (6)).

1.2 The Objectives of the Investigation

Literature on the response of structures to acoustic excitation is almost entirely limited to large, flat panels and cylindrical shells with diameters large compared with the acoustic wavelength. There is little information on beam-type structures. The primary objective of this investigation is to produce a method for theoretically predicting the response of slender beams to acoustic excitation.

Special attention will be given to establishing the importance of various parameters of the beam and the acoustic medium. In particular, the acoustic response of periodically supported beams will be considered in detail. The eventual aim of this part of the investigation is to produce solutions which will enable the designer to determine the best support system for a beam subjected to acoustic excitation.

Another objective of this research is to develop a procedure for calculating the acoustic energy radiated from a transversely vibrating beam. It will be shown in the analysis that this is actually a pre-requisite to the primary objective, i.e., the response of a structure excited by sound is intimately related to the sound radiation

characteristics of the vibrating structure. There are other practical applications for this objective in reducing the amount of undesirable sound radiated from vibrating beams and in calculating the acoustic damping due to sound radiation.

A large part of this research is devoted to calculating the response of a single beam excited by sound in a diffuse acoustic field. In some practical situations a beam will be adjacent to or surrounded by other structures. An exact solution for acoustic response would be difficult because of the complex boundary conditions presented by the geometry. The study of the behaviour of fibrous materials is an example of this multiple scattering problem (e.g. Attenbourgh (7)). If the vibrating beam could be replaced by its equivalent acoustic sources, it should be easier to determine the effects of these surrounding bodies because information is available on the interactions of simple point sources and reflecting surfaces. For this reason one of the objectives of this study is to devise acoustic models of vibrating beams in terms of idealized elementary source distributions.

Well established methods have been devised for measuring sound radiation and acoustic response of vibrating systems. However, special problems exist when the sound is pure tone or of narrow frequency bandwidth. Hence, considerable attention has been given to these problems for the case of the highly resonant structures under investigation. Some of the conclusions are considered to be of general interest for the development of reliable techniques of source power measurement.

1.3 The General Approach to the Problem

1.3.1 Review of the Literature

Considerable progress has been made in recent years toward gaining an understanding of the response of structures excited by sound (8, 9). The foundations of one method, which is particularly well suited to the problem under consideration, are presented in a classical paper by Smith (10) which utilizes the principle of reciprocity to show that the mean square acoustic response of a structural mode is proportional to the ratio of energy radiated to energy stored per cycle. Several assumptions are basic to the analysis which yields the above conclusion. Namely, the vibratory system must be linear and the structure must vibrate in a single, highly resonant mode. Also sound sources in the medium must be sufficiently far from the structure for the acoustic impedance of the sound wave radiated from the structure to be given by ρc where ρ is the fluid density and c is the speed of sound in the fluid. These three conditions are fulfilled in many real situations; however, two additional significant restrictions must be included. These are that sound energy must be radiated to the far field and the exchange of energy between the structure and the acoustic medium must be by the direct path only. These two conditions are rarely met in real situations. In nuclear power station applications for example, individual boiler tubes are surrounded by other structures which might interfere with radiation to the far field. Also tube supports provide other paths for the flow of energy between the structure and the acoustic medium. Therefore considerable care must be exercised in applying this method to real situations. However, the isolated beam configuration forms the essential basis for an understanding of the beam response problem. Therefore, it has been possible to use Smith's approach with confidence in this study, particularly because beam modes are usually well separated in frequency.

A currently fashionable approach to vibration analysis is the statistical energy method which has been developed to deal with complex structures having high modal densities. In general this theory indicates that the power flow and vibrational energy distribution in coupled acoustic-structural systems are governed by equations similar to those which control heat transfer and temperature distributions in thermal systems, i.e. power always flows from a high energy mode (hot region) to a lower energy mode (cold region) with the power flow being proportional to the difference in modal energy levels (temperature). The statistical energy method can be a powerful tool in the analysis of complex structures excited by broad band acoustic excitation. However, the method relies on statistical averaging of modes and is therefore not well suited to the study of one dimensional structures which have low modal density.

Theoretically it would be possible to study the present problem by considering the power flow between individual beam modes and the acoustic modes of the surrounding medium. This approach would require consideration of the distortion of the acoustic modes of the room by the presence of the static beam. The perturbation of the acoustic modes in a rectangular room by a two dimensional strip parallel to one wall has been considered by Morse and Feshbach (16). Application of this method to a three dimensional beam at an arbitrary position in a non-rectangular room would be very complicated. Therefore, Smith's analysis, in which the diffuse field is effectively produced by an infinite array of distant point sources, was thought to be preferable.

Classical normal mode approaches (e.g. 11, 12, 13) assume that the pressure at the surface of the vibrating body is known a priori. Surface pressure is generally unknown in the present study.

1.3.2 An Outline of the Presentation

1.3.2.1 Theory

Smith's theory of the response of structures excited by sound is outlined in Chapter II. The concept of radiation resistance is introduced and the equations for the response of a structure subjected to a reverberant sound field are presented.

Fundamentals of sound radiation from a vibrating body are presented in Chapter III. The classical wave equation is introduced and the appropriate boundary conditions are defined. As an introduction to the theoretical analysis presented in later chapters, the general equations in cylindrical co-ordinates are developed and applied as an example to the case of an infinitely long, pulsating cylinder.

The central theory of this investigation is contained in Chapter IV where the analysis of sound radiation from transversely vibrating beams is developed. Expressions are derived for the radiation resistances of an infinitely long, rigid cylinder and an infinitely long cylinder vibrating in a standing wave. Then an extensive investigation is conducted on the sound radiation from an infinitely long cylinder held motionless except for a finite section which vibrates in a standing wave. Radiation resistance and the equivalent acoustic sources are defined for this case. Finally, approximate solutions for the radiation resistance of periodically supported beams are obtained by defining an effective structural wavelength for sound radiation.

The theory developed in this work requires the use of numerical integration, computation of Hankel functions, and extensive algebraic manipulation. A computer program was developed to perform these functions. This program is briefly discussed in Chapter V.

1.3.2.2 Experimental

Special problems are associated with the measurement of pure-tone sound power in a reverberant room. The statistics governing the theoretical accuracy of measured results are presented in Chapter VI.

An experimental programme for measuring the radiation loss factors of vibrating beams is reported in Chapter VII. Investigations are conducted with freely-suspended and periodically supported beams.

A programme for measuring the resonant response of beams to acoustic excitation is reported in Chapter VIII. This study includes the response of freely-suspended and periodically supported beams and a freely-suspended circular ring to pure-tone sound in a reverberation chamber. An experiment in the anechoic room for measuring wavelength coincidence effects and polar directivity is also reported.

Conclusions and design criteria are given in Chapter IX.

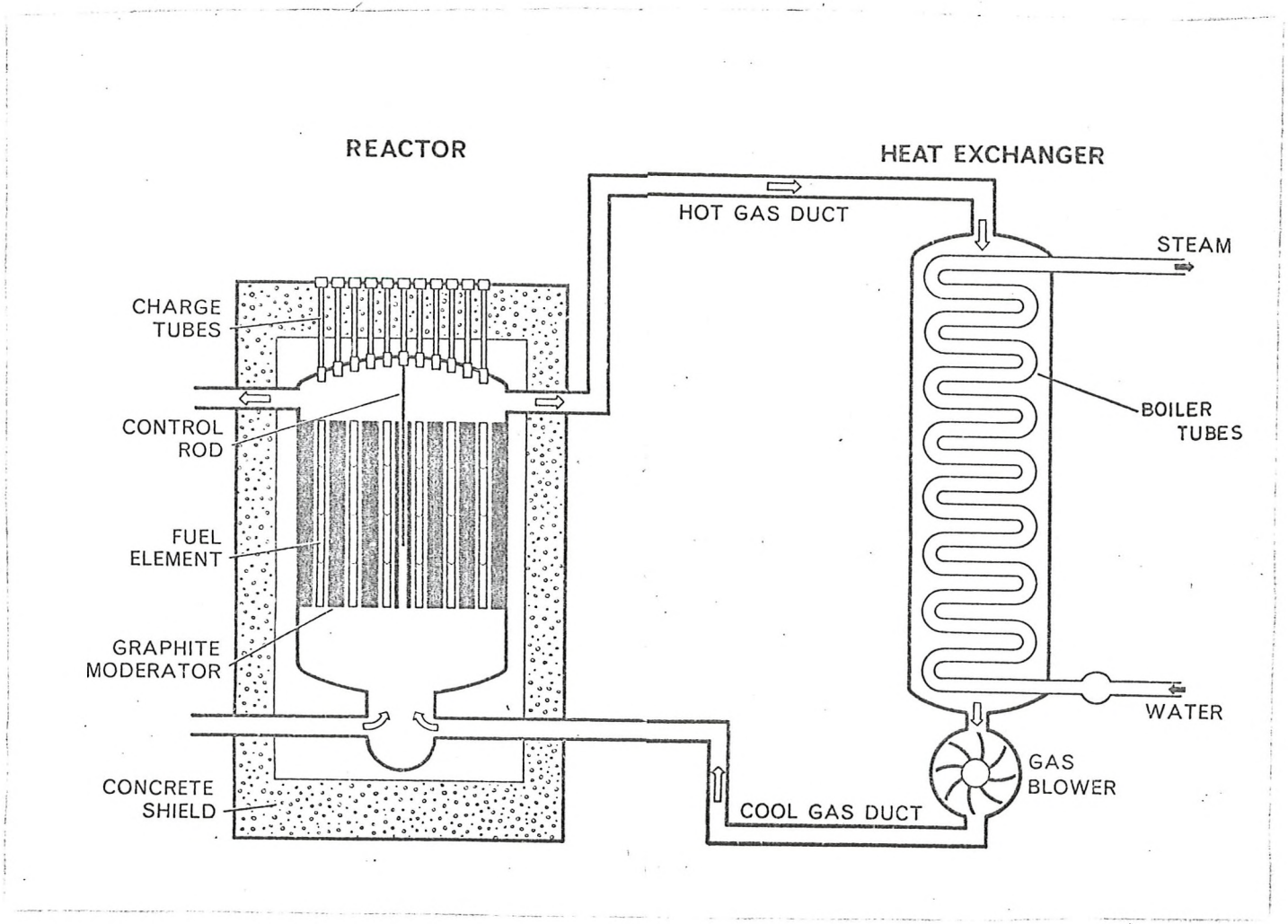

Fig. 1.1 Schematic of a nuclear power station.

CHAPTER II

RESPONSE OF STRUCTURES TO ACOUSTIC EXCITATION

2.1 Theory

The theory of modal response is developed in terms of a coupling parameter which relates incident free-field acoustic pressure to the generalised force acting on a single mode. This coupling parameter is generally a complex quantity which varies with frequency and angle of incidence. It can be defined by the following expression:

$$\Gamma_m = F_{m,bl}/p_o \quad , \qquad (2.1)$$

where Γ_m is the modal coupling parameter, p_o is the incident free-field sound pressure, and $F_{m,bl}$, the modal blocked force, is the effective force on the structure when it is held motionless. The pure-tone response of a structural mode is related to this coupling parameter by

$$\Gamma_m p_o = Z_m V_m \quad , \qquad (2.2)$$

where V_m is the modal velocity and Z_m is the modal impedance.

Of course, when a body vibrates under the action of an incident sound field, additional (radiation) pressures are created by the motion. The total pressure at the surface is the sum of the blocked and radiation pressures.

In general, sound energy is radiated from a vibrating body with the intensity varying with direction. This variation is called directivity. Similiarly, the effective driving force generated by a sound wave incident on a structure varies with the angle of incidence. It is an important conclusion of the principle of reciprocity that these variations with direction are identical. Thus, a mode which radiates sound strongly in one direction will also respond strongly to acoustic excitation from that direction.

An analytical expression relating sound radiation to the coupling parameter is given by Smith and Lyon (9) as

$$|P_{rad}(\Omega)/V_m| = (\rho_o \omega/4\pi R_o)| \Gamma_m(\omega,\Omega) | , \qquad (2.3)$$

where P_{rad} is the radiated sound pressure in the direction Ω, ρ_o is the density of the acoustic medium, ω is the circular frequency, and R_o is the distance from the vibrating body.

As will be pointed out in Section (2.3), the response of a structure to a diffuse sound field is of particular importance. For this case, it is convenient to relate response to radiated power or radiation resistance.

At large distances from the vibrating structure the mean intensity is given by

$$\langle I \rangle = |P_{rad}|^2 / 2 \rho_o c , \qquad (2.4)$$

where c is the speed of sound in the acoustic medium. Radiated power can be calculated by integrating the intensity over the surface of a sphere of large radius R_o. Substituting equation (2.3) into (2.4) yields the following equation for mean power:

$$\langle w \rangle_{rad} = \frac{\rho \omega^2 V_m^2}{8\pi c} \left[\frac{\int_\Omega |\Gamma_m|^2 \, d\Omega}{4\pi} \right]. \qquad (2.5)$$

The quantity in brackets above is equal to the average coupling factor for all angles of incidence and may be devoted by $\langle |\Gamma_m|^2 \rangle_{\text{all } \Omega}$.

Radiation resistance is defined in terms of radiated power as

$$R_{rad} = \langle w \rangle / \langle \bar{v}^2 \rangle , \qquad (2.6)$$

where $\langle \bar{v}^2 \rangle$ is the mean-square velocity of the structure, averaged with respect to time and space. R_{rad} can be expressed in terms of Γ_m by

$$R_{rad} = \frac{\rho\omega^2}{4\pi c} \; \langle |r_m|^2 \rangle_{\text{all } \Omega} \; . \qquad (2.7)$$

Explicit equations relating acoustic response to R_{rad} will be given in Section (2.3).

2.2 The Concept of Radiation Resistance

Since a large part of this study is devoted to calculating the radiation resistance of slender beams, it is appropriate that the concept of radiation resistance should be clearly defined at this stage.

The total impedance of a system is defined by equations (2.1) and (2.2) as the ratio of applied force to velocity. It is generally a complex number with the real part corresponding to the resistance of the system and the imaginary part corresponding to the reactance. A single degree of freedom system which includes radiation resistance is shown in Figure (2.1). The impedance of this system is given by

$$Z = (R_{rad} + R_{mech}) + i\,(M\omega - S/\omega). \qquad (2.8)$$

To be strictly correct the total impedance should include the imaginary or reactive part of the radiation impedance; but for mechanical structures vibrating in air, this term is usually negligible (9).

The real part of the impedance is the resistance of the system which is responsible for eventual decay of free vibrations and is of primary importance in controlling vibration response under steady state resonant excitation. In the present analysis, it is often convenient to represent the resistance by the total loss factor η_{TOT}, which is defined as the ratio of energy dissipated to energy stored per cycle. It is related to total resistance R by $R = \omega M \; \eta_{TOT}$ and to the magnification factor Q by $\eta_{TOT} = Q^{-1}$. The total loss factor may be considered as being the sum of

a mechanical loss factor η_{mech} associated with internal damping and a radiation loss factor η_{rad} corresponding to sound radiation. In general, η_{mech} may be due to the rubbing of two surfaces, the stressing of an imperfect elastic material or the passing of an electric conductor through a magnetic field. Radiation loss factor is defined in terms of radiated sound power by the following equation:

$$\eta_{rad} = \frac{\langle w \rangle_{rad}}{\omega M \langle \bar{v}^2 \rangle} , \qquad (2.9)$$

where M is the total mass of the vibrating structure.

A knowledge of radiation resistance is necessary in analysing the coupling of a sound field with a vibrating structure. It is also required in order to include acoustic damping in the analysis of ordinary structural vibrations and to calculate the sound power radiated from a vibrating structure. Morse (14), Rschevkin (15), Morse and Feshbach (16), Kinsler and Frey (17), Morse and Ingard (18), and Skudrzyk (19) are standard texts which deal with the fundamentals of sound radiation. The radiation resistances of flat panels and baffled beams have been studied by Smith (10), Lyon and Maidanik (5), Maidanik (20), and Smith and Lyon (9). Cylindrical shells have been considered by Junger (21, 22), Greenspon (23), Laird and Cohen (24), and Manning and Maidanik (25). An extensive study of cylindrical shells has also been made by Runkle and Hart (26). Most of this work, however, has been directed toward the problems of radiation from baffled structures or cylindrical shells with diameters large compared with the acoustic wavelength. With the exception of Morse (14), who considered radiation from an infinitely long cylinder vibrating with uniform transverse velocity, little information is available on the central subject of this research which is the radiation and response of slender beams.

2.3 Response to Diffuse Sound Fields

The response of structures subjected to a reverberant sound field is of considerable practical importance. This case will now be considered in detail because it most accurately represents the acoustic environment in a nuclear power station and the results can be applied directly to the experimental investigations reported in Chapters VII and VIII.

The sound field in a reverberant room is said to be diffuse if all angles of incidence are equally probable. Problems associated with the diffusivity of pure-tone sound energy in a reverberant chamber are discussed in detail in Chapter VI.

2.3.1 Pure-Tone Acoustic Excitation

The resonant response of a single mode excited by pure-tone sound is a case of special interest. The following equation relates mean square response to pressure and radiation loss factor:

$$\frac{\langle \bar{v}^2 \rangle}{\langle \bar{p}^2 \rangle} = \frac{4\pi c \ \eta_{rad}}{\omega^3 M \rho_o \eta_{TOT}^2} , \qquad (2.10)$$

where $\langle \bar{p}^2 \rangle$ is the mean-square sound pressure, averaged with respect to time and space.

2.3.2 Broad-Band Acoustic Excitation

A second special case of considerable interest is the resonant response of a structure vibrating in a single mode excited by broad-band random sound. The following equation relates response to excitation:

$$\frac{\langle \bar{v}^2 \rangle}{S_p(\omega)} = \frac{2\pi^2 c \ \eta_{rad}}{M \rho \omega^2 \eta_{TOT}} , \qquad (2.11)$$

where $S_p(\omega)$ is the pressure spectral density.

The above equation is restricted to analysis of modes with adequate spacing between resonant frequencies. This condition is usually found in beam-type structures where the modal density is inversely proportional to $\omega^{\frac{1}{2}}$. However, periodically supported beams have bands of resonant frequencies which might require a multimodal analysis if the damping of the individual modes is high enough to couple the modes together.

Of course, if the bandwidth of the acoustic excitation is much narrower than the resonant bandwidth of the structure, the excitation can be treated as pure-tone and the previous section is then pertinent.

2.3.3 Application to Slender Beams

Equations (2.10) and (2.11) can be used to analyse the response of slender beams to acoustic excitation by defining the appropriate mean square velocity. For simply supported beams, the velocity distribution of a resonant mode can be written as

$$v = V_o \sin(K_s Z) \cos \omega t, \qquad (2.12)$$

where V_o is the maximum amplitude and K_s is the structural wavenumber. The mean square velocity is given by

$$\langle \bar{v}^2 \rangle = \frac{1}{K_s \ell \cdot T} \int_0^T \int_0^\ell V_o^2 \sin^2(K_s Z) \cos^2(\omega t)\, dt\, dZ, \qquad (2.13)$$

$$\langle \bar{v}^2 \rangle = \frac{V_o^2}{4} \qquad (2.14)$$

Free-free beams, clamped beams and periodically supported beams have additional hyperbolic terms in the velocity distribution. A general expression is given by

$$v = V_o \cos \omega t \{ A \cos K_s Z + B \sin K_s Z + C \cosh K_s Z + D \sinh K_s Z \}, \qquad (2.15)$$

where A, B, C and D are constants determined by the boundary conditions. These constants have been evaluated by Bishop and Johnson (27), Timoshenko (28) and others. The mean square velocity can be obtained by substituting the appropriate constants into equation (2.15) and following the above procedure.

2.4 Summary

The basic equations relating acoustic response to sound radiation have been presented in this Chapter. The concept of radiation resistance has been introduced and it has been shown that the acoustic response of a structure can be predicted if the radiation resistance of the structure is known. The following Chapters III, IV, and V therefore concentrate on this parameter for transversely vibrating beams.

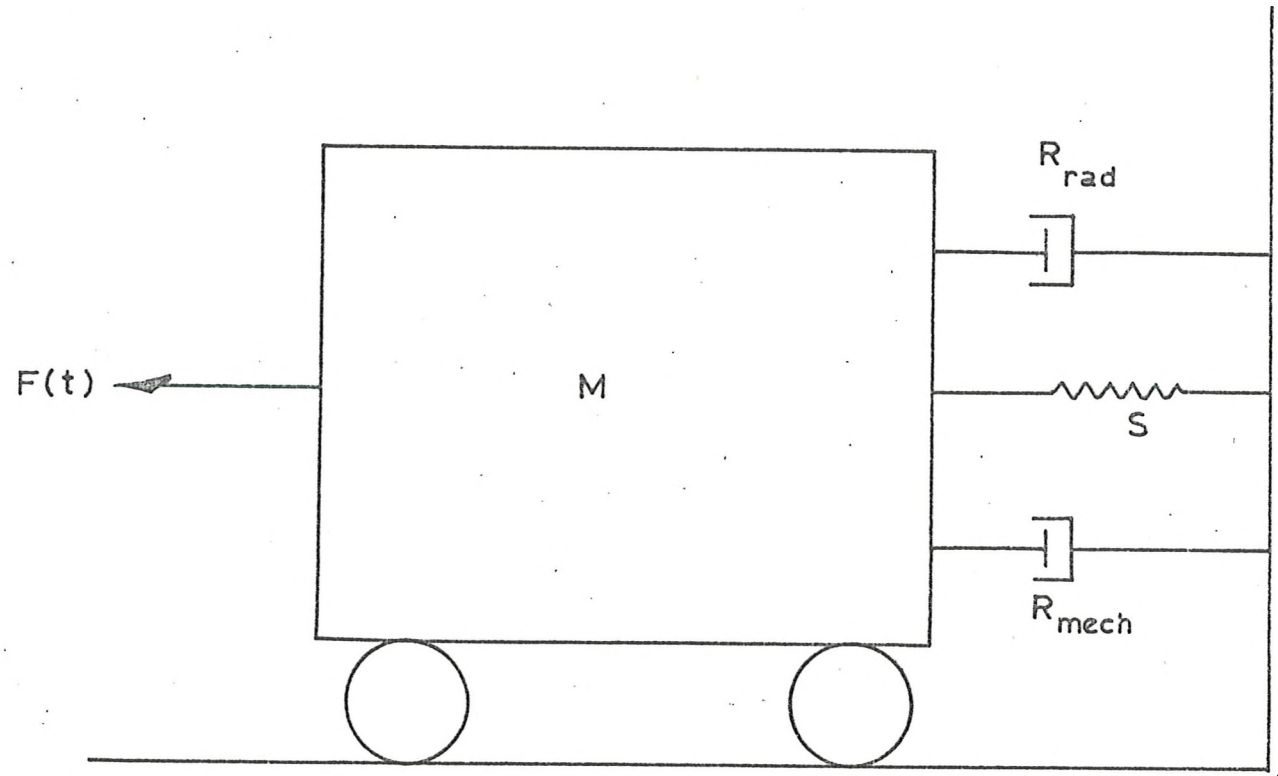

Fig. 2.1 Single degree of freedom system with radiation damping.

CHAPTER III

AN INTRODUCTION TO THE RADIATION OF SOUND BY CYLINDRICAL BODIES

3.1 Introduction

The power radiated from a vibrating structure can be determined by several methods. One approach is to calculate the far-field radiated sound pressure from which intensity and power can be ascertained. Another method is to find the acoustic pressure at the surface of the vibrating body and to obtain the time averaged power from the real part of the product of pressure or force times flux or velocity. Both of these methods require solution of the classical harmonic wave equation given by

$$\nabla^2 p + K_o^2 p = 0, \qquad (3.1)$$

where ∇^2 is the Laplace operator equal to the divergence of the gradient, p is acoustic pressure, and K_o is the acoustic wavenumber. The wave equation is developed in depth by Morse (14), Morse and Feshbach (16), Morse and Ingard (18), Kinsler and Frey (17), and Rschevkin (15). It can be derived from basic principles by assuming that the non linear fluctuations of the acoustic variables can be neglected, that the process is adiabatic, and that the acoustic medium obeys the perfect gas law. Newton's second law, the equation of continuity, and the equation of state then yield the desired result given by equation (3.1). The physical implication of the wave equation is simply that if there is a concentration of pressure at a point, the pressure at that point will tend to decrease.

The two boundary conditions required for solution of equation (3.1) depend on the extent of the acoustic medium and the motion of the vibrating body. The first boundary condition is that no reflections occur in the neighbourhood of the source. Mathematically this means that

only outgoing solutions of the wave equation are relevant. The second boundary condition is that at the body-medium interface, the acoustic particle velocity is equal to the velocity of the vibrating body. If the geometry of the vibrating body is complex, the Helmholtz integral method can be used to obtain solutions which match the boundary conditions, e.g. Chertock (29). This approach is unnecessary in the present analysis because of the simple geometry of cylindrical beams.

It is often convenient to work with velocity potential ψ which is related to acoustic pressure p by

$$p = -\rho \frac{\partial \psi}{\partial t} \quad . \tag{3.2}$$

For simple harmonic motion this equation becomes

$$p = i\omega\rho\psi \quad . \tag{3.3}$$

The second boundary condition at the surface of the vibrating body can be written in terms of velocity potential by

$$V_n = \left. \frac{\partial \psi}{\partial r} \right|_S \quad , \tag{3.4}$$

where V_n is the normal surface velocity of the body.

Solutions of the wave equation have been obtained for many simple acoustic sources. Acoustic monopoles, dipoles, quadrupoles and multipoles are discussed in Appendix 1. Details of these examples are presented in standard acoustic textbooks such as References (14) through (19). The results of Appendix I will be useful in subsequent discussions on sound radiation and response of slender beams.

3.2 The General Equations in Cylindrical Co-ordinates

For beam type structures it is often convenient to use the wave equation in cylindrical co-ordinates given by

$$\left[\frac{1}{r} \frac{\partial}{\partial r} \left(r \frac{\partial}{\partial r} \right) + \frac{1}{r^2} \frac{\partial^2}{\partial \phi^2} + \frac{\partial^2}{\partial z^2} \right] \psi = \frac{1}{c^2} \frac{\partial^2 \psi}{\partial t^2} \quad . \tag{3.5}$$

For simple harmonic motion the velocity potential can be written as

$$\psi(r,\phi,z,t) = \psi(r,\phi,z)\, e^{-i\omega t} \quad . \tag{3.6}$$

The second partial derivative with respect to time is

$$\frac{\partial^2 \psi}{\partial t^2} = \omega^2 \psi(r,\phi,z,t) \quad . \tag{3.7}$$

Substitution into equation (3.8) yields

$$\left[\frac{1}{r} \frac{\partial}{\partial r} \left(r \frac{\partial}{\partial r} \right) + \frac{1}{r^2} \frac{\partial^2}{\partial \phi^2} + \frac{\partial^2}{\partial z^2} \right] \psi + k_o^2 \psi = 0. \tag{3.8}$$

Equation (3.8) is known as the Helmholtz equation. Assuming that the variables can be separated, the velocity potential can be written as

$$\psi(r,\phi,z) = \psi(r,\phi) \cdot \bar{\psi}(z), \tag{3.9}$$

where $\bar{\psi}(z)$ is the inverse Fourier transform of $\psi(K)$ as shown in the following pair of equations:

$$\psi(K) = \int_{-\infty}^{\infty} \bar{\psi}(z)\, e^{-iKz}\, dz \tag{3.10}$$

$$\bar{\psi}(z) = \frac{1}{2\pi} \int_{-\infty}^{\infty} \psi(K)\, e^{iKz}\, dK \quad . \tag{3.11}$$

Velocity potential can thus be written as

$$\psi(r,\phi,z) = \psi(r,\phi) \frac{1}{2\pi} \int_{-\infty}^{\infty} \psi(K)\, e^{iKz}\, dK \, . \tag{3.12}$$

Now the Fourier transform of equation (3.8) can be taken:

$$\int_{-\infty}^{\infty} \left[\frac{1}{r} \frac{\partial}{\partial r} \left(r \frac{\partial}{\partial r} \right) + \frac{1}{r^2} \frac{\partial^2}{\partial \phi^2} + \frac{\partial^2}{\partial z^2} \right] \psi e^{-iKz}\, dz + k_o^2 \int_{-\infty}^{\infty} \psi e^{-iKz}\, dz = 0. \tag{3.13}$$

The second partial derivative with respect to z is given by

$$\frac{\partial^2 \psi}{\partial z^2} = -K^2 \psi(r,\phi) \frac{1}{2\pi} \int_{-\infty}^{\infty} \psi(K) \, e^{-iKz} \, dK, \tag{3.14}$$

$$\frac{\partial^2 \psi}{\partial z^2} = -K^2 \psi(r,\phi) \, \bar{\psi}(z) \quad . \tag{3.15}$$

Substituting into (3.13) yields

$$\left[\frac{1}{r} \frac{\partial}{\partial r} \left(r \frac{\partial}{\partial r}\right) + \frac{1}{r^2} \frac{\partial^2}{\partial \phi^2} - K^2\right] \psi(r,\phi) \int_{-\infty}^{\infty} \bar{\psi}(z) \, e^{-iKz} \, dz$$

$$+ k_o^2 \psi(r,\phi) \int_{-\infty}^{\infty} \bar{\psi}(z) \, e^{iKz} \, dz = 0 \quad . \tag{3.16}$$

Thus the wave equation is reduced to

$$\left[\frac{1}{r} \frac{\partial}{\partial r} \left(r \frac{\partial}{\partial r}\right) + \frac{1}{r^2} \frac{\partial^2}{\partial \phi^2} + (k_o^2 - K^2)\right] \psi(r,\phi) = 0. \tag{3.17}$$

An outgoing solution of (3.17) is given by

$$\psi(r,\phi) = \sum_{m=0}^{\infty} A_m \cos m\phi \, [J_m(kr) + iN_m(kr)] \tag{3.18}$$

where $k^2 = k_o^2 - K^2$, $k_o > K$,

$J_m(kr)$ = Bessel function of order m,

$N_m(kr)$ = Neumann function of order m,

A_m = coefficients determined by the boundary conditions.

The Hankel function of order m is given by

$$H_m(kr) = J_m(kr) + iN_m(kr), \tag{3.19}$$

so that equation (3.18) can be written as

$$\psi(r,\phi) = \sum_{m=0}^{\infty} A_m \cos m\phi \, H_m(kr) \quad . \tag{3.20}$$

The inverse Fourier transform of (3.20) is given by

$$\psi(r,\phi,z) = \frac{1}{2\pi}\int_{-\infty}^{\infty} \psi(r,\phi)\, e^{iKz}\, dK. \qquad (3.21)$$

$$\psi(r,\phi,z) = \frac{1}{2\pi}\int_{-\infty}^{\infty} \Big[\sum_{m=0}^{\infty} A_m \cos m\phi\, H_m(kr)\Big]\, e^{iKz}\, dK. \qquad (3.22)$$

For simple harmonic motion,

$$\psi(r,\phi,z,t) = \psi(r,\phi,z)e^{-i\omega t} \qquad (3.23)$$

Substituting into (3.22) yields

$$\psi(r,\phi,z,t) = \frac{e^{-i\omega t}}{2\pi}\int_{-\infty}^{\infty} \Big[\sum_{m=0}^{\infty} A_m \cos m\phi\, H_m(kr)\Big] e^{iKz}\, dK. \qquad (3.24)$$

Equation (3.24) is a general expression for velocity potential in cylindrical co-ordinates. Acoustic pressure can be expressed by utilizing equation (3.3). The result is

$$p(r,\phi,z,t) = \frac{i\omega\rho e^{-i\omega t}}{2\pi}\int_{-\infty}^{\infty} \Big[\sum_{m=0}^{\infty} A_m \cos m\phi\, H_m(kr)\Big] e^{iKz}\, dK \,. \qquad (3.25)$$

Equation (3.24) must satisfy the boundary condition imposed by the structure. Thus, the particle velocity at the surface must equal the normal surface velocity of the structure. This boundary condition is stated mathematically by equation (3.4). A general expression relating surface velocity to velocity potential can be obtained by performing the partial differentiation of velocity potential with respect to r.

$$\frac{\partial \psi}{\partial r} = \frac{\partial}{\partial r}\Big\{\frac{e^{-i\omega t}}{2\pi}\int_{-\infty}^{\infty} \Big[\sum_{m=0}^{\infty} A_m \cos m\phi\, H_m(kr)\Big] e^{iKz}\, dK\Big\} \qquad (3.26)$$

$$\frac{\partial \psi}{\partial r} = \frac{e^{-i\omega t}}{2\pi}\int_{-\infty}^{\infty} \Big[\sum_{m=0}^{\infty} A_m \cos m\phi\, H_m'(kr)\Big]\, e^{iKz}\, dK \,, \qquad (3.27)$$

where,

$$H_m'(kr) = \frac{\partial}{\partial r}\Big[H_m(kr)\Big] \qquad (3.28)$$

For a given surface velocity the following equation can be used to determine the coefficients A_m.

$$V_n\Big|_{r=a} = \frac{e^{-i\omega t}}{2\pi} \int_{\infty}^{\infty} \Big[\sum_{m=0}^{\infty} A_m \cos m\phi \; H_m'(kr)\Big] e^{iKz}\, dK. \qquad (3.29)$$

Equations (3.25) and (3.29) are sufficient for calculation of the sound radiation from cylinders with arbitrary surface velocity distributions. Useful approximations and properties of the Hankel Function are listed in Appendix II.

3.3 An Example: The Pulsating Cylinder

Consider an infinitely long cylinder of radius a which is expanding and contracting uniformly with surface velocity $V = V_o e^{-i\omega t}$. The boundary condition is that the particle velocity must equal the normal velocity of the cylinder at the surface.

$$V_n = V_o e^{-i\omega t} = \frac{\partial \psi}{\partial r}\Big|_{r=a} . \qquad (3.30)$$

Now, by equation (3.44),

$$V_o e^{-i\omega t} = \frac{e^{-i\omega t}}{2\pi} \int_{\infty}^{\infty} \Big[\sum_{m=0}^{\infty} A_m \cos m\phi \; H_m'(kr)\Big] e^{iKz}\, dK . \qquad (3.31)$$

By using the orthogonal properties of the trigonometric functions, it can be shown that all the A_m's equal zero except A_o. Equation (3.31) thus becomes

$$V_o = \frac{1}{2\pi} \int_{\infty}^{\infty} A_o H_o'(kr) \Big| e^{iKz}\, dK \Big|_{r=a} . \qquad (3.32)$$

Taking the inverse Fourier Transform yields

$$A_o H_o'(kr)\Big|_{r=a} = \int_{\infty}^{\infty} V_o e^{-iKz}\, dz . \qquad (3.33)$$

The coefficient A_o can therefore be written as

$$A_o = \frac{V_o 2\pi}{H_o'(kr)\Big|_{r=a}} \delta(K) \quad , \tag{3.34}$$

where δ = Dirac delta function.

Radiated sound pressure as given by equation (3.25) can be written as

$$p(r,\phi,z,t) = \frac{i\omega\rho e^{-i\omega t}}{2\pi} \int_{-\infty}^{\infty} A_o H_o(kr)\Big|_{r=a} e^{iKz} dK. \tag{3.35}$$

Substituting A_o yields

$$p(r,\phi,z,t) = \frac{i\omega\rho e^{-i\omega t}}{2\pi} \int_{-\infty}^{\infty} \frac{2\pi V_o \delta(K) H_o(kr) e^{iKz} dK}{H_o'(kr)\Big|_{r=a}} . \tag{3.36}$$

The above integral can be evaluated by noting the following general characteristic of the delta function:

$$\int_{\infty}^{\infty} F(t) \delta(t-a) dt = F(a) \quad . \tag{3.37}$$

This yields the following expression for radiated pressure:

$$p(r,\phi,z,t) = \frac{i\omega\rho e^{-i\omega t} V_o H_o(k_o r)}{H_o'(k_o r)\Big|_{r=a}} \quad , \tag{3.38}$$

where $k_o = \omega/c$.

Equation (3.38) can be simplified by substituting from equation (A.2.2.)

$$p(r,\phi,z,t) = \frac{2\rho c V_o e^{-i(\omega t + \gamma_o)} H_o(k_o r)}{E_o} . \tag{3.39}$$

At large distances from the cylinder, equation (A.2.9) can be used to yield

$$p(r,\phi,z,t) = \frac{2\rho c V_o}{E_o} \sqrt{\frac{2}{\pi k_o r}} e^{-i(\omega t + \gamma_o - kr + \pi/4)} . \tag{3.40}$$

The mean intensity is given by

$$\langle I \rangle = \frac{1}{2} \frac{p_o p^*}{\rho c} = \frac{4\rho c V_o^2}{\pi k_o r E_o^2} \quad . \tag{3.41}$$

Power per unit length ℓ can be calculated by integrating over the surface of a cylinder of large radius r.

$$\langle w \rangle = \int_0^{\ell} \int_0^{2\pi} \langle I \rangle r \, dz \, d\theta \quad . \tag{3.42}$$

$$\langle w \rangle = \frac{8\rho c V_o^2}{K_o E_o^2} \quad . \tag{3.43}$$

Now, the mean-square velocity averaged with respect to time and space is given by $\langle \overline{v^2} \rangle = V_o^2/2$. Therefore, radiation resistance can be written as

$$R_{rad} = \frac{16\rho c \ell}{K_o E_o^2} \quad . \tag{3.44}$$

Limiting values of radiation resistance can be obtained by using the approximations for E_o given in equations (A.2.4) and (A.2.6). The result is

$$R_{rad} \simeq \begin{cases} \rho c \, (\pi^2 a \ell) \, (ka), & ka \ll 1; \\ \rho c \, (2\pi a \ell) & ; \; ka \gg 1. \end{cases} \tag{3.45}$$

It is interesting to compare the above equation with equation (A.1.7) which gives the radiation resistance of a simple source. When $ka \gg 1$, R_{rad} for both cases is equal to ρc times the total surface area. This is often found at high frequencies.

3.6 Summary

The classical wave equation has been introduced and the boundary conditions for sound radiation have been defined in this chapter.

Fundamental acoustic point sources have been reviewed in Appendix I where expressions are presented for the radiation resistance of monopoles, dipoles, quadrupoles, and multipoles.

Fourier Transform techniques have been used to set-up the general equations for sound radiation in cylindrical co-ordinates. These equations have shown that sound pressure radiated from cylinders is dependent on the Hankel Function. Useful approximations and properties of the Hankel Function have been listed in Appendix II.

Finally, the basic procedure for calculating radiation resistance has been established by considering in detail the case of an infinitely long pulsating cylinder.

CHAPTER IV

THEORY OF SOUND RADIATION FROM TRANSVERSELY VIBRATING CYLINDRICAL BEAMS

4.1 Introduction

The theory of sound radiation in this work so far has been limited to fundamental acoustic sources and the relatively simple case of an infinitely long, pulsating cylinder. Now we are ready to proceed with the primary objectives of this study; namely, to consider sound radiation from transversely vibrating cylindrical beams.

We will begin this chapter by considering the sound radiation from infinitely long beams. The first case will be that of a rigid cylinder vibrating in a plane with uniform transverse velocity. Then we will continue with the case of a cylinder vibrating in an infinitely long standing wave.

Of course, an infinitely long beam will seldom be encountered in real, physical situations. Hence, approximations must be obtained for beams of finite length. When the structural wavelength of the beam is larger than the acoustic wavelength in the medium, a general solution for radiated power will be achieved by working with pressure and velocity at the surface of the cylinder. On the other hand, when the acoustic wavelength is larger than the structural wavelength, it will be advantageous to work with the sound pressure radiated to the far-field. This approach will yield an integral equation for radiated sound power which can be calculated numerically. It will also give us considerable insight into the type of acoustic sources involved so that equivalent acoustic sources for transversely vibrating, slender beams can be defined.

Finally, the sound radiation from periodically supported beams will be considered. Approximate solutions will be obtained by defining an

effective structural wavelength for sound radiation.

As in the previous chapter, it will be convenient to present the results in terms of radiation resistance.

4.2 An Infinitely Long, Rigid Cylinder Vibrating in a Plane

Consider the axially independent case of an infinitely long cylinder of radius a, vibrating back and forth in a direction perpendicular to its axis with a uniform velocity $V_o e^{-i\omega t}$. The normal velocity can be written as

$$V_n = V_o \cos \phi \, e^{-i\omega t} \quad . \tag{4.1}$$

The boundary condition expressed by equation (3.29) yields

$$V_o \cos \phi \, e^{-i\omega t} = \frac{e^{-i\omega t}}{2\pi} \int_{-\infty}^{\infty} \left[\sum_{m=0}^{\infty} A_m \cos m\phi \, H_m'(kr) \right] e^{iKz} dK. \tag{4.2}$$

Again utilizing the orthogonality of trigonometric functions, all the A_m's can be shown to be zero except A_1. Equation (4.2) thus reduces to

$$V_o = \frac{1}{2\pi} \int_{\infty}^{\infty} A_1 H_1'(kr) \Big|_{r=a} e^{iKz} \, dK. \tag{4.3}$$

Taking the inverse Fourier Transform yields

$$A_1 H_1'(kr) \Big|_{r=a} = \int_{-\infty}^{\infty} V_o \, e^{-iKz} \, dz. \tag{4.4}$$

Integration yields the following expression for A_1.

$$A_1 = \frac{2\pi \, V_o \delta(K)}{H_1'(kr) \Big|_{r=a}} \quad . \tag{4.5}$$

Pressure can now be written as

$$p(r,\phi,z,t) = \frac{i\omega\rho e^{-i\omega t}}{2\pi} \int_{-\infty}^{\infty} A_1 \cos \phi H_1(kr) \, e^{iKz} \, dK. \tag{4.6}$$

Substituting for A_1 yields

$$p(r,\phi,z,t) = \frac{i\omega\rho e^{-i\omega t}}{2\pi} \int_{-\infty}^{\infty} \frac{2\pi V_o \delta(K) \cos\phi H_1(kr)}{H_1'(kr)\Big|_{r=a}} e^{iKz}\, dK. \quad (4.7)$$

Integration yields

$$p(r,\phi,z,t) = \frac{i\omega\rho e^{-i\omega t} V_o \cos\phi H_1(k_o r)}{H_1'(k_o r)\Big|_{r=a}} . \quad (4.8)$$

Substituting from equation (A.2.3) yields

$$p(r,\phi,z,t) = \frac{\rho c \cos\phi V_o H_1(k_o r) e^{-i(\omega t + \gamma_1)}}{E_1} . \quad (4.9)$$

Now, equation (A.2.7) can be used to yield the following equation for pressure at large distances from the cylinder.

$$p(r,\phi z,t) = \frac{\rho c V_o \cos\phi}{E_1} \sqrt{\frac{2}{\pi k_o r}}\, e^{-i(\omega t + \gamma_1 - k_o r + 3\pi/4)} . \quad (4.10)$$

The mean intensity can therefore be written as

$$\langle I \rangle = \frac{\rho c V_o^2 \cos^2\phi}{\pi k_o r\, E_1^2} . \quad (4.11)$$

Radiated power per unit length ℓ can be calculated by integrating over the surface of a cylinder of large radius. The result is

$$\langle w \rangle = \frac{\rho c V_o^2 \ell}{k_o E_1^2} . \quad (4.12)$$

Now, the mean square velocity averaged with respect to time and space is given by $\langle \overline{v}^2 \rangle = V_o^2/2$. Substituting into (4.12) yields the following expression for radiation resistance:

$$R_{rad} = \frac{2\rho c \ell}{k_o E_1^2} \quad . \qquad (4.13)$$

Using the approximations of equations (A.2.5.) and (A.2.6) yields

$$R_{rad} = \begin{cases} \dfrac{\rho c(\pi^2 a\ell)(ka)^3}{2} & , \ ka<<1; \\ \rho c(\pi a \ell) & , \ ka>>1. \end{cases} \qquad (4.14)$$

The above result for ka<<1 agrees with that obtained in Reference (18).

A check on these results can be obtained by working with the pressure and velocity at the surface of the vibrating cylinder. The pressure at the surface can be written by substituting from equation (A.2.7) into equation (4.9). The result is

$$p(a,\phi,z,t) = \frac{-i\rho c \cos\phi \ V_o E_o \ e^{-i(\omega t + \gamma_1 - \gamma_o)}}{2 E_1} \quad . \qquad (4.15)$$

The real part of the pressure is thus given by

$$p(a,\phi,z,t)_{real} = \frac{-\rho c \cos\phi \ V_o E_o}{2 E_1} \sin(\omega t + \gamma_1 - \gamma_o). \qquad (4.16)$$

The real part of velocity can be written as

$$V_{real} = V_o \cos\phi \cos \omega t \quad . \qquad (4.17)$$

Power radiated by unit length ℓ can be calculated by the following integration:

$$\langle w \rangle = \int_{-\ell/2}^{\ell/2} \int_{o}^{2\pi} \langle p_{real} \cdot v_{real} \rangle \ a \ dz \ d\phi \quad . \qquad (4.18)$$

The result is

$$\langle w \rangle = \frac{-\rho c \ V_o^2 \ E_o}{4 E_1} (\pi a \ell) \sin(\gamma_1 - \gamma_o) \quad . \qquad (4.19)$$

For ka <<1, substitution for E_o, E_1, γ_o, and γ_1 yields

$$\langle w \rangle \simeq \tfrac{1}{2}\rho c \; V_o^2 \; (\pi a^2 \ell) \; K \sin\left(\frac{\pi k^2 a^2}{2}\right) . \qquad (4.20)$$

$$\simeq \frac{\rho c \; V_o^2 \; (\pi^2 a \ell)(ka)^3}{4} . \qquad (4.21)$$

Radiation resistance is thus given by

$$R_{rad} = \frac{\rho c(\pi^2 a \ell) \; (ka)^3}{2} , \quad ka<<1 . \qquad (4.22)$$

Similar substitutions for ka>>1 yield

$$R_{rad} \simeq \rho c(\pi a \ell) . \qquad (4.23)$$

Radiation resistance as expressed by equations (4.22) and (4.23) is identical with that given by equation (4.14).

4.3 An Infinitely Long Cylinder Vibrating in a Standing Wave

We now consider the case shown in the top of Figure (4.1) of an infinitely long cylinder of radius a, which is vibrating at resonance in a standing wave with normal velocity given by

$$V_n = V_o \cos\phi \begin{matrix}\cos \\ \sin\end{matrix}(K_s z) e^{-i\omega t} , \qquad (4.24)$$

where the structural wavenumber K_s is equal to 2π times the inverse of the structural wavelength, the plane of vibration is denoted by $\phi = 0$, and $\cos(K_s z)$ is used if the origin is placed at an antinode; $\sin(K_s z)$ if the origin is at a nodal point. Using equation (3.29) and the orthogonal properties of the trigonometric functions yields the following equation:

$$V_o \cos\phi \begin{matrix}\cos \\ \sin\end{matrix}(K_s z) e^{-i\omega t} = \frac{e^{-i\omega t}}{2\pi} \int_{\infty}^{\infty} A_1 \cos\phi H_1'(kr) e^{iKz} \, dK . \qquad (4.25)$$

Taking the inverse transform yields

$$A_1 H_1'(kr) = \int_{-\infty}^{\infty} V_o \cos\phi \begin{matrix}\cos\\ \sin\end{matrix}(K_s z) e^{-iKz}\, dz \quad . \qquad (4.26)$$

Now,

$$\cos(K_s z) = \frac{e^{iK_s z} + e^{-iK_s z}}{2} \qquad (4.27)$$

and

$$\sin(K_s z) = \frac{e^{iK_s z} - e^{-iK_s z}}{2i} \quad . \qquad (4.28)$$

Substituting into equation (4.26),

$$A_1 H_1'(kr) = \frac{V_o}{2} \int_{-\infty}^{\infty} \left[e^{i(K + \frac{n\pi}{\ell})z} + e^{i(K - \frac{n\pi}{\ell})z}\right] dz \quad , \text{(origin at antinode)}$$

$$= \frac{V_o}{2i} \int_{-\infty}^{\infty} \left[e^{i(K + \frac{n\pi}{\ell})z} - e^{i(K - \frac{n\pi}{\ell})z}\right] dz. \quad \text{(origin at antinode)} \qquad (4.29)$$

Integration yields

$$A_1 H_1'(kr) = \pi V_o \left[\delta(K + \tfrac{n\pi}{\ell}) + \delta(K - \tfrac{n\pi}{\ell})\right] \text{ (origin at antinode)}, \qquad (4.30)$$

$$= \frac{\pi V_o}{i} \left[\delta(K + \tfrac{n\pi}{\ell}) - \delta(K - \tfrac{n\pi}{\ell})\right], \text{(origin at node)}$$

where δ = Dirac delta function.

Now, using equation (3.25) and integrating yields the following expression for pressure:

$$p(r,\phi,z,t) = i\omega\rho V_o \cos\phi \begin{matrix}\cos\\ \sin\end{matrix}(K_s z) e^{-i\omega t} \frac{H_1(qr)}{H_1'(qa)} \quad , \qquad (4.31)$$

where

$$q^2 = K_o^2 - K_s^2 \quad .$$

Now

$$\frac{H_1(X)}{H_1'(X)} = \frac{J_1(X) + iN_1(X)}{J_1'(X) + iN_1'(X)} \cdot \frac{J_1'(X) - iN_1'(X)}{J_1'(X) - iN_1'(X)} , \tag{4.32}$$

$$\frac{H_1(X)}{H_1'(X)} = \frac{J_1(X)\,J_1'(X) + N_1(X)\,N_1'(X) + iN_1(X)\,J_1'(X) - iJ_1(X)N_1'(X)}{J_1'(X)^2 + N_1'(X)^2} \tag{4.33}$$

$$J_1(X)\,N_1'(X) - J_1'(X)\,N_1(X) = \frac{2}{\pi X} \quad . \tag{4.34}$$

The real part of the pressure at the surface can be written by substituting equations (4.33) and (4.34) into (4.31). The result is

$$p(a,\phi,z,t)_{real} = \frac{2\omega\rho V_o \cos\phi \begin{matrix}\cos\\ \sin\end{matrix}(K_s z)\cos\omega t}{\pi q^2 a \{[J_1'(qa)]^2 + [N_1'(qa)]^2\}} . \tag{4.35}$$

The real part of velocity is given by

$$V_{real} = V_o \cos\phi \begin{matrix}\cos\\ \sin\end{matrix}(K_s z)\cos\omega t \quad . \tag{4.36}$$

Radiated power can be calculated by substituting into equation (4.18). The result of the integration is

$$\langle w\rangle = \frac{\omega\rho\, V_o^2\, \ell}{2q^2\{[J_1'(qa)]^2 + [N_1'(qa)]^2\}} \tag{4.37}$$

Now, $\langle \overline{v^2} \rangle = \frac{V_o^2}{4}$. Radiation resistance is therefore given by

$$R_{rad} = \frac{2\omega\rho\ell}{q^2\{[J_1'(qa)]^2 + [N_1'(qa)]^2\}} \quad . \tag{4.38}$$

But,

$$[J_1'(qa)]^2 + [N_1'(qa)]^2 = E_1^2 \quad . \tag{4.39}$$

Thus,

$$R_{rad} = \frac{2\omega\rho\ell}{q^2 E_1^2} \quad . \qquad (4.40)$$

Values of E_1 are tabulated in Reference (18) so that equation (4.40) can be used to calculate R_{rad} for any given qa.

It is often convenient to work with the non-dimensional radiation loss factor related to radiation resistance by $\eta_{rad} = R_{rad}/\omega M$. A plot of η_{rad} vs. qa is shown in Figure (4.4) for a steel cylinder vibrating in air. It should be noted that η_{rad} is zero when $K_o < K_s$. Therefore, the frequency corresponding to $K_o = K_s$ may be considered as a lower cut-off frequency. Below this frequency the structural wavelength of the beam is less than the wavelength in the acoustic medium and q, the radial acoustic wavenumber, is imaginary. The acoustic energy is entirely reactive and no sound is radiated to the far field.

The maximum η_{rad} occurs at qa = 1, where the radial acoustic wavelength is equal to the circumference of the beam. Above this frequency η_{rad} falls off with increasing frequency. At these high frequencies radiation resistance will be independent of frequency. Physically this simply means that acoustic short circuiting around the circumference of the beam decreases as the dimensions of the beam become much larger than an acoustic wavelength. Limiting values of R_{rad} are given below:

$$R_{rad} = \begin{cases} 0, & q^2 < 0 \ ; \\ \dfrac{\rho c(\pi^2 a\ell)(K_o a)(qa)^2}{2}, & qa \ll 1 ; \\ \rho c(\pi a\ell), & qa \gg 1. \end{cases} \qquad (4.41)$$

It is interesting to compare the above equation with the results obtained for the infinitely long cylinder. As a check on the above result, we can let $K_s = 0$; i.e., remove the axial distribution. For

this case q will be equal to K_o and the above equations for R_{rad} will be identical with equations (4.14) for the rigid cylinder.

4.4 An Infinitely Long Cylinder, Held Motionless Except for a Finite Section Which Vibrates in a Standing Wave

Expressions were obtained in the previous section for the radiation resistance of an infinitely long beam vibrating in a standing wave. A more realistic situation is, of course, the case of a finitely long beam vibrating in a standing wave. To avoid difficulties in matching the acoustic boundary conditions at the ends of the beam, it is convenient to consider the beam as having infinite length but being held motionless except for a finite section. The effect of this assumption will be insignificant if the radius of the cylinder is small compared with the length.

Therefore, consider the case shown in the bottom of Figure (4.1) of an infinitely long cylinder of radius a, vibrating between supports at $\pm\ell/2$ with normal velocity

$$V_n = \begin{cases} 0 & z < -\ell/2 \\ V_o \cos \begin{matrix}\cos \\ \sin\end{matrix} \left(\frac{n\pi z}{\ell}\right) e^{-i\omega t} & -\ell/2 \leq z \leq \ell/2 \\ 0 & z > \ell/2, \end{cases} \qquad (4.42)$$

where the mode number n = 1,2,3,4,... is the number of antinodes in the standing wave and $\cos\left(\frac{n\pi z}{\ell}\right)$ is used if n is odd; $\sin\left(\frac{n\pi z}{\ell}\right)$ if n is even.

The boundary conditions at the surface is that the particle velocity must equal the normal velocity of the surface. Thus,

$$V_o \cos\phi \begin{matrix}\cos \\ \sin\end{matrix}\left(\frac{n\pi z}{\ell}\right) e^{-i\omega t} = \frac{e^{-i\omega t}}{2\pi} \int_{-\infty}^{\infty} A_1 \cos\phi H_1'(kr) e^{iKz}\, dK. \quad (4.43).$$

Taking the inverse yields

$$A_1 H_1'(kr)\Big|_{r=a} = V_o \int_{-\ell/2}^{\ell/2} \begin{matrix}\cos \\ \sin\end{matrix} \left(\frac{n\pi z}{\ell}\right) e^{-iKz}\, dz. \qquad (4.44)$$

Performing the integration yields

$$A_1 H_1'(ka) = \begin{cases} \dfrac{2V_o \left(\frac{n\pi}{\ell}\right) \sin\left(\frac{n\pi}{2}\right) \cos\left(\frac{k\ell}{2}\right)}{\left[\left(\frac{n\pi}{\ell}\right)^2 - K^2\right]}, & n \text{ odd} \\ \dfrac{2iV_o \left(\frac{n\pi}{\ell}\right) \cos\left(\frac{n\pi}{2}\right) \sin\left(\frac{k\ell}{2}\right)}{\left[\left(\frac{n\pi}{\ell}\right)^2 - K^2\right]}, & n \text{ even.} \end{cases} \qquad (4.45)$$

Pressure can now be written as

$$p(r,\phi,z,t) = \frac{-i\omega\rho V_o \left(\frac{n\pi}{\ell}\right) \begin{matrix}\sin \\ \cos\end{matrix} \left(\frac{n\pi}{2}\right) \cos\phi\, e^{-i\omega t}}{\pi} \int_{\infty} \frac{\begin{matrix}\cos \\ i \sin\end{matrix}\left(\frac{k\ell}{2}\right) H_1(kr)\, e^{iKz}\, dK}{H_1'(ka)\left[\left(\frac{n\pi}{\ell}\right)^2 - K^2\right]} \qquad (4.46)$$

4.4.1. Near-field Calculations

At this stage one can choose to calculate the pressure at the surface of the cylinder or the pressure in the far-field. Let us first consider pressures at the surface which can be written as

$$p(a,\phi,z,t) = \frac{i\rho c V_o \left(\frac{n\pi}{\ell}\right) \begin{matrix}\sin \\ \cos\end{matrix} \left(\frac{n\pi}{2}\right) \cos\phi\, e^{-i\omega t}}{2\pi} \int_{-\infty} \frac{\begin{matrix}\cos \\ i \sin\end{matrix}\left(\frac{K\ell}{2}\right) E_o\, e^{i(\gamma_o - \gamma_1 + Kz)}}{E_1\left[\left(\frac{n\pi}{\ell}\right)^2 - K^2\right]} dK \qquad (4.47)$$

For odd mode numbers, the integral in equation (4.47) can be written as.

$$I_{odd} = \int_{\infty} \frac{E_o \cos\left(\frac{K\ell}{2}\right) e^{i(\gamma_o - \gamma_1 + Kz)}}{E_1\left[\left(\frac{n\pi}{\ell}\right)^2 - K^2\right]} dK. \qquad (4.48)$$

Using the trigonometric identity of equation (4.27) yields

$$I_{odd} = \int_{-\infty}^{\infty} \frac{E_o \left[e^{\frac{iK\ell}{2}} + e^{\frac{-iK\ell}{2}} \right] e^{i(\gamma_o - \gamma_1 + Kz)}}{2E_1 \left[\left(\frac{n\pi}{\ell}\right)^2 - K^2 \right]} \, dK. \qquad (4.49)$$

For $k_o > \frac{n\pi}{\ell}$, the above integral can be evaluated by contour integration. Using the contours shown in Figure (4.2), the appropriate contour for the exponential $e^{i(Kz + K\ell/2 + \gamma_o - \gamma_1)}$ can be closed by a semicircle around the upper half of the K-plane. This can be reduced to the contours C_n around the simple poles at $(\frac{n\pi}{\ell})$.

For the exponential $e^{i(Kz + K\ell/2 + \gamma_o - \gamma_1)}$, the contour can be closed by a semicircle around the lower half of the K-plane. This can be reduced to the contours C_n' around the simple poles at $(-n\pi/\ell)$. Thus, I_{odd} can be shown by residue theory to be given by

$$I_{odd} = \frac{E_o \, \pi \sin(n\pi/2) \cos(n\pi z/\ell)}{E_1 \left(\frac{n\pi}{\ell}\right)} e^{i(\gamma_o - \gamma_1)} . \qquad (4.50)$$

For even mode numbers, the trigonometric identity of equation (4.28) can be used with contour integrations to yield

$$I_{even} = \frac{-iE_o \, \pi \cos(n\pi/2) \sin(n\pi z/\ell) e^{i(\gamma_o - \gamma_1)}}{E_1 \left(\frac{n\pi}{\ell}\right)} . \qquad (4.51)$$

In both equation (4.50) and (4.51), E_o, E_1, γ_o and γ_1 are now functions of Q, where Q is related to the acoustic wavenumber K_o and the structural wavenumber $(n\pi/\ell)$ by

$$Q^2 = K_o^2 - \left(\frac{n\pi}{\ell}\right)^2 . \qquad (4.52)$$

A general expression for pressure at the surface can now be written as

$$p(a,\phi,z,t) = \frac{-i\rho c V_o \cos\phi \, E_o \sin\left(\frac{n\pi z}{\ell}\right)}{2 E_1} e^{i[\gamma_o - \gamma_1 - \omega t]} . \qquad (4.53)$$

The real part of pressure is thus

$$p(a,\phi,z,t)_{real} = \frac{\rho c V_o \cos\phi \; E_o \; \begin{matrix}\cos\\ \sin\end{matrix}(\frac{n\pi z}{\ell})}{2\,E_1} \sin(\gamma_o - \gamma_1 - \omega t) \; . \qquad (4.54)$$

The real part of surface velocity is given by

$$V_{real} = V_o \; \begin{matrix}\cos\\ \sin\end{matrix}(\frac{n\pi z}{\ell}) \cos\phi \cos\omega t \; . \qquad (4.55)$$

Radiated power can be calculated by integrating the time average of the product of the real parts of pressure and velocity over the surface of the cylinder.

$$\langle w \rangle = \frac{1}{T}\int_{-\ell/2}^{\ell/2}\int_{o}^{2\pi}\int_{o}^{T} \frac{\rho c\, E_o}{2E_1}\left[V_o \begin{matrix}\cos\\ \sin\end{matrix}(\frac{n\pi z}{\ell})\cos\phi\right]^2 \sin(\gamma_o-\gamma_1-\omega t)\cos\omega t\, a\,dz\,d\phi\,dt \qquad (4.56)$$

Carrying out the above integrations yields

$$\langle w \rangle = \frac{\rho c\,(\pi a\ell) V_o^2\, E_o}{8\,E_1} \sin(\gamma_o - \gamma_1) \; . \qquad (4.57)$$

The mean square velocity averaged with respect to time and space is given by $\langle \overline{v^2} \rangle = V_o^2/4$. Therefore, radiation resistance is given by

$$R_{rad} = \frac{\rho c(\pi a\ell)\, E_o \sin(\gamma_o - \gamma_1)}{2\,E_1} \; , \quad Q^2 > 0 \; . \qquad (4.58)$$

The above equation is a general expression for radiation resistance of a finite cylinder vibrating in a standing wave when $Q^2 > 0$.

A normalised plot of η_{rad} from this equation for a beam of density ρ_M, outer radius a_o, and inner radius a_i is shown by the solid line in Figure (4.5).

Approximate values for R_{rad} are given below:

$$R_{rad} \simeq \begin{cases} \rho c(\pi a \ell)\ Qa \sin\frac{\pi(Qa)^2}{2} \simeq \frac{\rho c(\pi^2 a\ell)(Qa)^3}{2}, & Qa<<1, \\ \rho c(\pi a \ell), & Qa>>1. \end{cases} \tag{4.59}$$

The above equations are seen to be identical with the results obtained for the infinitely long cylinder vibrating in a standing wave. However, there is one important difference between infinite and finite standing waves. This occurs for the case $K_o < \frac{n\pi}{\ell}$. Returning to equation (4.46) and using the approximation of equation (A.2.10) yields,

$$p(a,\phi,z,t) = \frac{i\omega\rho a V_o (\frac{n\pi}{\ell}) \cos\phi e^{-i\omega t} \begin{matrix}\sin \\ \cos\end{matrix}(\frac{n\pi}{2})}{\pi} \quad x \quad \ldots$$

$$\ldots \int_{-\infty}^{\infty} \frac{\begin{matrix}\cos \\ \sin\end{matrix}(\frac{K\ell}{2}) \left[-1 - a^2(K^2 - K_o^2)\ell n(C_a\sqrt{K^2 - K_o^2})\right] e^{iKz}\, dK}{\left[(\frac{n\pi}{\ell})^2 - K^2\right]} \tag{4.60}$$

Using the contours of integration shown in Figure (4.3) it can be seen that the simple poles at $\pm (\frac{n\pi}{\ell})$ will not result in real pressure terms. However, the difference between the incoming and outgoing parts of the logarithmic factor is $i\pi$ for F and $-i\pi$ for F' so that the branch points at $\pm K_o$ do contribute to energy radiation. Thus, a finite cylinder vibrating in a standing wave can radiate energy when the structural wavelength is less than the acoustic wavelength.

When $K_o < n\pi/\ell$, a closed form solution cannot be obtained because of difficulties in evaluating the contribution of the logarithmic branch point at $K = K_o$. However, it can be noted that the relevant terms in the expression for radiated sound power are not proportional

to the velocity of the beam which indicates that $V \begin{matrix}\cos \\ \sin\end{matrix}(\frac{n\pi z}{\ell})$ is not an exact solution for the shape of a vibrating beam in contact with an acoustic medium. This also implies that the source of energy loss is the finite extent of the beam, i.e. the sudden change in the slope at $z = \pm \ell/2$.

Some understanding of the source of this radiation can be obtained by reformulating the problem. Instead of working with the pressure at the surface let us now consider the alternative method of analyzing the far-field sound radiation.

4.4.2. Far-Field Calculations

At large distances from the cylinder we can use the approximation of equation (A.2.8) for the Hankel function with equation (4.47) to yield the following expression for radiated pressure:

$$p(r,\phi,z,t) = -\sqrt{\frac{2}{\pi r}}\ \frac{\omega\rho\ V_o(\frac{n\pi}{\ell})\ \begin{matrix}\sin \\ \cos\end{matrix}(\frac{n\pi}{2})\ \cos\phi\ e^{-i\omega t}}{\pi} \quad x \ \ldots$$

$$\ldots \int_{-\infty}^{\infty} \frac{\begin{matrix}\cos \\ \sin\end{matrix}(\frac{K\ell}{2})\ e^{i(Kr - \frac{3\pi}{4} - \gamma_1 + Kz)}}{E_1 K^{3/2}\left[(\frac{n\pi}{\ell})^2 - K^{-2}\right]} dK \qquad (4.61)$$

Changing to spherical co-ordinates:

$$\begin{aligned} r &= R \sin\theta \\ z &= R \cos\theta \\ \phi &= \phi \end{aligned} \qquad (4.62)$$

$$p(R,\phi,\theta,t) = -\sqrt{\frac{2}{\pi R \sin\theta}}\ \frac{\omega\rho\ V_o(\frac{n\pi}{\ell})\ \begin{matrix}\sin \\ \cos\end{matrix}(\frac{n\pi}{2})\ \cos\phi\ e^{-i(\omega t - \frac{3\pi}{4})}}{\pi}\ X\ I, \qquad (4.63)$$

where

$$I = \int_{-\infty}^{\infty} \frac{\cos(\frac{K\ell}{2})}{\sin} \frac{e^{iKR\sin\theta + iKR\cos\theta - i\gamma_1}}{E_1 K^{3/2}\left[(\frac{n\pi}{\ell})^2 - K^2\right]} dK. \qquad (4.64)$$

The above integral can be evaluated by the method of stationary phase integration as suggested by Laird and Cohen (24). (Details of this method are given by Erdelyi (30)). The approximate result as $R \to \infty$ is given by

$$I \simeq \frac{i\sqrt{\frac{2\pi}{R\sin\theta}} \frac{\cos(\frac{k_o\ell}{2}\cos\theta)}{\sin} e^{-i\gamma_1}}{k_o E_1\left[(\frac{n\pi}{\ell})^2 - k_o^2\cos^2\theta\right]}, \qquad (4.65)$$

where the argument for E_1 and γ_1 is $(k_o a \sin\theta)$. For small ka (i.e. $k_o a \sin\theta << 1$) pressure can be written as

$$p(R,\phi,\theta,t) \sim \frac{-\rho c\, k_o^2 a^2 V_o (\frac{n\pi}{\ell}) \frac{\sin}{\cos}(\frac{n\pi}{2})\cos\phi \frac{\cos}{\sin}(\frac{k_o\ell}{2}\cos\theta)\sin\theta e^{-i\omega t + ik_o R}}{R\left[(\frac{n\pi}{\ell})^2 - k_o^2\cos^2\theta\right]} \qquad (4.66)$$

Mean intensity can now be written as

$$\langle I\rangle = \frac{|p|^2}{2\rho c} = \frac{\rho c\, V_o^2 (\frac{n\pi}{\ell})^2 (ka)^4 \cos^2\phi\left[\frac{\cos}{\sin}(\frac{k_o\ell}{2}\cos\phi)\right]^2 \sin^2\theta}{2R^2\left[(\frac{n\pi}{\ell})^2 - k_o^2\cos^2\theta\right]} \qquad (4.67)$$

Radiated power can be calculated by integrating the intensity over the surface of a sphere of large radius R.

$$\langle w\rangle = \int_0^{\pi}\int_0^{2\pi} \langle I\rangle R^2 \sin\theta d\theta d\phi = \frac{\pi\rho c V_o^2 (\frac{n\pi}{\ell})^2 (ka)^4}{2} \int_0^{\pi} \frac{\left[\frac{\cos}{\sin}(\frac{k_o\ell}{2}\cos\theta)\right]^2 \sin^3\theta d\theta}{\left[(\frac{n\pi}{\ell})^2 - k_o^2\cos^2\theta\right]^2} \qquad (4.68)$$

Now, $\langle \bar{v}^2\rangle = V_o^2/4$. Substitution yields

$$R_{rad} = \rho c(2\pi)\left(\frac{n\pi}{\ell}\right)^2 (ka)^4 \int_0^{\pi} \frac{\left[\begin{matrix}\cos \\ \sin\end{matrix}\left(\frac{k_o \ell}{2}\cos\theta\right)\right]^2 \sin^3\theta d\theta}{\left[\left(\frac{n\pi}{\ell}\right)^2 - k_o^2 \cos^2\theta\right]^2} \quad . \qquad (4.69)$$

A computer program has been written to evaluate the above integral numerically by the Runge-Kutta method (42). In using this program it is once again convenient to work with the non-dimensional radiation loss factor. A normalised plot of the resulting η_{rad} for a cylindrical beam is shown by the dashed line in Figure (4.5), for comparison with the result obtained from equation (4.58). As expected, η_{rad} calculated by equation (4.69) approaches the previously obtained values when the structural wavelength is larger than the acoustic wavelength. The value of using equation (4.69) is that we can now express η_{rad} as a continuous function of $k_o a$. Thus, we can approximate radiation and acoustic response for any ratio of structural to acoustic wavelength.

4.4.3. Equivalent Acoustic Sources

One of the important objectives of this study is to define the equivalent acoustic sources for transversely vibrating beams. Having derived an expression for pressure radiated to the far-field, we are now in a position to proceed with this objective. The directivity D of radiated sound pressure can be expressed by suppressing the non-directional terms in equation (4.66). The result is

$$D(\phi,\theta) = \frac{\cos\phi \begin{matrix}\cos \\ \sin\end{matrix}\left(\frac{\pi\ell}{\lambda_a}\cos\theta\right)\sin\theta}{\left[\left(\frac{\lambda_a}{\lambda_s}\right)^2 - \cos^2\theta\right]} \qquad (4.70)$$

where we have introduced the structural wavelength λ_s and the acoustic wavelength λ_a.

If the acoustic wavelength is longer than the structural wavelength for a given mode of the beam, the mode is said to be sub-critical because the denominator in the above equation is always greater than zero. From a response viewpoint, this means that the acoustic trace wavelength of a plane wave incident on the cylinder at an angle θ with the axis is always greater than the structural wavelength of the beam.

For higher order modes of the beam, the structural wavelength will be longer than the acoustic wavelength. These modes, termed super-critical, will radiate strongly in the direction for which cos θ is equal to λ_a/λ_s. This also implies that the beam will have maximum response to a plane wave which is incident on the beam at an angle such that the acoustic trace wavelength is equal to the structural wavelength. If the frequency of the acoustic excitation is also equal to the resonant frequency of the beam, this condition is called dual coincidence.

Calculations with equation (4.70) show that the fundamental mode of a beam will have a figure eight directivity pattern for <u>all</u> ratios of structural to acoustic wavelength. Thus, a beam vibrating in the fundamental mode is essentially a dipole acoustic source. This is as expected since every point of the beam is in-phase with every other point. Directivity patterns for the fundamental mode are plotted in Figure (4.6).

Directivity patterns for the second, third, fourth and fifth modes are shown in Figures (4.7), (4.8), (4.9) and (4.10) respectively. When the acoustic wavelength is much longer than the length (or structural wavelength) of the beam, it can be observed that all the odd modes have dipole directivity patterns and all the even modes have quadrupole

directivity patterns. This characteristic is also exhibited by the ninth and tenth modes as shown in Figures (4.11) and (4.12). This phenomenon can be explained by modelling a beam as a line of coupled dipole sources as shown in Figure (4.13). Each quarter wavelength of the beam can be represented by an equivalent dipole source. (Of course, each quarter wavelength could also be divided into a number of individual in-phase dipoles). When the acoustic wavelength is much longer than the structural wavelength, destructive interference would tend to cancel sound radiation from the interior dipoles, leaving only the quarter-wavelengths at each end of the beam. For odd modes, the two end dipoles would be in-phase resulting in a net dipole distribution of double strength. For even modes, the two end dipoles would be exactly 180° out-of-phase so that a net quadrupole distribution would result.

In the intermediate frequency range, where the structural and acoustic wavelengths are of the same order, the radiation is seen to be multipole in nature with one loop in the directivity pattern for each quarter wavelength of the mode. Thus, a beam vibrating transversely in the n^{th} mode radiates sound as a multipole with 2n loops in the directivity pattern. The order m of the multipole can be established by noting that 2n simple sources would be required to produce the multipole. Therefore

$$\begin{aligned} 2^{m} &= 2n, \\ 2^{(m-1)} &= n, \\ (m-1) &= \log_2 (n) = \ell n(n)/\ell n(2), \\ m &= 1 + \ell n(n)/\ell n(2). \end{aligned} \tag{4.71}$$

At higher frequencies, when the structural wavelength becomes much larger than the acoustic wavelength, sound radiation is dominated by the component in the direction for which $\cos\theta = \lambda_a/\lambda_s$. In the

limiting case of an infinitely long structural wavelength the net result is once again dipole radiation. From the acoustic source viewpoint the individual dipoles will now be far enough apart to radiate independently. Both odd and even modes have the same characteristics at these high frequencies. This is as expected since the end quarter-wavelengths are so widely separated that the relative phases will not matter.

4.5 Periodically Supported Beams

A basic understanding of the acoustic behaviour of slender beams vibrating in standing waves has now been established. In this section we shall consider a more practical situation; namely, the case of periodically supported beams. The purpose of this section will be to develop a method for estimating the sound radiation and acoustic response of periodically supported beams. This will be accomplished by defining an effective structural wavelength for sound radiation. The previous sections will then be utilized to approximate the radiation loss factor.

The main sound radiation analysis will be preceded by presentation of the classical frequency equation and a discussion of the mode shapes of periodically supported beams.

4.5.1 Natural Frequencies

The classical method for calculating the natural frequencies of transversely vibrating beams has been well established by Timoshenko (28), Bishop and Johnson (27) and others. For periodically supported beams with uniform span length, the natural frequencies are given by

$$f_i = \frac{(n_i \pi)^2}{2\pi \ell^2} \sqrt{\frac{E I g}{\gamma}} \quad , \qquad (4.72)$$

where f_i = natural frequency of the i^{th} mode,

$n_i\pi$ = i^{th} root of the frequency equation,

ℓ = length of each span,

E = Young's Modulus,

I = cross sectional moment of inertia,

γ = mass per unit length,

g = gravitational constant.

The roots of the above equation have been determined graphically by Ayre & Jacobson (31). In general, the natural frequencies tend to fall in groups with one mode for each span of the beam.

4.5.2. Mode Shapes with Simply Supported Ends

The fundamental mode of a periodically supported beam is obviously equivalent to the fundamental of the single span beam. The second mode of a two span beam is equivalent to the fundamental of a single span beam with one end clamped and the other simply supported. Similarly the higher order modes in each group can be reduced to the equivalent single span cases with the internal supports acting as points of inflection. Typical mode shapes are shown by the solid lines in Figures (4.14) and (4.15) for the first two groups of natural modes of a beam with five simple supports.

4.5.3. Effective Wavelengths for Sound Radiation

An expression for the radiation resistance of a finite beam vibrating in a standing wave was obtained in Section (4.4) by solving the classical wave equation subject to the boundary conditions imposed by the motion of the vibrating beam. Solutions were obtained by assuming that the mode shapes of the vibrating beam could be expressed in terms of sine or cosine. For periodically (or non-periodically) supported beams this is no longer possible because the supports can act as points of inflection, resulting in additional

hyperbolic terms. The total sound power radiated from a particular mode could be approximated by summing the contributions from the Fourier components of the velocity distribution. Radiation resistance could then be calculated in the usual manner.

It would obviously be a mammoth task to follow this procedure to calculate the radiation resistance of every mode of a periodically supported beam. Fortunately, it has been found that an adequate approximation for radiation resistance can be obtained by assuming that the majority of the radiation is due to the fundamental wavelength component. This assumption is justified because it has been shown that radiation is highly dependent on the difference between the structural and the acoustic wavelengths. Thus, even if the higher order Fourier components are of the same magnitude as the fundamental, the radiation is still dominated by the fundamental wavelength component.

The fundamental wavelengths, which will be considered as equivalent wavelengths for sound radiation, are shown by the dashed lines in Figures (4.14) and (4.15).

It should be noted that these approximations are only valid when the acoustic field is diffuse. All the Fourier components would have to be included to consider the directional characteristics of sound radiation and response.

4.5.4. Radiation Resistance

Radiation resistance of periodically supported beams will now be estimated by using the equivalent structural wavelengths. The equivalent wavenumber is given by

$$k_e = 2\pi/\lambda_{eff} \quad . \qquad (4.73)$$

Substituting into equation (4.58) yields

$$R_{rad} = \frac{\rho c(\pi a \ell)\, E_o \sin(\gamma_o - \gamma_1)}{2\, E_1} \quad , \tag{4.74}$$

where E_o, E_1, γ_o and γ_1 are now functions of q_e as defined by

$$q_e^2 = k_o^2 - k_e^2 \quad . \tag{4.75}$$

Limiting values are given by substituting into (4.59). The result is

$$R_{rad} \simeq \begin{cases} \dfrac{\rho c(\pi^2 a \ell)(q_e a)^3}{2} & , \; q_e a << 1 \\ \rho c(\pi a \ell) & , \; q_e a >> 1 \end{cases} \quad . \tag{4.76}$$

For the case $q_e^2 < 0$, equation (4.69) is applicable with $(n\pi/\ell)$ replaced by k_e.

The results of assuming an equivalent wavelength for sound radiation are shown in Figure (4.16). The curve which establishes the upper limit in this plot is the radiation loss factor of an infinitely long, rigid beam vibrating in a plane. The lower curve is the radiation loss factor of a simply supported beam. At higher frequencies the two curves converge. As expected the two groups of modes shown in Figures (4.14) and (4.15) lie between these two curves with the first mode in both groups being on the lower curve and the last mode approaching the upper curve.

Obviously, the equivalent wavelength for the first mode in each group is the actual structural wavelength of the beam. Thus the calculations for these modes should be exact. Perhaps the calculations

for the higher modes in each group could be improved by including other Fourier components. However, the considerable effort involved would be difficult to justify for the following reasons. First of all, from a design viewpoint, converging upper and lower limits for response have been established. Also, approximations for the Hankel function have been used in all the calculations and it has been assumed that a finite beam is equivalent to an infinitely long beam, held rigid except for a finite portion which vibrates in a standing wave. Finally, application of the results to predict the response of a beam to acoustic excitation would require an approximation of the total damping of the beam and a detailed knowledge of the acoustic field. In the midst of all these approximations the assumption of an equivalent structural wavelength would seem to be adequate.

4.5.5. Comments on Clamped Beams

The previous discussion has been limited to periodically supported beams. It has been observed that the natural modes occur in groups with one mode for each span of the beam. The first natural mode in each group has the resonant frequency of a single span with simply supported ends. The last mode has a natural frequency which is slightly less than the natural frequency of a single span with clamped ends. From a sound radiation viewpoint the primary difference between clamped and supported beams is that with clamped beams the phase of adjacent spans is indeterminate. Thus, a clamped beam could have effective structural wavelengths less than or equal to any of the simply supported modes, depending on the relative phase of each span. The worst case would always occur when all the spans are in-phase. The effective structural wavelength for this case would be slightly less than the wavelength for the simply supported case with all the spans in-phase and the frequency would be slightly higher. Thus, the sound radiation and acoustic

response of periodically clamped beams must be equal to or less than that calculated for beams with periodic simple supports.

Of course, it is extremely difficult to predict the behaviour of any support system. If simple supports are assumed all the possible mode shapes are included. For this reason, simple supports should be assumed in the design of periodically supported beams subjected to acoustic excitation.

4.6 Summary

Three of the primary objectives of this research have been achieved in this chapter. Firstly, a procedure for calculating the acoustic energy radiated from a transversely vibrating beam has been established. Secondly, it has been shown that a transversely vibrating beam can be represented by an ensemble of coupled dipole sources. Finally, an approximate solution for the radiation resistance of a periodically supported beam has been obtained.

The important parameters for sound radiation are clearly shown in the following table of radiation resistances. For every case, radiation resistance is seen to be proportional to $\rho c \ell$ where ρc is the specific impedance of the acoustic medium and ℓ is the length of the vibrating beam. When $k_a << 1$, radiation resistance is proportional to a^4. Thus the radius of a vibrating beam is a very critical parameter at low frequencies.

The importance of the ratio of structural to acoustic wavelengths is also evident with radiation resistance being proportional to k^3 where $k^2 = (k_o^2 - Q_e^2)$. If the structural wavelength is of the same order of magnitude as the acoustic wavelength, i.e., $Q_e^2 \simeq k_o^2$, radiation resistance will be closely linked to the exact velocity distribution of a particular mode. On the other hand, when the ratio

TABLE OF RADIATION RESISTANCES

TYPE OF SOURCE	RADIATION RESISTANCE (Unit Length ℓ)		
	General Expression*	ka<<1**	ka>>1
Infinitely Long, RIGID cylinder	$\frac{2\rho c\ell}{k_o E_1^2}$	$\frac{\rho c(\pi^2 a\ell)(k_o a)^3}{2}$	$\rho c(\pi a\ell)$
Infinitely Long Standing Wave ($q^2 > 0$)	$\frac{2\rho c\ell k_o}{q^2 E_1^2}$	$\frac{\rho c(\pi^2 a\ell)k_o a(qa)^2}{2}$	$\rho c(\pi a\ell)$
STANDING WAVE of length ℓ ($Q^2 > 0$)	$\frac{\rho c(\pi a\ell)E_o \sin(\gamma_o-\gamma_1)}{2E_1}$	$\frac{\rho c(\pi^2 a\ell)(Qa)^3}{2}$	$\rho c(\pi a\ell)$
Periodically Supported Cylindrical Beam ($q_e^2 > 0$)	$\frac{\rho c(\pi a\ell)E_o \sin(\gamma_o-\gamma_1)}{2E_1}$	$\frac{\rho c(\pi^2 a\ell)(q_e a)^3}{2}$	$\rho c(\pi a\ell)$

* The argument for E_o, E_1, γ_o, and γ_1 in these equations is ka where $k^2 = k_o^2 - Q_e^2$ with Q_e being the appropriate structural wavenumber for each case.

** k_o, q, Q and q_e are defined in the sections corresponding to each case.

of structural to acoustic wavelengths is much larger than 1, k will approach k_o and radiation resistance will be relatively insensitive to the exact shape of the velocity distribution. This result is particularly useful in approximating the radiation resistance of periodically supported beams. The ratio of structural to acoustic wavelengths is also important in differentiating between finite and infinitely long beams. When the ratio is greater than 1, the radiation resistance per unit length of an infinitely long beam is identical with that of a finite beam. In contrast, when the ratio is less than 1, a finite beam will radiate as a multipole source but an infinitely long beam will not radiate sound to the far-field.

For small ka radiation resistance is proportional to k^3. Thus, radiation resistance is highly dependent on frequency and the speed of sound in the acoustic medium.

At high frequencies radiation resistance is given by $\rho c(\pi a \ell)$ for every case. This is in agreement with the basic principle that wave motions are insensitive to details smaller than an acoustic wavelength. It is interesting to compare this result with the radiation resistance of a pulsating sphere. For equal dimensions and velocities the ratio is

$$\frac{R_{pul.cyl.}}{R_{osc.cyl.}} = \frac{\rho c(2\pi a \ell)}{\rho c(\pi a \ell)} = 2. \qquad (4.77)$$

Thus, a pulsating cylinder is a more efficient radiator than an oscillating cylinder at high frequencies. This is consistent with the comparison of pulsating and oscillating spheres in Appendix I.

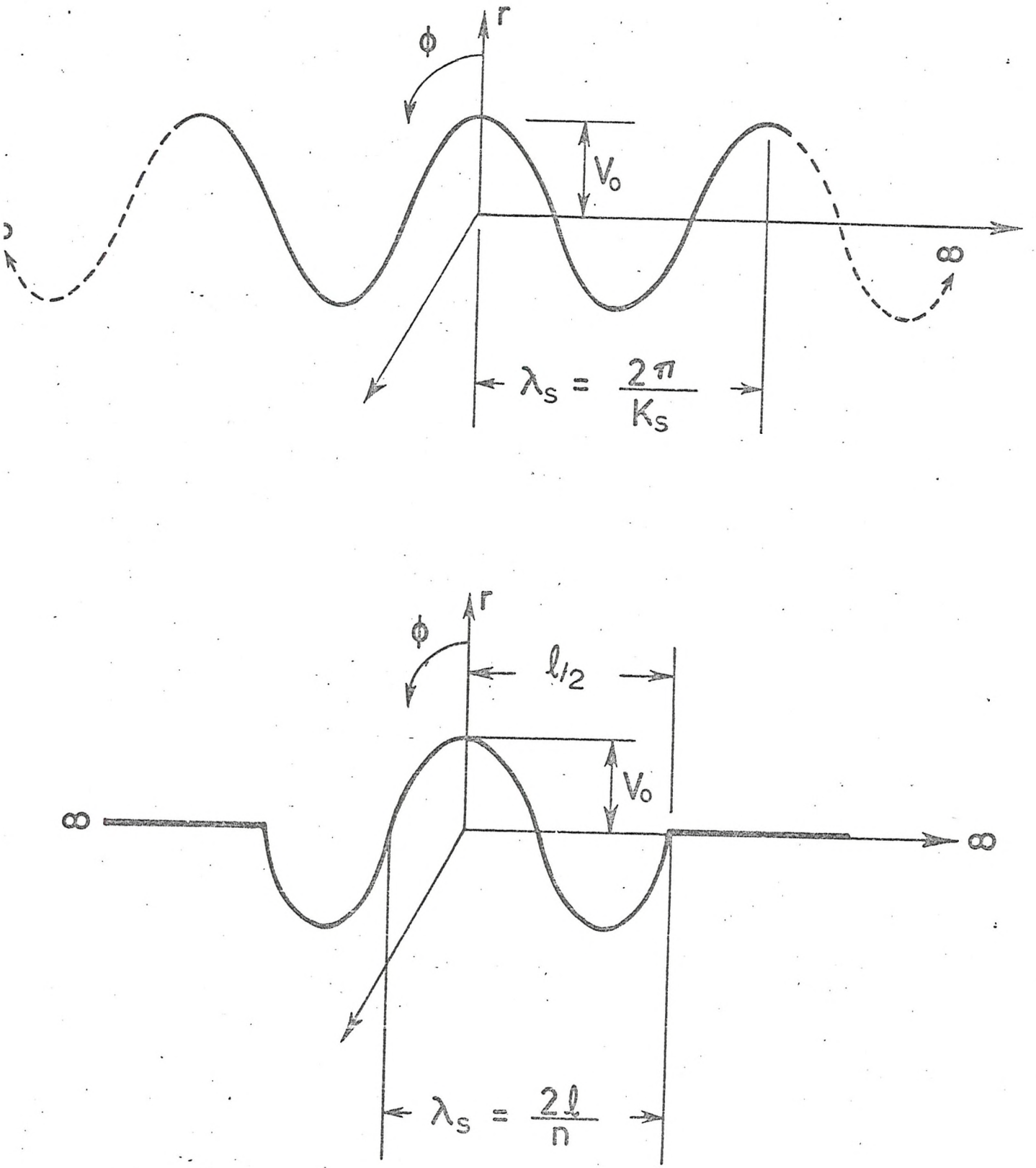

Fig. 4.1 Top - An infinitely long standing wave.
Bottom - A finite standing wave.

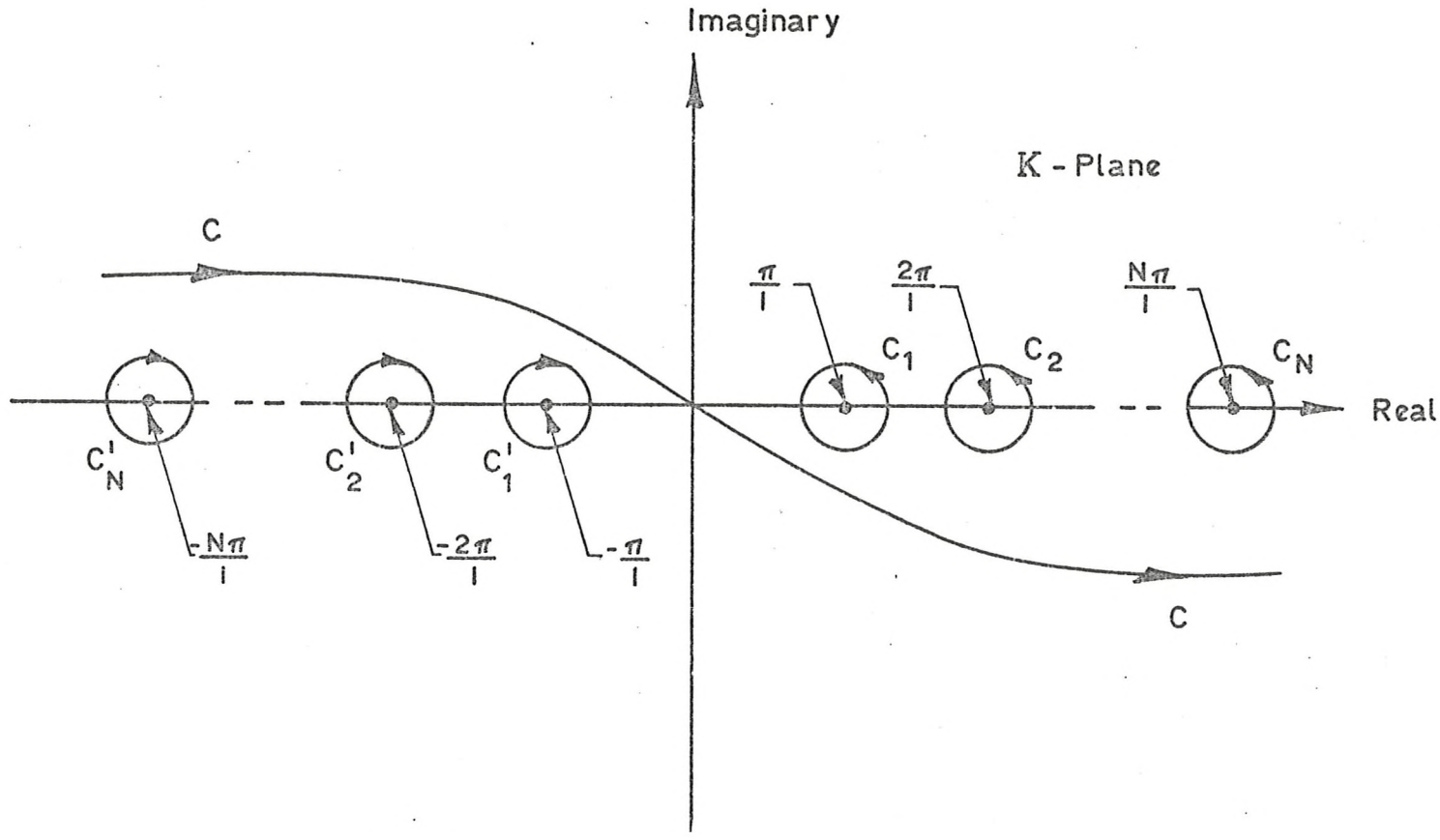

Fig. 4.2 Contours of integration for equation (4.49).

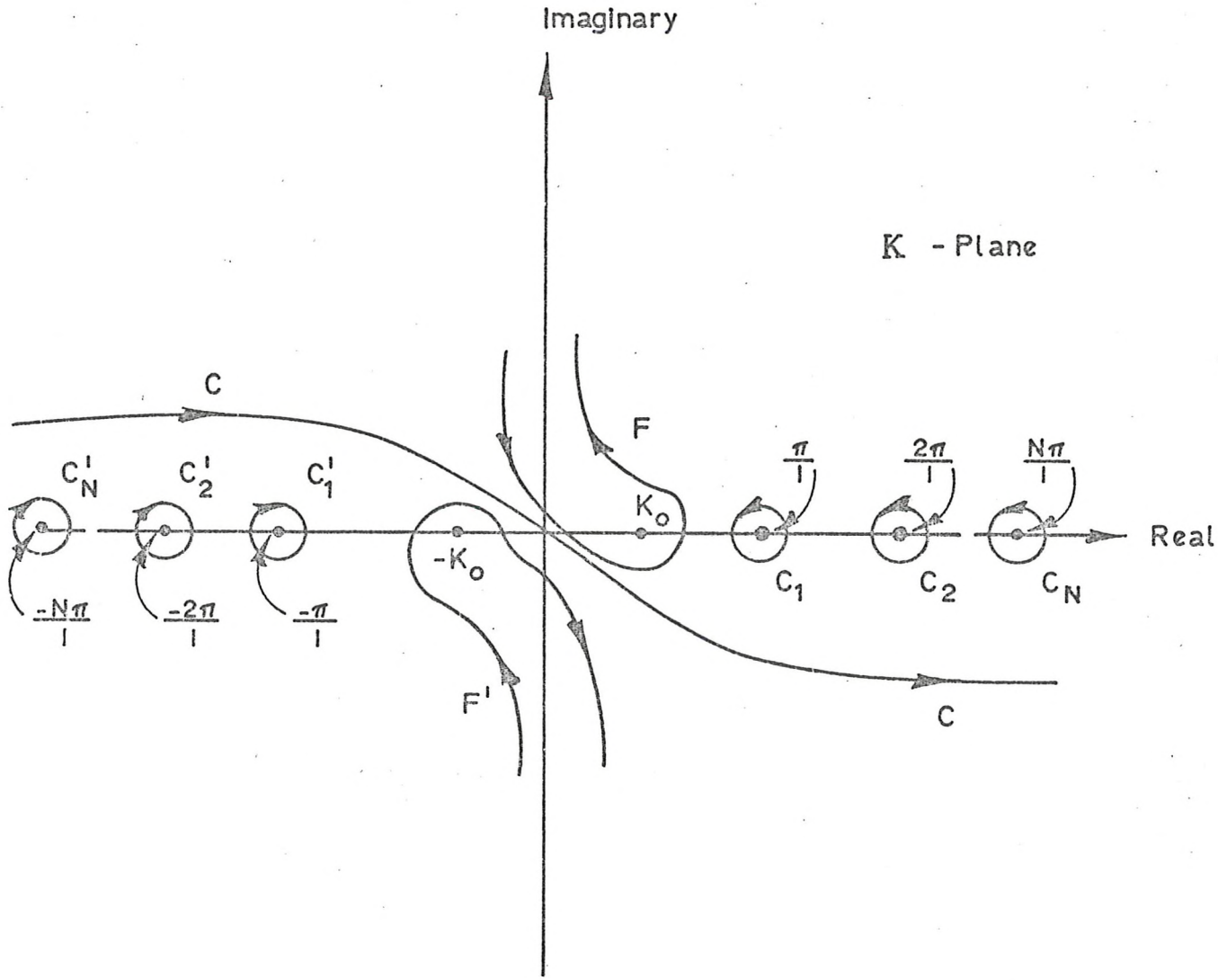

Fig.4.3 Contours of integration for equation (4.60).

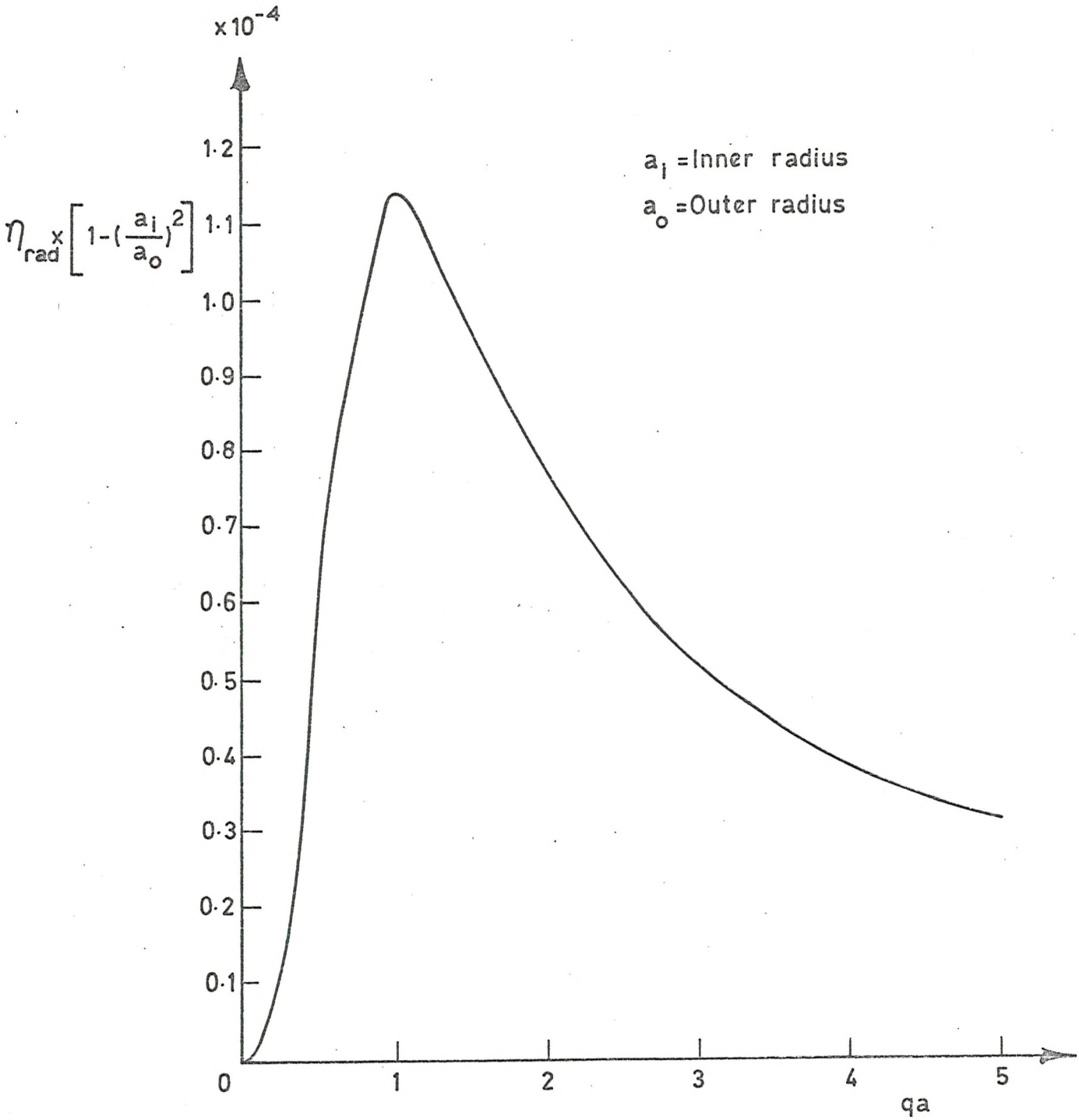

Fig. 4.4 Radiation loss factor of a steel cylinder vibrating transversely in air.

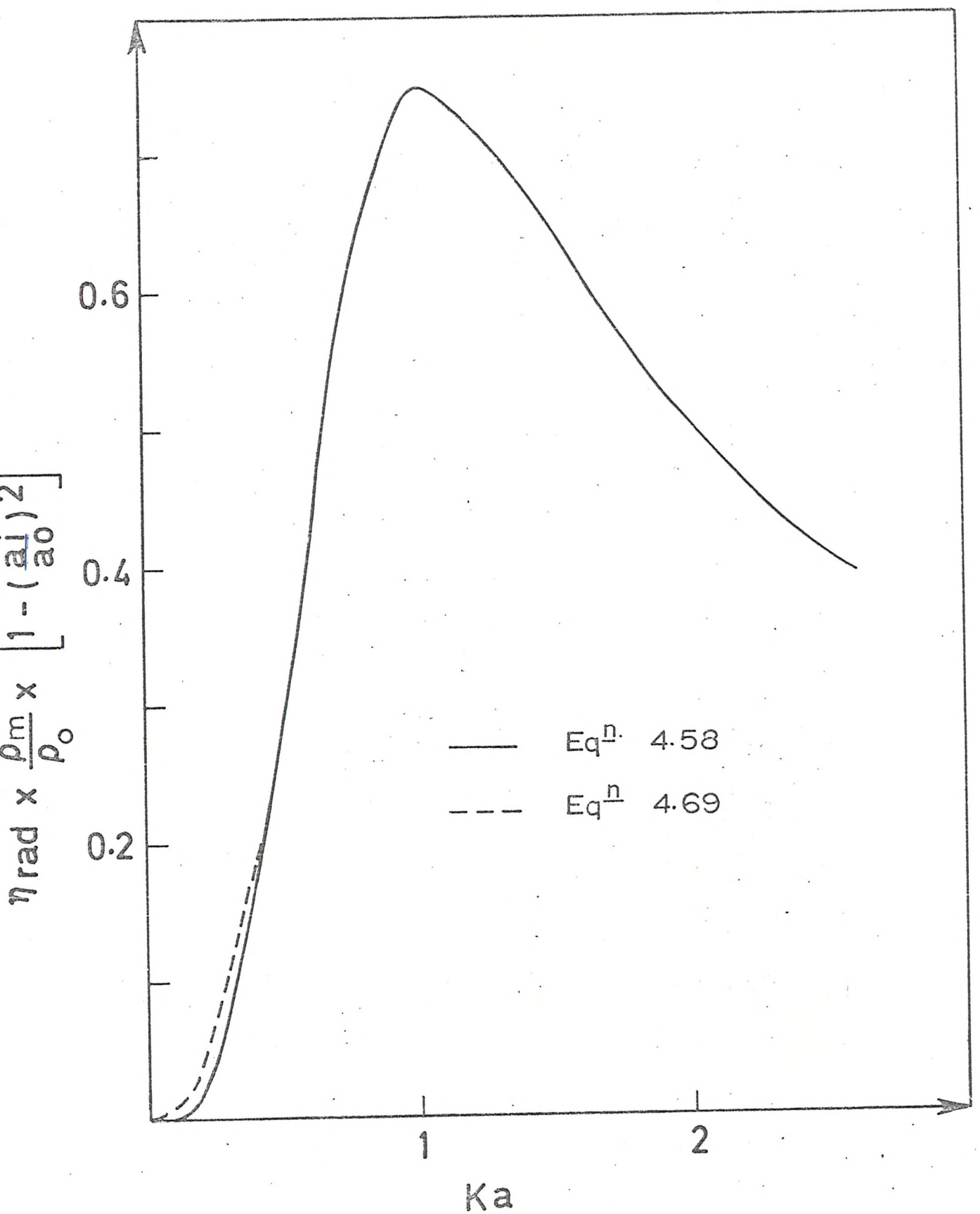

Fig. 4.5 Normalized η_{rad} for a cylindrical beam.

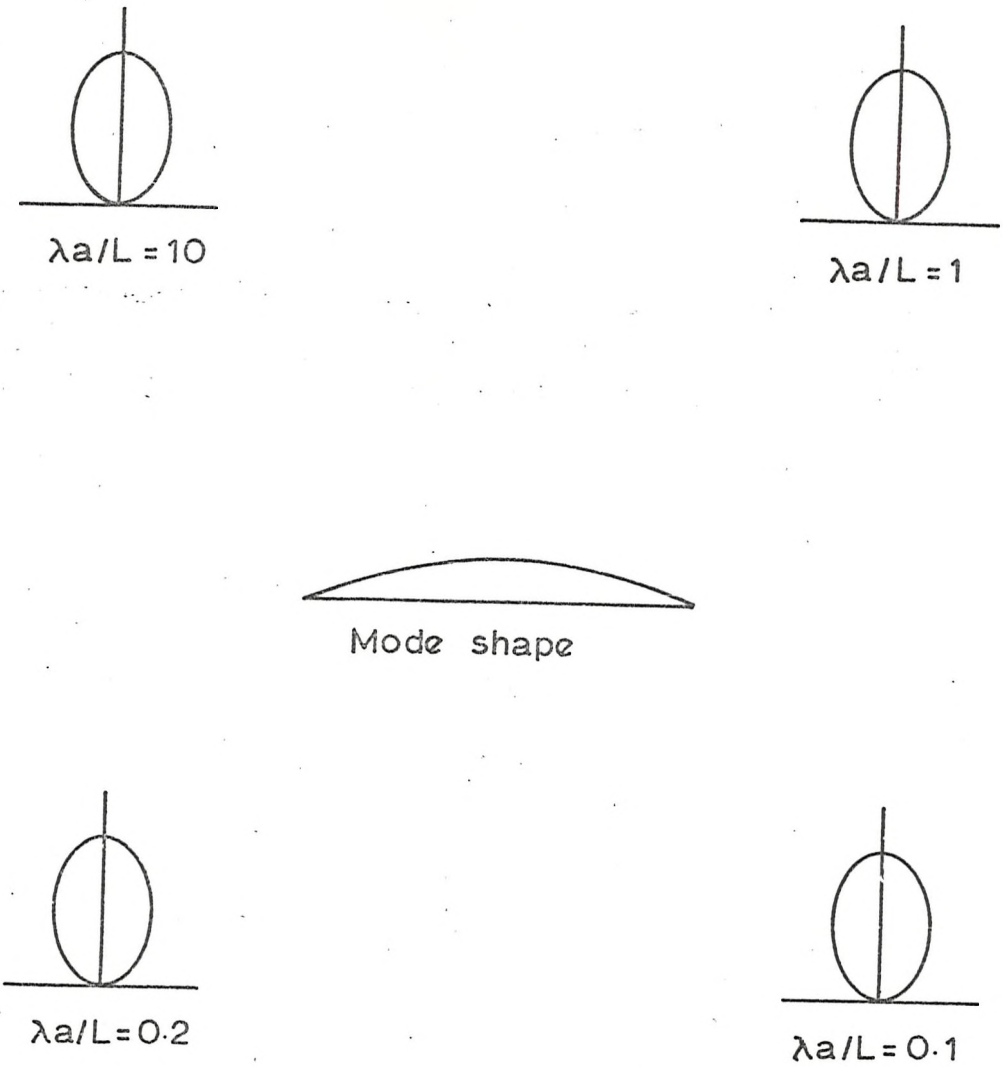

Fig. 4.6 Directivity patterns - fundamental mode.

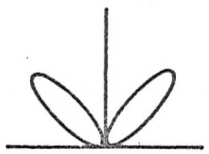

λa/L = 10

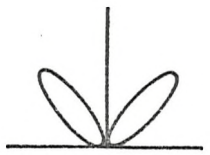

λa/L = 1

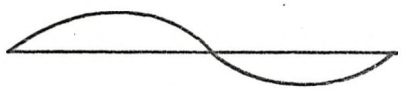

Mode shape

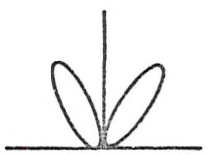

λa/L = 0·2

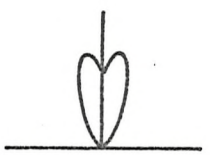

λa/L = 0·1

Fig. 4.7 Directivity pattern - second mode.

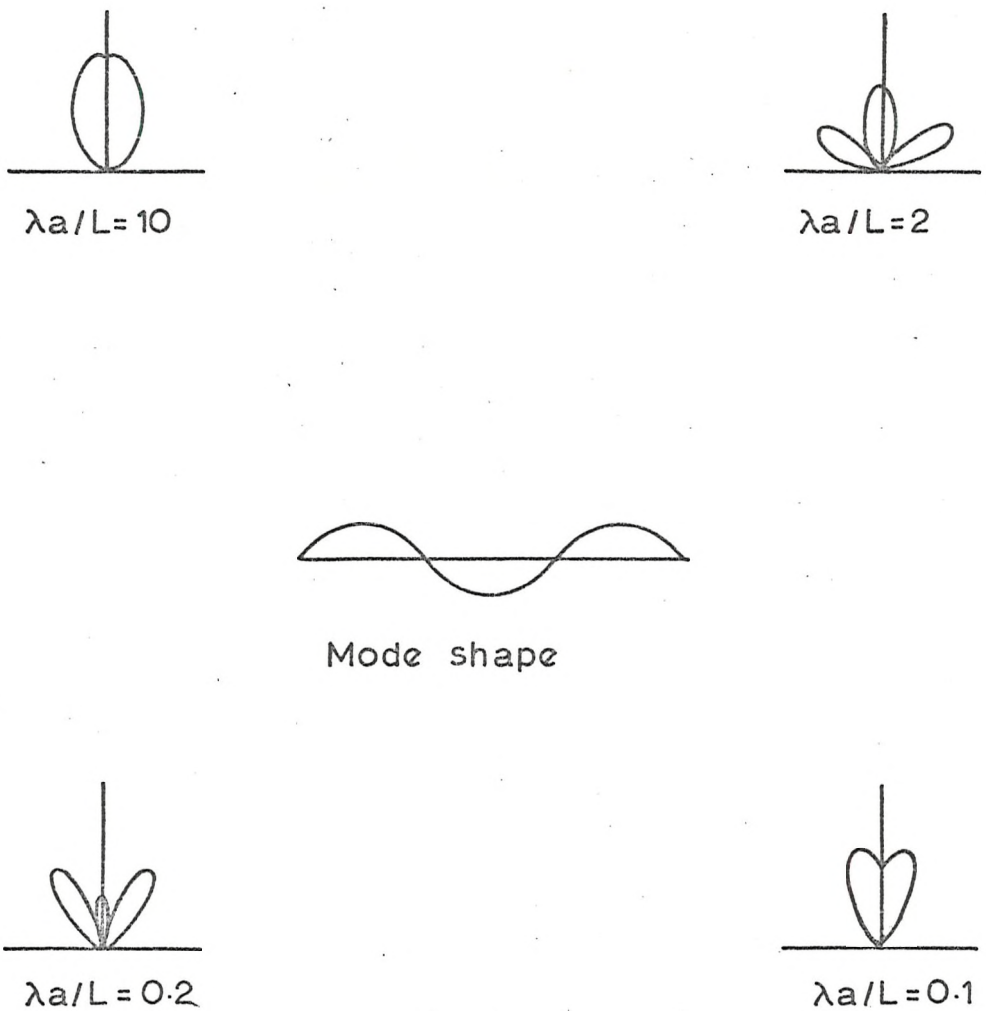

Fig. 4.8 Directivity pattern - third mode.

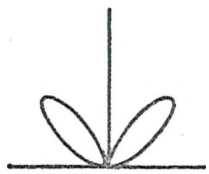

λa /L = 10

λa /L = 1

Mode shape

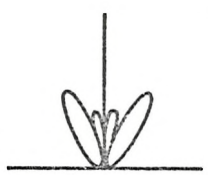

λa = 0·2

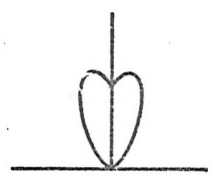

λa = 0·1

Fig. 4·9 Directivity patterns - fourth mode.

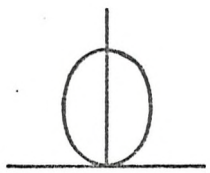

λa/L = 10

λa/L = 1

Mode shape

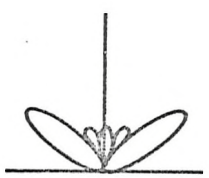

λa/L = 0·2

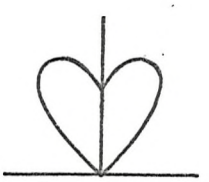

λa/L = 0·1

Fig. 4·10 Directivity patterns - fifth mode.

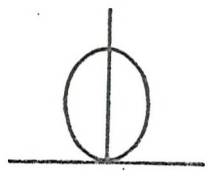

λa/L= 10

λa/L = 1

Mode shape

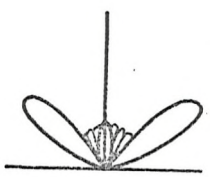

λa/L = 0.2

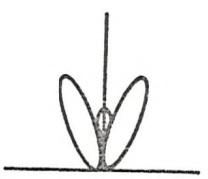

λa/L = 0.1

Fig. 4.11 Directivity patterns - ninth mode.

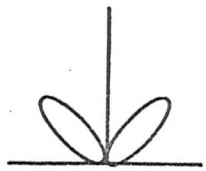

$\lambda a/L = 10$

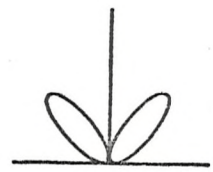

$\lambda a/L = 1$

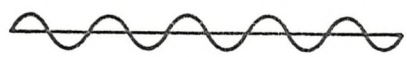

Mode shape

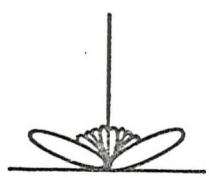

$\lambda a/L = 0.2$

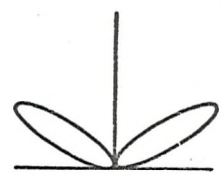

$\lambda a/L = 0.1$

Fig. 4.12 Directivity patterns - tenth mode.

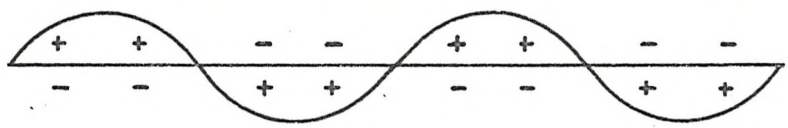

\+ Positive monopole

\- Negative monopole

Fig. 4.13 Acoustic source model.

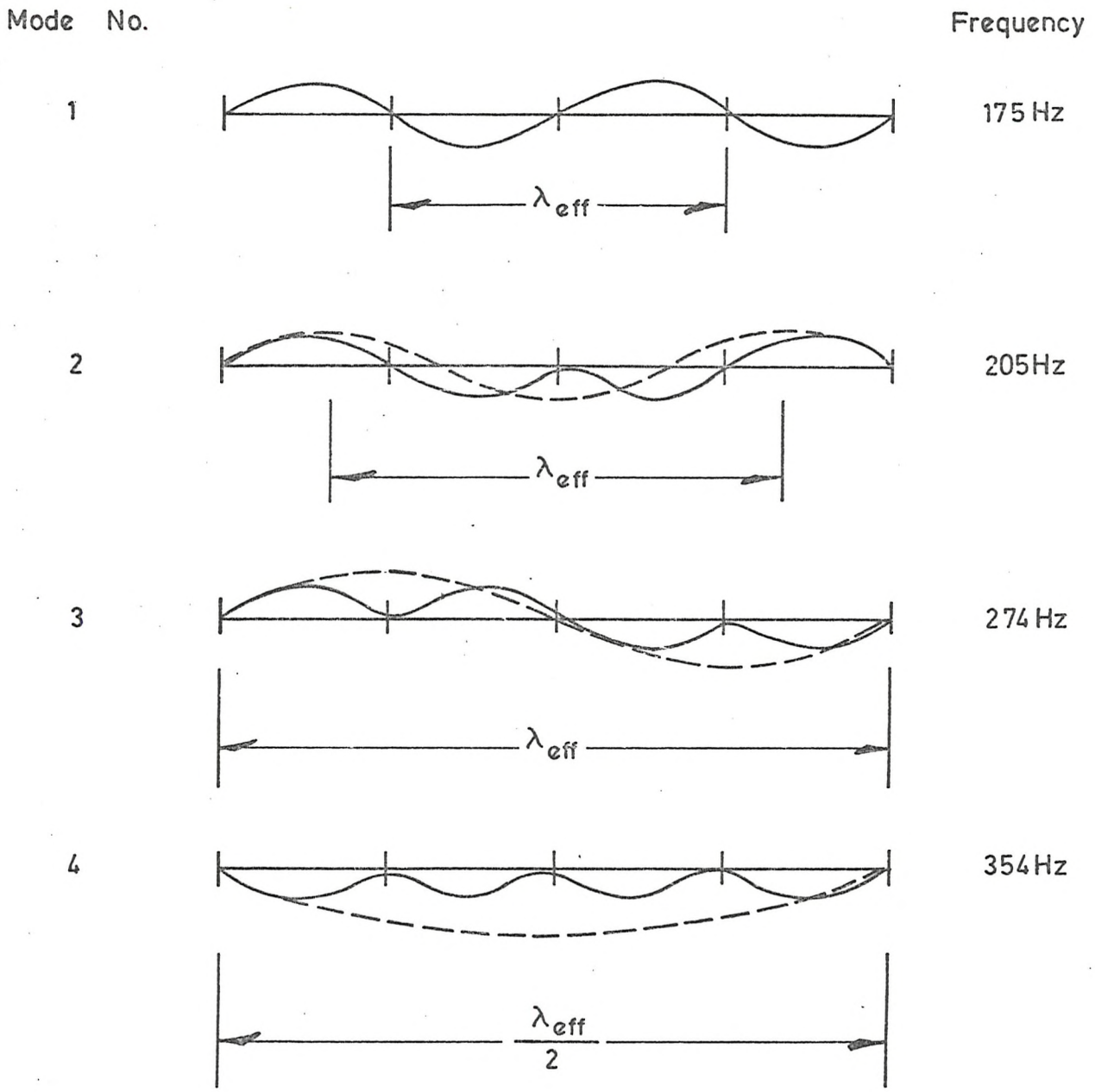

Fig.4.14 Effective wavelengths for the first group of modes - beam 4 with five supports.

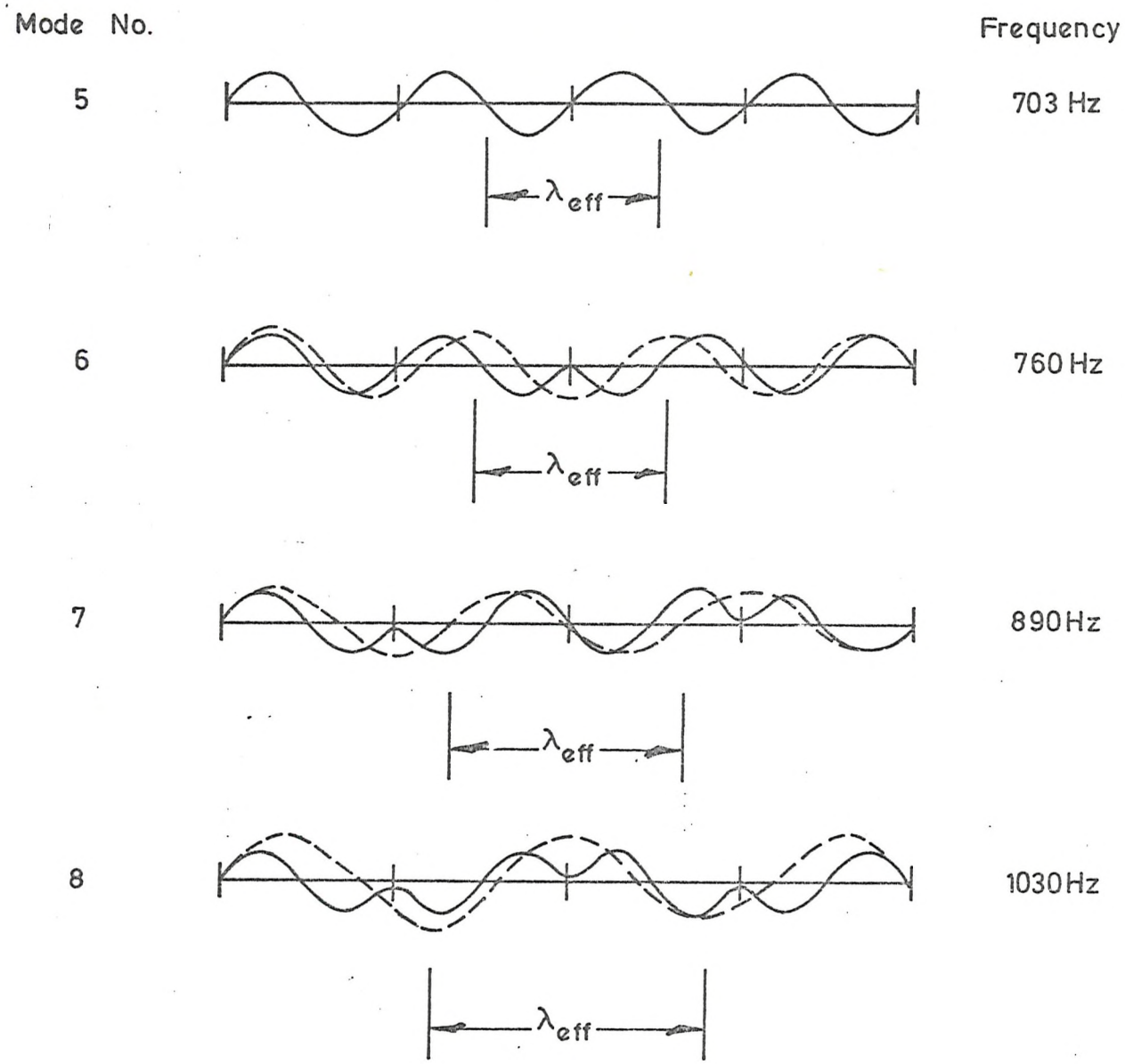

Fig. 4.15 Effective wavelength for the second group of modes - beam 4 with five supports.

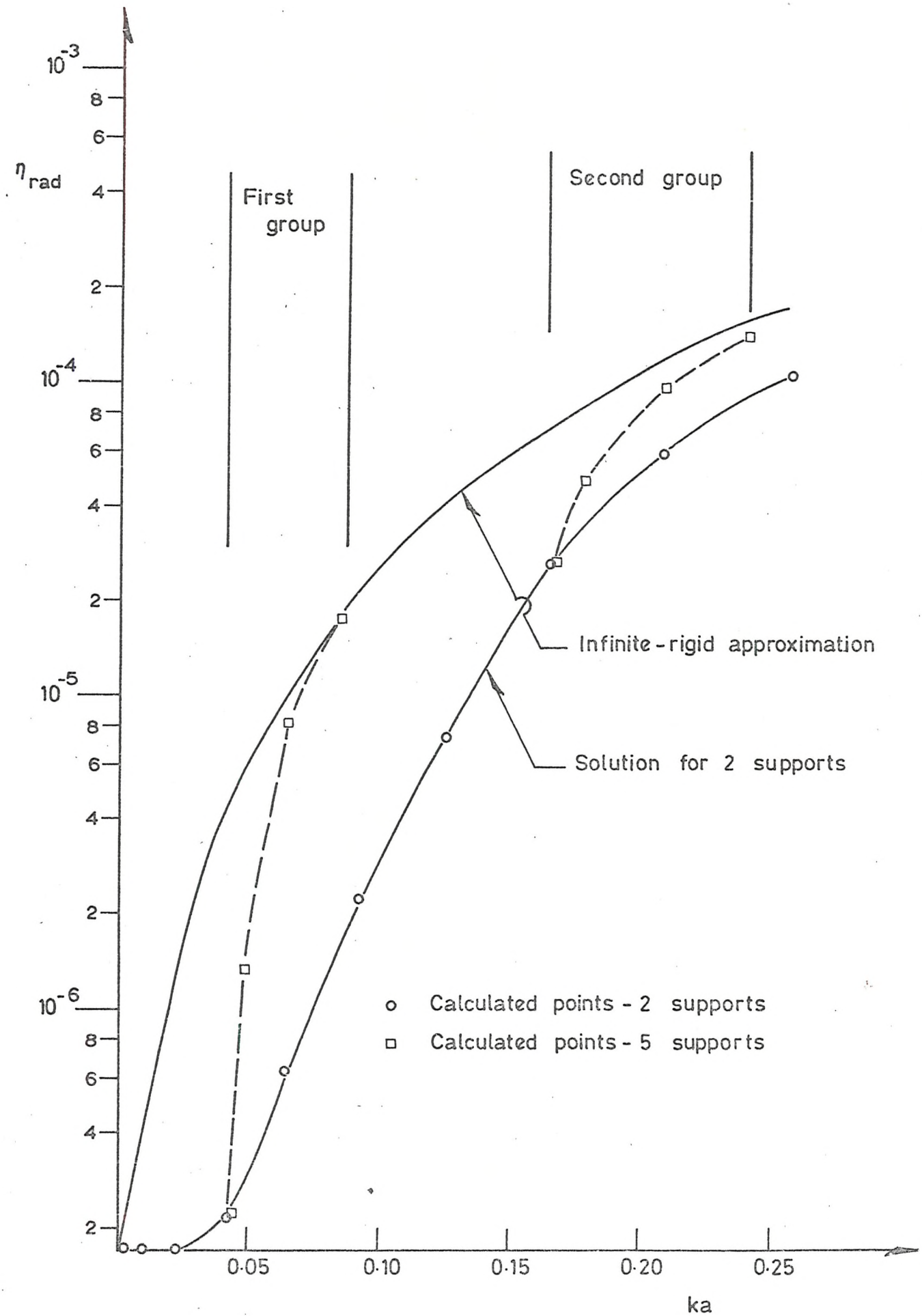

Fig.4.16 η_{rad} - First two groups - five periodic supports - beam four.

CHAPTER V

NOTES ON COMPUTATION

5.1 The MASTER PROGRAM

Several parameters have been shown to be important in determining the response of a beam to acoustic excitation. In particular, the number of supports for a given length of beam would be of interest to the designer. The mathematical models which have been derived require the use of numerical integration and computation of Hankel functions. A computer program has been written in Fortran 1900 to perform these functions. The flow diagram is shown in Figure (5.1). For given beam dimensions the program will calculate all the natural frequencies, radiation loss factors and acoustic responses of the beam in a given frequency range. The program will then automatically add additional supports one at a time, and repeat the above calculations. Up to thirteen supports can be included in the analysis.

The numerical integrations are performed by Subroutine S4 Runk which is an application of the Runge-Kutta method. Subroutine DERY defines the differential for the integration and Subroutine F(BETA) is used to set up the proper equations for odd and even modes. The Subroutine BESSEL is used to compute the Hankel functions.

5.2 Typical Calculations

The following beam parameters have been used in typical calculations with the MASTER PROGRAM:

Material	Aluminium
Outside diameter	1.0 inches
Bore	0.8593 inches

Length	96 inches
Young's Modulus	10×10^6 p.s.i.
Density	0.101 lbm/in^3

The effect of changing the number of supports is shown in Figure (5.2) which is a plot of normalized response to pure-tone sound vs. Ka. At first glance, it would appear that adding supports will always reduce the maximum response to acoustic excitation. This can be misleading, however, unless the source of the acoustic excitation is taken into consideration. The following example will demonstrate this point.

Suppose the above beam is to be subjected to noise generated by a gas circulator with a flat spectrum from 100 to 1000 Hz. This corresponds to the range of Ka from 0.023 to 0.23 shown in Figure (5.2). The mode which will have maximum response with two supports occurs at Ka = .21 corresponding to 890 Hz.

If four supports are used, the mode with maximum response occurs at Ka = 0.44 corresponding to 185 Hz. For this particular mode all three spans of the beam vibrate in-phase, resulting in increased response because the coupling with the sound field has been greatly enhanced by the longer effective structural wavelengths. The amplitude of response has been increased by a factor of 2.8. Thus, for equal damping, the addition of two more supports has actually increased the response of the beam to the acoustic excitation.

The peculiar behaviour of the response of the beam with two supports can be explained by recalling the simple acoustic source model of section (4.4.3). The first mode is essentially a dipole acoustic source which should radiate and respond strongly. The second mode is equivalent to a quadrupole source which is a relatively weak radiator. Hence, the response of the second mode is greatly reduced. The third mode is a

multipole radiator, but the acoustic wavelength is longer than the structural wavelength so that radiation is dominated by the center lobe and is essentially dipole in nature. Consequently, the response of the third mode is slightly higher than that of the second mode. The next four or five modes are multipole radiators with response increasing with frequency because the radiation is beginning to be controlled by the major lobe of the directivity pattern. At higher frequencies, where the structural wavelength is much greater than the acoustic wavelength, the radiation once again becomes dipole in nature.

Similar explanations can be offered for the response behaviour of beams with additional supports. For example, the first mode of the beam with four supports should radiate as a multipole. The second mode, having an effective structural wavelength equal to the length of the beam, should radiate as a quadrupole, and the third mode, with every span in-phase, should radiate as a strong dipole. Because of phase cancellation between spans, the fourth mode should be a relatively weak multipole. Hence, the acoustic response of a beam with four supports increases with frequency to a maximum at the third mode. Then the response drops sharply as the nature of the radiation becomes multipole and increases with frequency to a second maximum at the sixth mode, etc.

Further calculations using the MASTER PROGRAM are given in Chapter VII for comparison with experimental results.

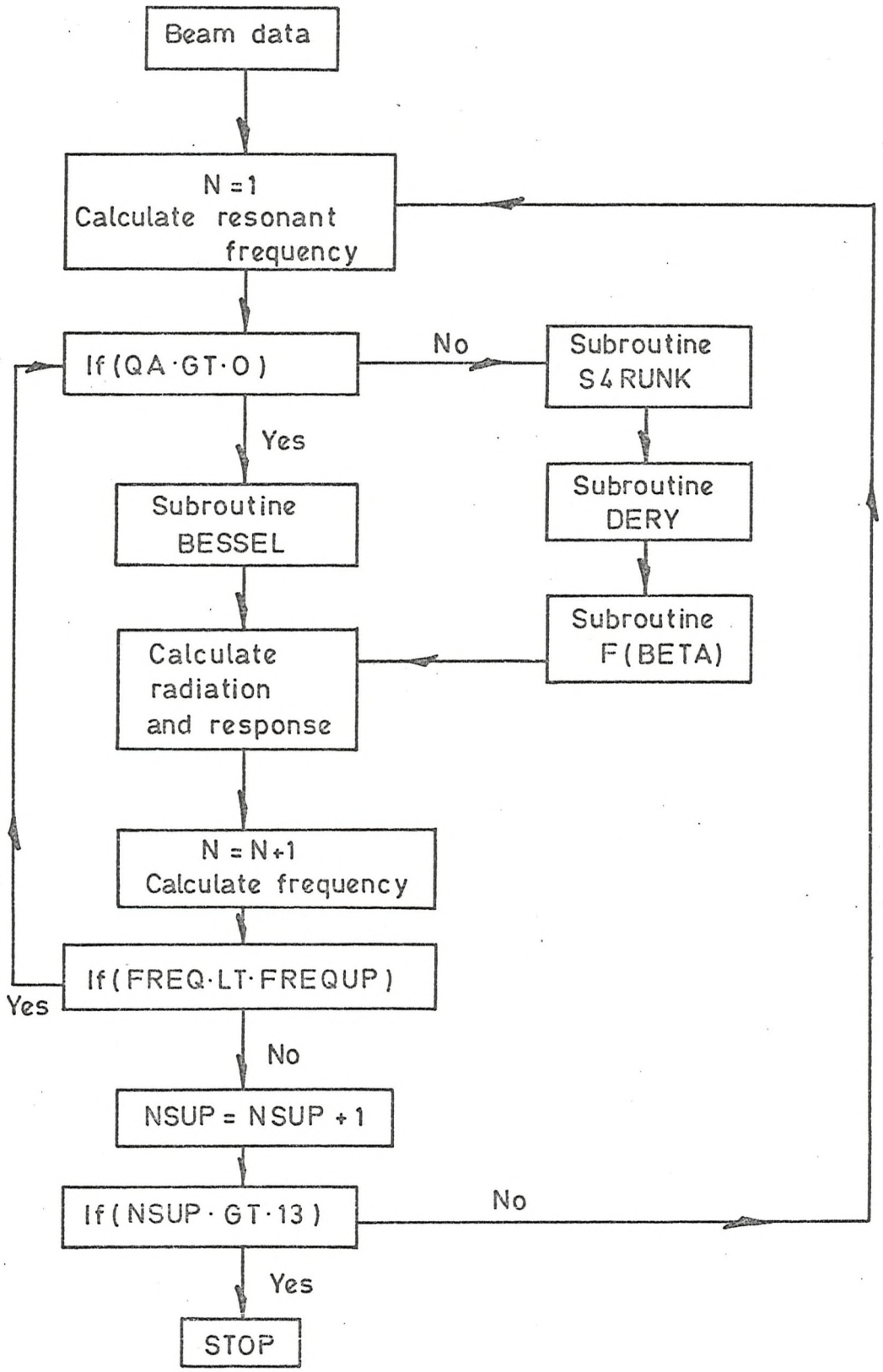

Fig.5.1 Flow diagram for master program

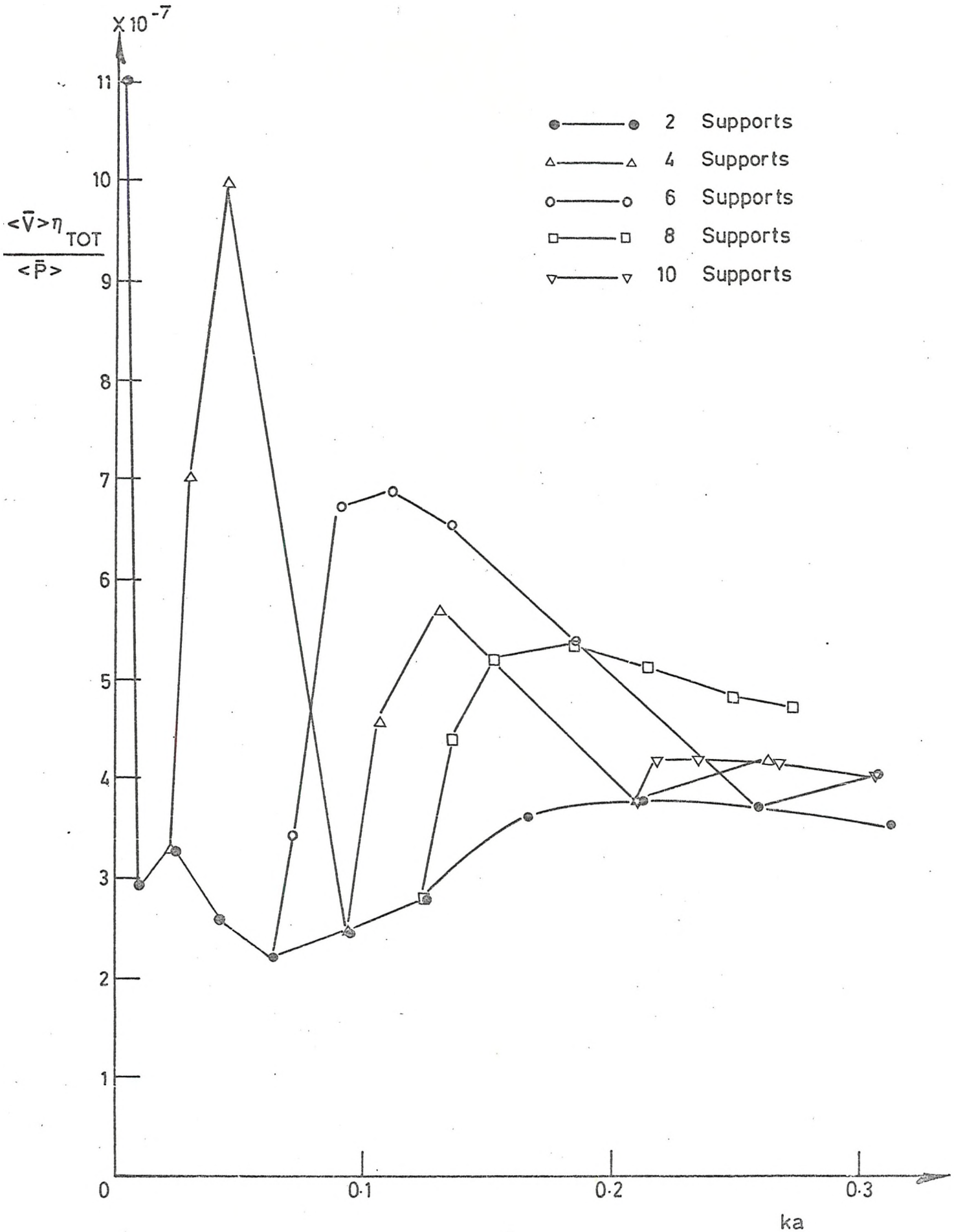

Fig.5.2 Variation of response with number of supports.

CHAPTER VI

INTRODUCTION TO THE PROBLEMS OF SOUND MEASUREMENTS IN REVERBERANT ROOMS

This chapter discusses some aspects of the measurement of sound radiation and response in reverberant rooms. This discussion is vital to the experimental investigations reported in Chapters VII and VIII.

6.1 Comments on Diffusivity

There are several methods of measuring the sound power radiated from a vibrating body. Measurements in the free-field provide information about the directivity of a source and define radiated power. However, the large number of microphone measurement points and the corresponding data analysis result in a relatively high test effort. Measurements in a reverberant field require fewer microphone readings and consequently less test effort. The procedure used in this research has been to compute the radiated sound power from sound pressure measurements in a large reverberant room. The mean acoustic power output $\langle w \rangle$ in watts of a source in such a room is given by the following equation:

$$\langle w \rangle = 2.8 \, (\langle \bar{p}^2 \rangle \quad V/T) \times 10^{-8} , \qquad (6.1)$$

where V is the room volume in ft^3, $\langle \bar{p} \rangle$ is the sound pressure in microbars, and T is the reverberation time of the room in seconds. The above equation is based on the assumption that the sound field is completely diffuse.

Uniformity of energy distribution in a reverberant room is dependent on the number of modes present in the frequency band of interest and the spectrum of the source. In general, sound sources which emit broad band noise will excite many modes in the room and produce reasonably diffuse

sound fields. Narrow band or pure-tone sources will generally produce non-uniform fields. Schroder (32) has shown that a sufficient number of modes will be excited in a reverberant room if the frequency is above the "large room" frequency given by

$$f_{L.R.} = 1.19 \times 10^{4} \, (T/V)^{\frac{1}{2}} \, . \qquad (6.2)$$

The "large room" frequency of the reverberation chamber used in this research is approximately 320 Hz. Above this frequency the assumption of a diffuse field would seem to be valid.

6.2 Fluctuations of Sound Pressure

6.2.1 General Theory

The sound pressure at a point in a reverberant room varies as either the frequency or the source position varies. Above the "large room" frequency Schröder (32) has shown that for variation of pure-tone frequency the sound pressure level at a point has a Gaussian probability distribution with the standard deviation from the mean value equal to 5.5 dB.

Doak (33) investigated the fluctuations of sound pressure level in rooms when the receiver position was varied. He was able to show that the standard deviation of pure-tone sound pressure level at a point from its mean value is 5.5 dB above the "large room" frequency. This value does not hold near the source where the directivity of the source would affect the spatial variation of sound pressure.

Obviously, excessive errors would result from using a single microphone position to measure sound pressure. As pointed out by Baade (34), the uncertainty of measuring sound pressure can be reduced by taking separate readings at a number of points in the room. By averaging N

independent samples, the standard deviation will be reduced by a factor of $\sqrt{N}$. A more practical method is to calculate the average sound pressure from the output of a microphone which is moved along a traverse. The number of statistically independent samples obtained from a traverse of length X is given by Lubman (35) and Schroder (36, 37) as $N = 1 + 2X/\lambda$, where λ is the acoustic wavelength. The equivalent sample size can be increased by using a two-dimensional traverse (34).

6.2.2 Measurements of the Standard Deviation of Pure-tone Sound Pressure Levels

An experimental investigation was conducted to measure the fluctuations of pure-tone sound pressure. A loud speaker, placed in one corner of a large reverberant room, was driven through a power amplifier by a beat-frequency oscillator. The sound pressure level from a microphone traverse was recorded with a high speed level recorder. Typical sound pressure traces are shown in Figures (6.1), (6.2) and (6.3) taken from traverses at 172, 1600 and 3700 Hz, respectively. As the frequency increases the spacing between maxima and minima of sound pressure level along the traverse decreases. This is consistent with arguments of the preceding section and reflects the fact that the acoustic wavelength is inversely proportional to frequency.

The statistical characteristics of the sound pressure levels in the room can be established by analysing the traverse recordings. The mean sound pressure level and the standard deviation of sound pressure level at a single point from the mean value was calculated by dividing the level recorder traces into 50 equal parts. The measured standard deviations are plotted vs frequency in Figure (6.4). The results are seen to be in good agreement with the theoretical even at frequencies

below the "large room" frequency.

It can be concluded from these results that pure-tone sound pressure levels can be accurately measured if a sufficiently large number of microphone readings are taken.

6.3 Spatial Variation of Room Impedance

6.3.1 Theory

The acoustic power output of a source depends on the impedance of the acoustic medium. The impedance presented by a reverberant room is determined by the volume and absorption of the room and the spectrum of the excitation. The variance of room impedance and hence power input from point sources has been investigated by Lyon (38). For a simple source radiating into a reverberant room, Lyon derives the following equation for normalised variance of radiation resistance:

$$\sigma_N^2 = {}^{27}/_{16M} \quad , \qquad (6.3)$$

where M is the modal overlap equal to the product of the modal density $n_v(f.)$ and the modal bandwidth Δ_v.

Modal density of a reverberant room is given by Morse and Ingard (18) as

$$n_v(f) = \frac{4\pi f^2 V}{c^3} \qquad (6.4)$$

The modal bandwidth is given by

$$\Delta_v = \frac{\pi f. \eta}{2} \quad , \qquad (6.5)$$

where

$$\eta = \frac{2.2}{f.T} \quad . \qquad (6.6)$$

Substituting into equation (6.3) yields

$$\sigma_N^2 = \frac{1.58 \times 10^6 \, T}{f^2 \, V} \quad , \qquad (6.7)$$

where V is the room volume in m^3.

Normalised standard deviation of sound power at a point is therefore given by

$$\sigma_N = \frac{1.256 \times 10^3}{f} \sqrt{\frac{T}{V}} \qquad (6.8)$$

From this equation it can be seen that the sound power radiated from a point source can be accurately measured with the source at a single point if the frequency is high, the volume of the room is large, and the reverberant time is short.

A plot of equation (6.8) is shown by the solid line in Figure (6.5) for the reverberant room used in this research.

The greatest contribution to the standard deviation comes from source positions near the walls. Baade (34) suggests that for points at least a quarter wavelength from the walls, the standard deviation should be only 70% of that shown in Figure (6.5). Using this assumption, the standard deviation of radiation resistance is plotted by the dashed line in Figure (6.5) for points not near a wall. This result implies that at 300 Hz, 68% of the source points not near a wall should result in measured sound power within ± 50% of the true mean value. At 1000 Hz the uncertainty is reduced to ± 13%.

6.3.2 Experimental Investigation

The theory presented in the previous section is strictly applicable to a simple source. This research is primarily concerned with transversely vibrating beams which radiate sound as an ensemble of dipole sources

(see Section 4.4.3). Intuitively, one would expect such a distribution of sources to see an average impedance of the room; especially when the length of the beam is longer than an acoustic wavelength. An experimental investigation has been conducted to test this assumption. The apparatus is shown in Figure (6.6). The beam response rig, which consists of a dexion angle frame bolted to a 300 lb. concrete base, was placed at ten different positions near the centre of the large reverberant room. At each position, the beam (5 ft. long, 1 in. dia.) was driven mechanically at three resonant frequencies and the output of a microphone traverse was recorded. From these traces the radiated sound power was calculated for each position, the mean radiation resistance was determined, and the normalised standard deviation was calculated. The results are shown in the following table:

Mode No.	FREQ.	σ_N
3	322 Hz	0.239
5	542	0.105
7	1450	0.016

These results are plotted in Figure (6.5) for comparison with the theory of the previous section. The standard deviation of the radiation resistance of the beam is seen to be lower by a factor of approximately three. A theoretical explanation for this is offered by Doak (39) who suggests that the standard deviation of the radiation resistance of a distribution of dipoles should be reduced by a factor approximately equal to the number of dipoles in the ensemble. This is consistent with the observed phenomenon.

6.3.3 Near Wall Effect

As mentioned in Chapter I, solid objects may be in the immediate proximity of a vibrating beam in some practical situations. The simplest example would be that of an adjacent plane reflecting surface. A preliminary attempt to measure this effect was made by placing the beam response rig near to one wall of the reverberation chamber. The variation in the radiation resistance of the beam, vibrating in a plane perpendicular to the wall, is shown in Figure (6.7) for comparison with the theoretical change in the radiation resistance of a point dipole with the same orientation. The results agree with theory as well as can be expected in light of the statistical problems associated with the sound field near the wall. A more precise measurement of the near wall effect would have required considerable effort since the experiment would have to be repeated at many positions around the room to account for the spatial variation of room impedance. This was not pursued as it was considered to be of secondary importance for the present research.

6.4 Summary

The sound field in a reverberant room can be assumed to be diffuse for pure-tone sound above the "large room" frequency. However, the standard deviation of sound pressure level from the mean value is approximately 5.5 dB. Therefore, many microphone readings must be used if accurate calculations of mean sound pressure are required.

Spatial variations of room impedance have also been considered. It has been shown that meaningful measurements of the sound power radiated from a vibrating beam can be made at a single source point because the beam tends to see the average impedance of the room if the length of the beam is longer than an acoustic wavelength.

A preliminary measurement of the effect of placing a vibrating beam

near a rigid wall has been made. The image source presented by the wall causes destructive interference as the beam is moved closer to the wall. This is in basic agreement with the theory of the interactions of point sources and reflecting surfaces, but more extensive experiments would be needed to produce fully reliable results.

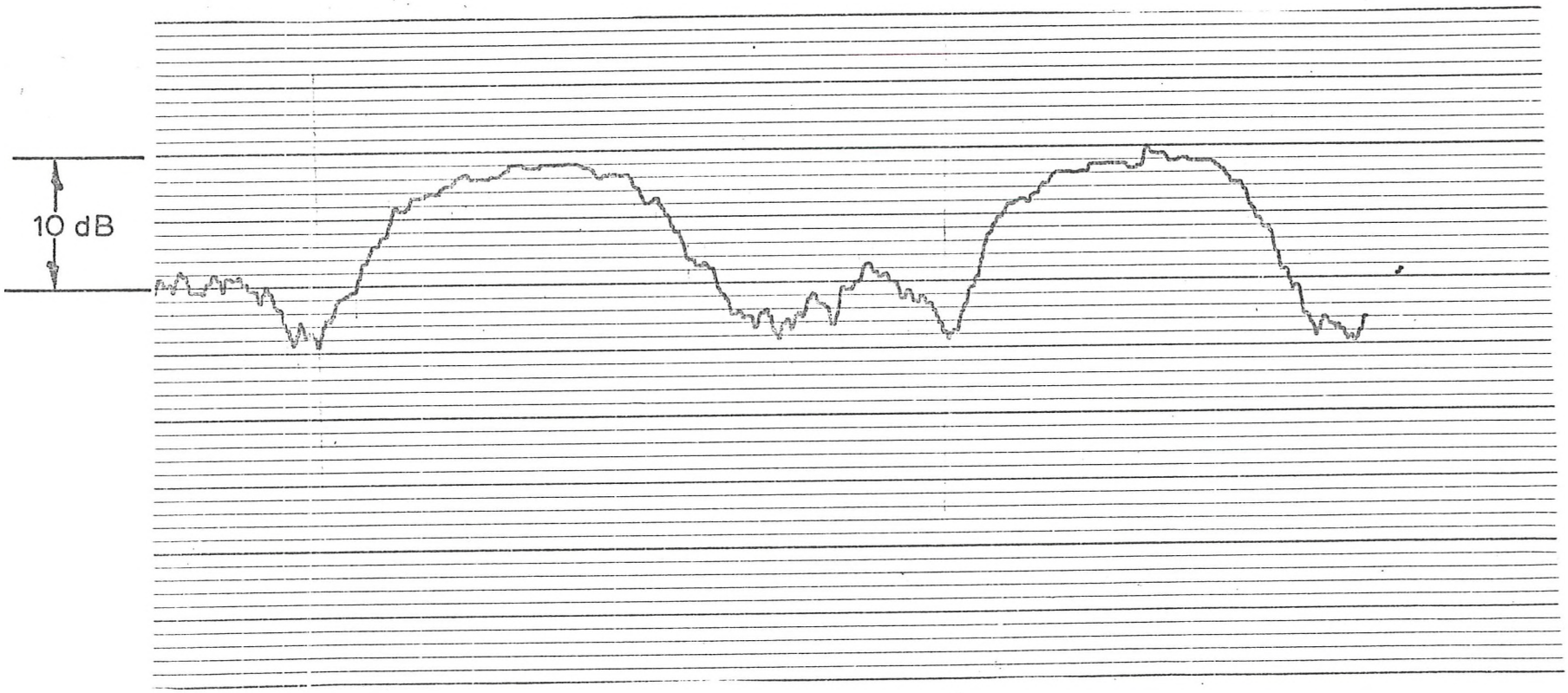

Fig. 6.1 Microphone traverse at 172 Hz.

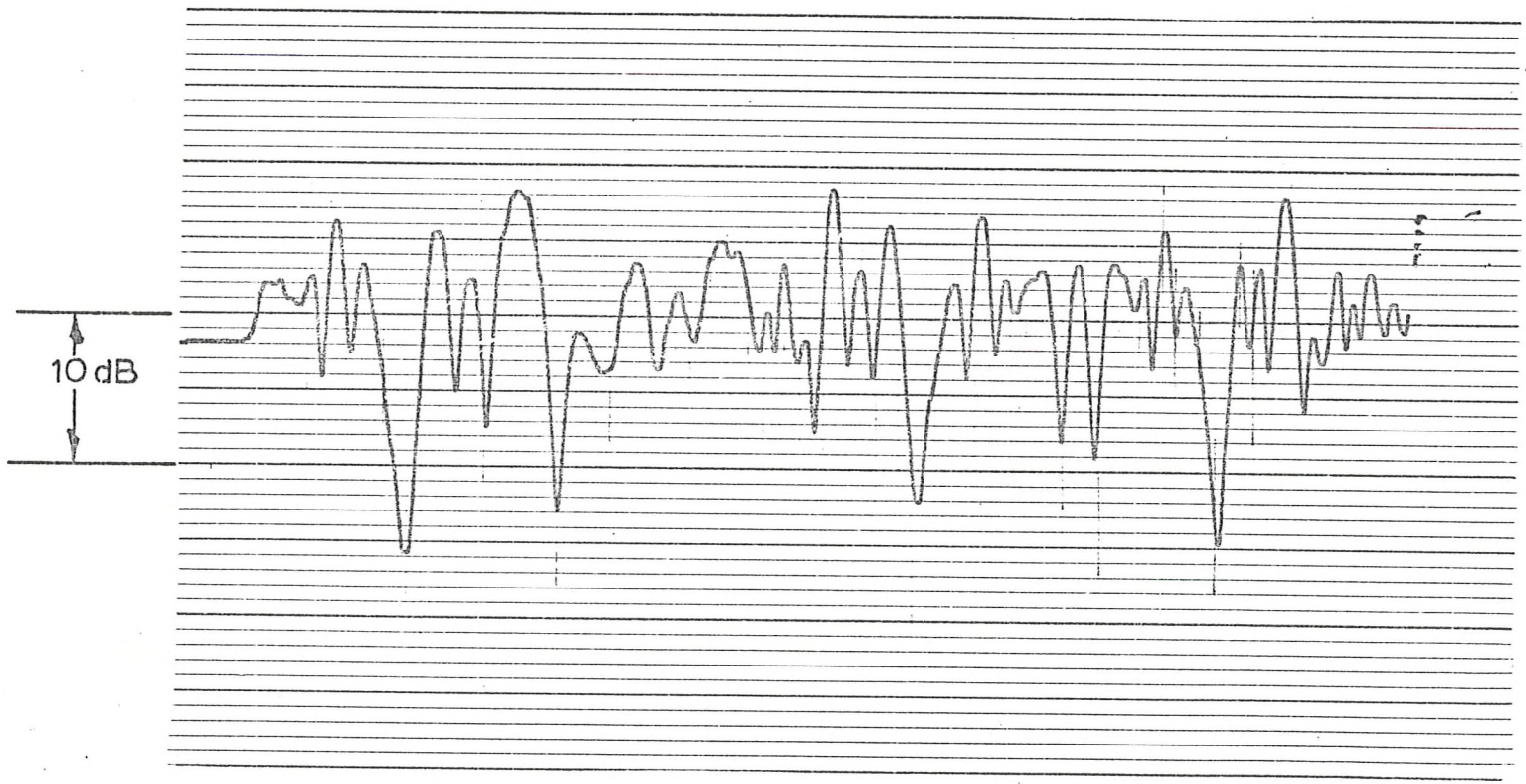

Fig. 6.2 Microphone traverse at 1600 Hz.

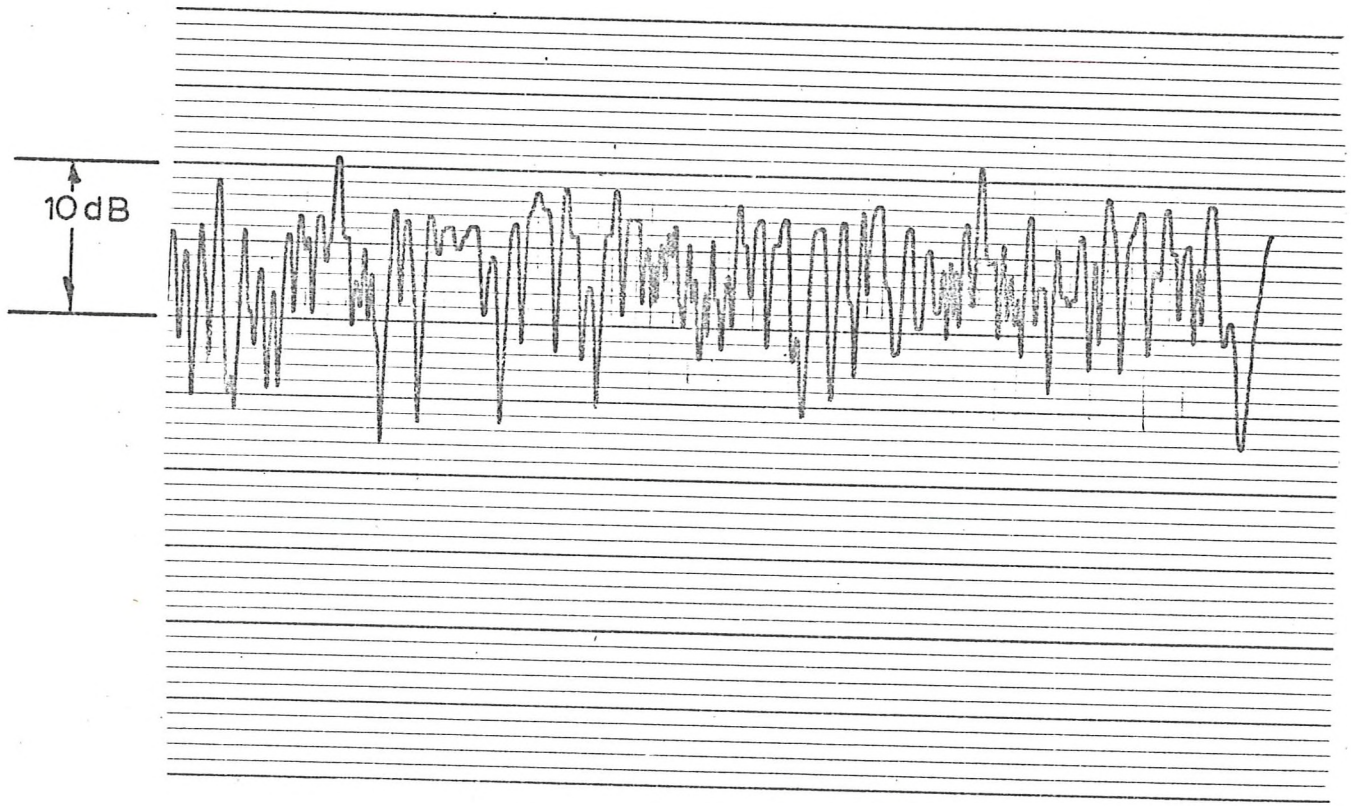

Fig. 6.3 Microphone traverse at 3700 Hz

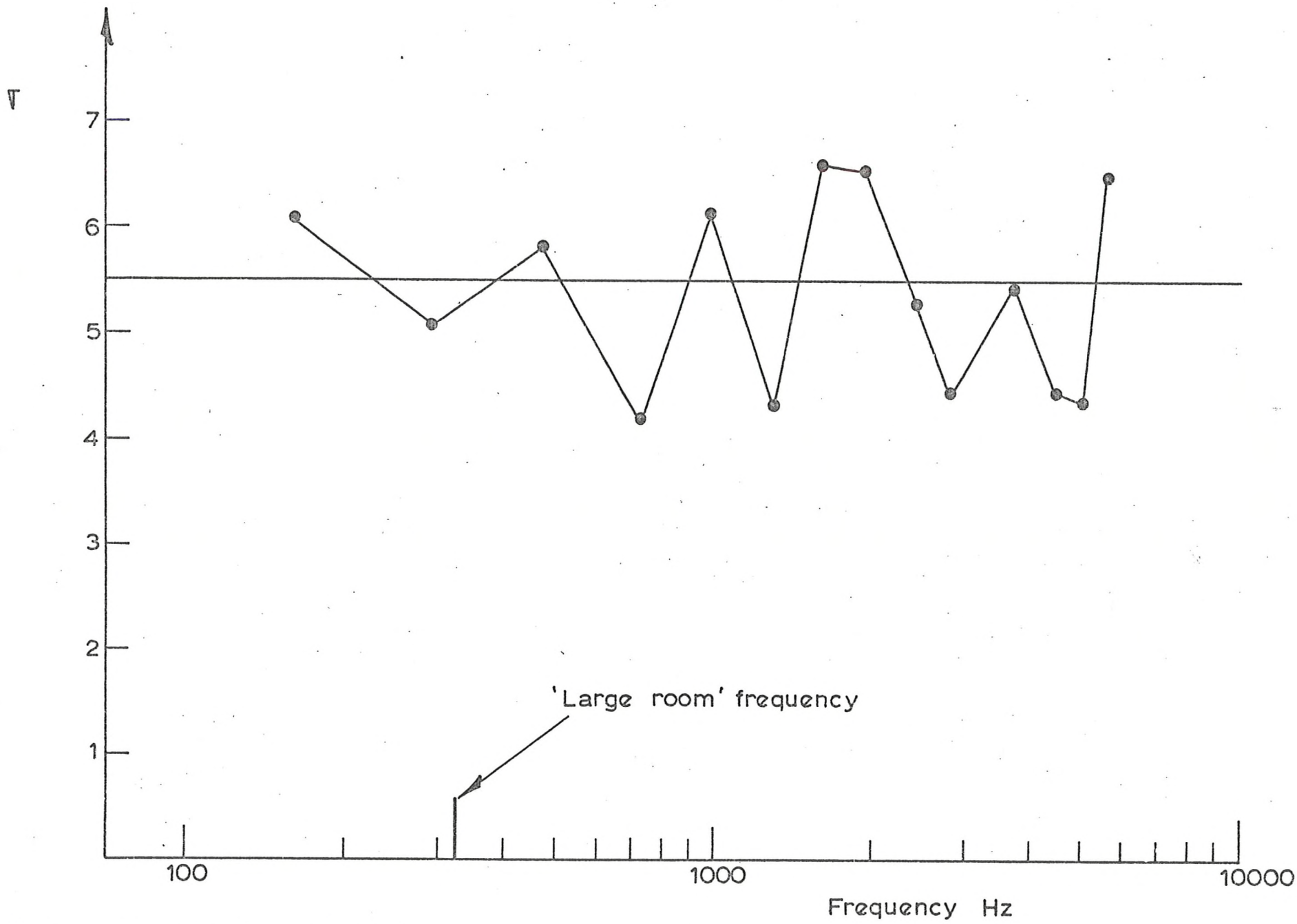

Fig. 6.4 Standard deviation of sound pressure level.

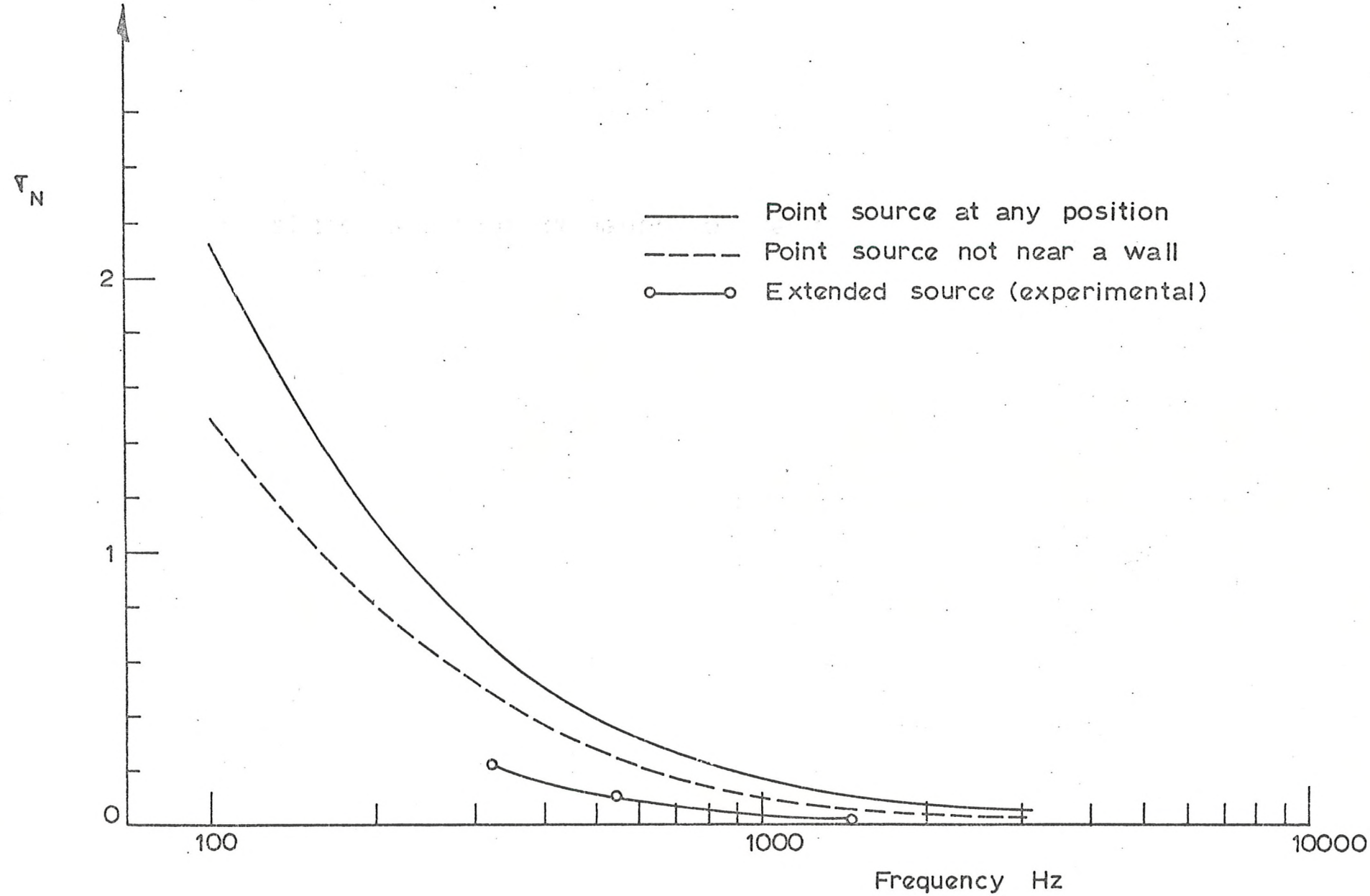

Fig. 6.5 Normalized standard deviation of radiation resistance.

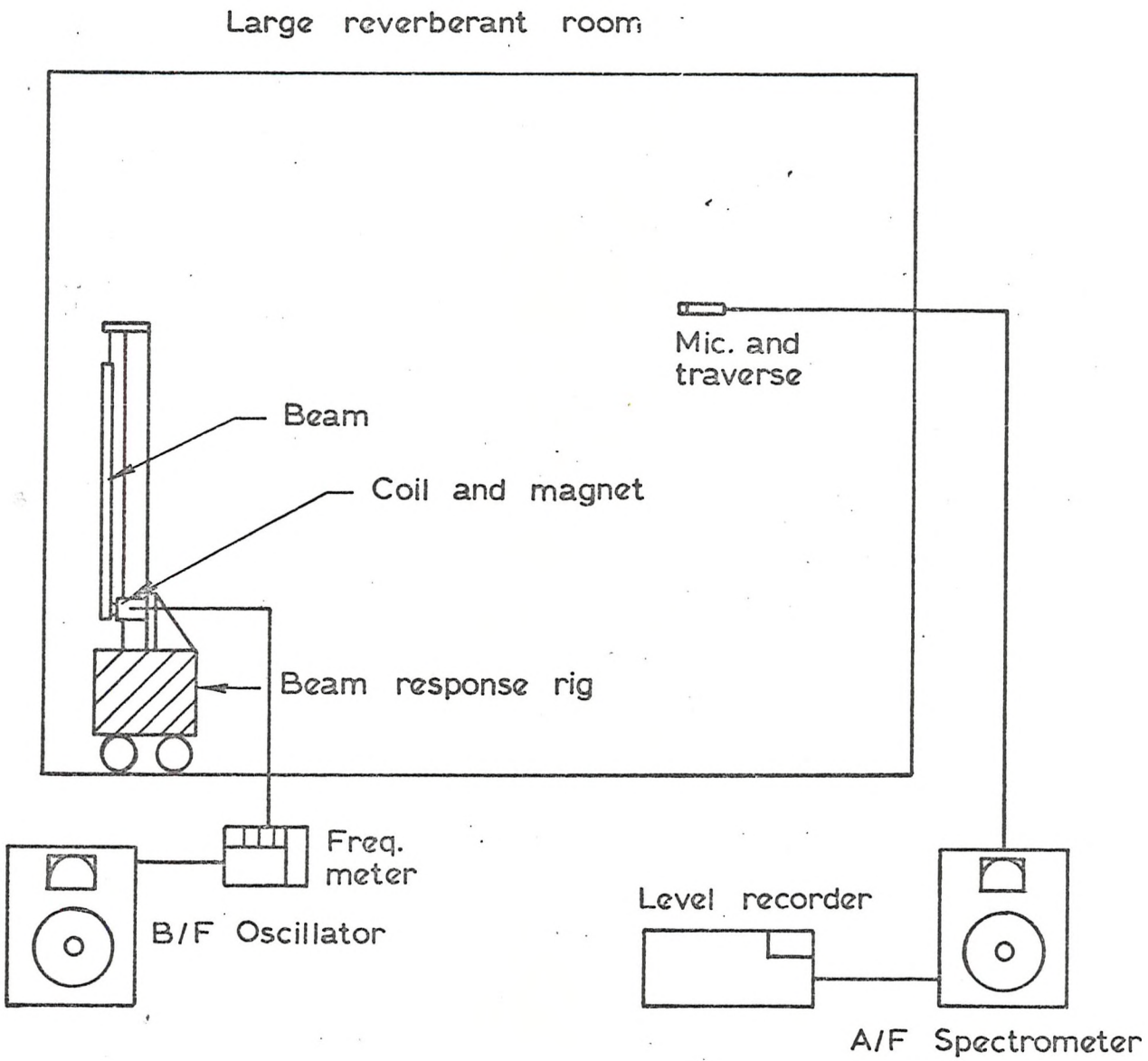

Fig.6.6 Arrangement for measuring spatial variation of room impedence.

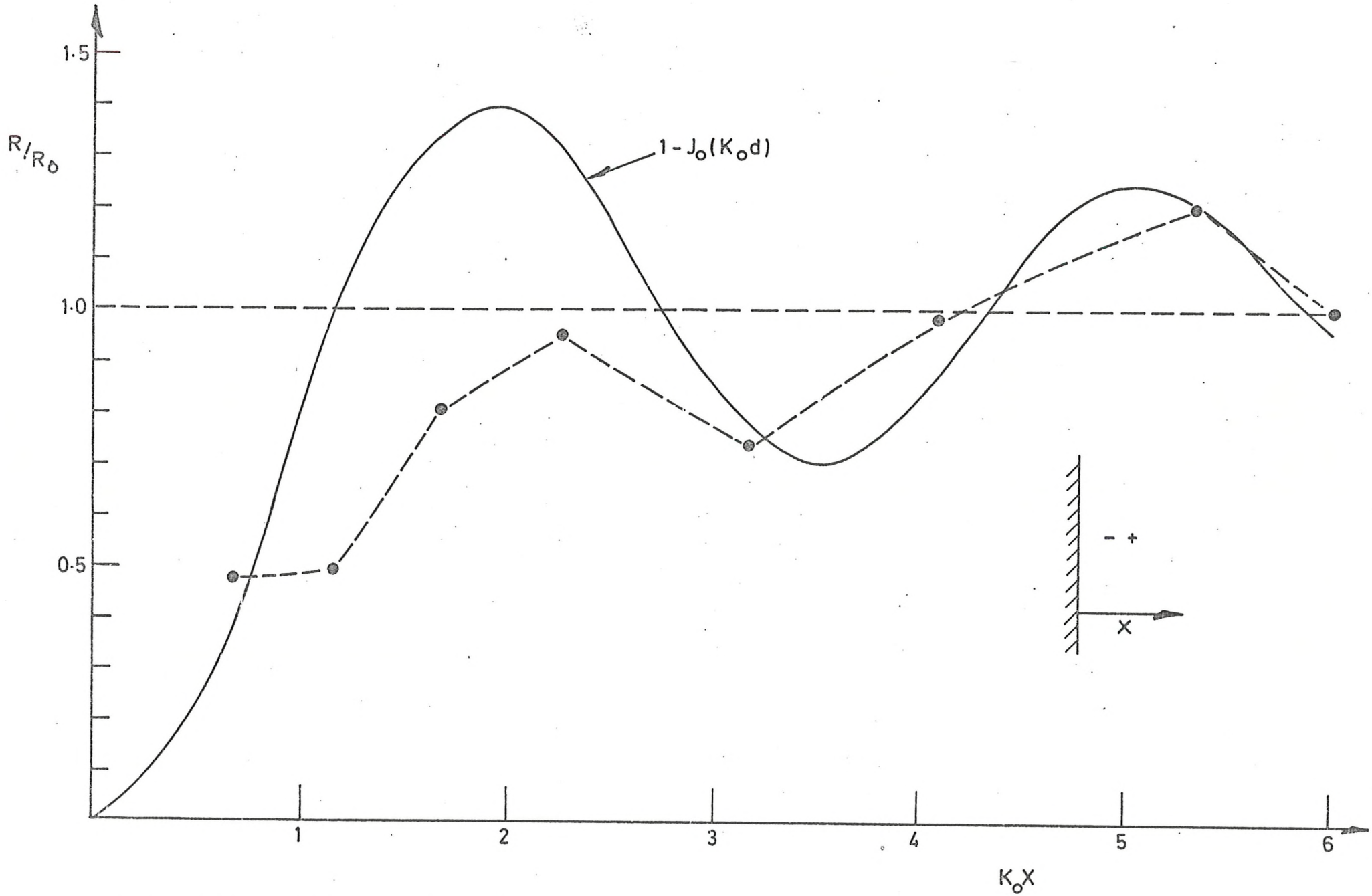

Fig. 6·7 Near wall effect.

CHAPTER VII

Experimental Programme for Measuring Radiation Loss Factor of Slender Beams

The purpose of this experimental programme was to measure the sound power radiated from resonant, transversely vibrating cylindrical beams. Three freely-suspended beams were used in the first part of this investigation to show the effects of changing various parameters. Particular consideration was given to the importance of the radius of the beam and the ratio of structural wavelength to acoustic wavelength.

A periodically supported beam was used in the second part of this study to show the importance of support spacing.

7.1 Investigations with Three-Freely-Suspended Beams

7.1.1 Description of the Apparatus

The apparatus used in this experiment is shown in Figure (7.1). The beam response rig, described in Chapter VI, was positioned near the centre of the large reverberant chamber. The rig was designed so that it would cause minimum obstruction to the acoustic near-field of the beam. It was found by experimentation that minimum distortion of the mode shapes of the beam could be achieved by suspending the beam with a wire attached to a pin through the first nodal point of the fifth transverse resonant mode. The suspension wire was made as small as possible (.012" dia.) to avoid resonant frequencies of the wire and to minimize the flow of energy between the beam and the rig.

A small coil, protruding into the field of an annular permanent magnet, was attached to the bottom end of the beam to provide a means of mechanical excitation with minimum external interference. The response of the beam was measured with three Bruel and Kjaer accelerometers. One of the

accelerometers was attached with wax to the bottom end of the beam opposite the coil. The other two were placed at the top end of the beam, one in the same plane as the coil, the other at 90^{o} rotation. The sound pressure level was measured with a one-inch Bruel and Kjaer condensor microphone mounted on a microphone traverse unit.

The specifications of the beams used in this experiment are given in the following table:

TABLE OF BEAM SPECIFICATIONS

Specification	Beam 1	Beam 2	Beam 3
Material	Copper	Aluminium	Copper
Outside Diameter	1.112 inches	1.00 inches	1.312 inches
Inside Diameter	1.016	0.75	1.00
Length	60	60	60
Elastic modulus	$18 \times 10^{6} P/in^{2}$	$10 \times 10^{6} P/in^{2}$	$18 \times 10^{6} P/in^{2}$
Density	$0.335 lbm/in^{3}$	$0.101 lbm/in^{3}$	$0.335 lbm/in^{3}$

7.1.2 Measured Results

The reverberation time of the room was measured at each frequency by switching off the loudspeaker and recording the slope of the decay in sound pressure level. A typical trace is shown in Figure (7.2).

The frequency response of each beam was measured by driving the beam with the coil and slowly sweeping the frequency of the excitation. Typical accelerometer outputs are shown in Figures (7.3) and (7.4) measured at the bottom of the beam opposite the coil and at the top end of the beam in the plane of the coil. The antiresonance effect is clearly shown in Figure (7.3) by the sharp dip in response just before each

resonant frequency. The first fifteen to twenty resonant frequencies can easily be distinguished but the higher order modes are lost because the sweep is on a logarithmic scale. By manually tuning the oscillator the first fifteen modes of each beam could be determined and all the resonant frequencies were found to be within 5% of the theoretical values. The good agreement between theoretical and experimental natural frequencies implies that the added masses of the accelerometers did not appreciably affect the mode shapes of the beam. This is as expected since the weight of each accelerometer was only two grams.

The procedure for measuring η_{rad} was to drive the beam at resonance by tuning the oscillator to a natural frequency of the beam, record the accelerometer outputs, then traverse the microphone over a distance of 15 feet continuously recording the sound pressure level in the room. The results for the three beams are plotted in Figure (7.5) with the theoretical values which are calculated by assuming that the mode shapes of the beam can be described with trigonometric functions. Of course, the mode shape of a free-free beam will also contain hyperbolic terms, but these are probably insignificant from a radiation viewpoint because wave motions are generally insensitive to details smaller than an acoustic wavelength.

It is significant that the first two modes of each beam did not radiate measurable sound to the far-field. The acoustic wavelength was longer than the total length of the beam for these cases. Hence, it is not surprising that these relatively weak multipoles did not radiate strongly (see Section (4.4.3)).

The beams used in this experiment were designed to investigate the two most important parameters in sound radiation; namely, (i) radius of the beam and (ii) ratio of structural to acoustic wavelengths. The

importance of the radius parameter alone was studied by comparing the modes of beams 2 and 3 which had the same resonant frequencies and mode shapes. The wavelength ratio parameter was investigated independently by comparing the modes of beams 1 and 2 which had the same mode shapes at different frequencies. The predicted behaviour was observed for both parameters.

7.2 Investigations with a Periodically Supported Beam

The main objective of this part of the experiment was to determine the changes in sound radiation from a slender beam when the number of periodic supports was varied. This was achieved by measuring the radiation loss factor of a beam with two, three and five simple supports.

7.2.1 Description of the Apparatus

The importance of taking the tube supports into account when assessing acoustic response has been established in previous work by Beaney & Yeh (40). In particular, it has been shown that a tube must be isolated from other structures if meaningful results are to be obtained. The support used in these experiments is shown in Figure (7.6). The base stand can be bolted rigidly to the vibration isolation pad in the large reverberation room to minimise mechanical coupling of the tube to other structures.

Tapered pins on the sides of the collar fit into hardened steel cone bearings mounted in the yoke. This leaves the beam free to rotate so that the support is essentially "simple" with zero moment and deflection at the support.

A schematic of the experimental arrangement is shown in Figure (7.7). The beam was mounted on the vibration isolation pad near the centre of

the large reverberant room. The five simple supports, positioned periodically along the beam, could be disconnected independently so that different combinations of supports could be investigated. A small coil, protruding into an annular magnet, was attached to the beam to provide a means of mechanical excitation. The response of the beam was measured with four accelerometers attached with wax to the beam, one in each span. A one-inch microphone, mounted on a traverse, was provided for measuring the sound pressure in the room. A 25 watt loudspeaker was available for acoustic excitation.

The output of the accelerometers was fed into an audio-frequency spectrometer. A four beam oscilloscope and a level recorder were also available for analysis of the results. The frequency of the excitation was measured with a digital frequency meter.

The specifications of the beam used in this experiment are given in Chapter V.

7.2.2 Natural Frequencies and Mode Shapes

Analysis of the sound radiation from vibrating beams requires some knowledge of the resonant frequencies and mode shapes. The natural frequencies of the beams used in this experiment were determined by driving the beams mechanically and tuning the oscillator until a maximum accelerometer output was obtained. The ratios of measured to calculated natural frequency are shown in Figures (7.8), (7.9), (7.10) for two, three and five supports, respectively.

The natural frequencies of several modes could not be measured because the accelerometers or the driving coils were at nodal points for those particular modes. Thus only the first, third and fifth groups of modes were considered for the case with five supports.

The experimental results are seen to be within 15% of the theoretical predictions for most of the modes. Lower experimental frequencies probably indicate that the supports are not completely rigid in the plane of vibration.

Some of the modes are repeated in all three support arrangements. For example, the fourth mode with two supports is the same as the third mode with three supports and the first mode with five supports. The measured frequency was 172 Hz for all three cases. Similarly, the 20th mode with two supports is equivalent to the 19th mode with three supports and the 17th mode with five supports. The measured frequencies of these three modes were 4003, 4008, and 3990 Hz, respectively.

For pure, resonant vibration, the mode shapes would have equal amplitude in each span. With mechanical excitation at a single point in one span, the measured results tended to have maximum amplitude in the driven span and slightly reduced amplitudes in adjacent spans. When this was observed the average amplitude was taken to be the mean of the amplitudes measured in each span. A typical example of the accelerometer outputs in each span is shown by the oscillascope traces in Figure (7.11) for the second mode of the beam with five supports. The amplitudes in each span are seen to be of the same order of magnitude for this mode with the first two spans (the upper traces) vibrating in-phase and the second two spans (the lower traces) vibrating 180° out-of-phase.

7.2.3 Measured Radiation Loss Factors

The procedure for measuring radiation loss factor is essentially the same as that used with the freely-suspended beams. Basically, this involves driving the beam mechanically at resonance, measuring the accelerometer outputs and recording the radiated sound pressure levels in the room.

The results with two supports are shown in Figure (7.12) which is a plot of radiation loss factor vs. Ka; where K is the acoustic wave-number (ω/c) and a is the radius of the beam. The theoretical curve was calculated by the computer program presented in the previous chapter. It is significant to note that the fourth mode of the beam,

occurring at 172 Hz, was the first mode to radiate measurable sound. This is as expected since below this frequency the acoustic wavelength is longer than the total length of the beam.

The support at the centre of the beam was then connected and the experiment repeated. The results are shown in Figure (7.13) for comparison with the theoretical predictions. Finally, all five supports were connected with the result shown in Figure (7.14).

The basic characteristics of sound radiation from periodically supported beams is seen to be identical with that from simply supported beams. Radiation loss factor increases with frequency to a maximum at Ka = 1. Above this frequency radiation loss factor decreases with increasing frequency. The primary difference between periodically supported beams and simply supported beams is the slope of the radiation loss factor curve at low frequencies. This is more clearly observed in Figure (4.15) which has an expanded Ka axis. The implications of this will be discussed in the next chapter which deals with resonant response to acoustic excitation.

7.3 Discussion of Results

The experimental results of this investigation largely verify the theory presented in Chapter IV. As predicted radiation loss factor increases with frequency to a maximum at Ka = 1 where the radial acoustic wavelength is equal to the circumference of the beam. Above this frequency radiation loss factor decreases with frequency.

The statistical problems discussed in Chapter VI have been encountered. With the 50 microphone positions used in these experiments, it can be shown that there is a 68% probability of measuring radiation loss factor within ±20% of the true value. Additional uncertainties are

encountered at low frequencies (see Figure (6.5)) because of the spatial variation of room impedance. Hence, it is not surprising that individual measured results differ from the theory by as much as a factor of two.

The theoretical predictions of radiation loss factor for the periodically supported beam are based on the assumption that sound radiation is dominated by the longest wavelength component of the velocity distribution. This assumption has been verified; again demonstrating the basic principle that wave motions are insensitive to small details.

Measurable sound pressure was not radiated by any mode when the acoustic wavelength was longer than the total length of the beam. This evidence supports the theory of Chapter IV which suggests that these modes should be relatively weak multipole radiators.

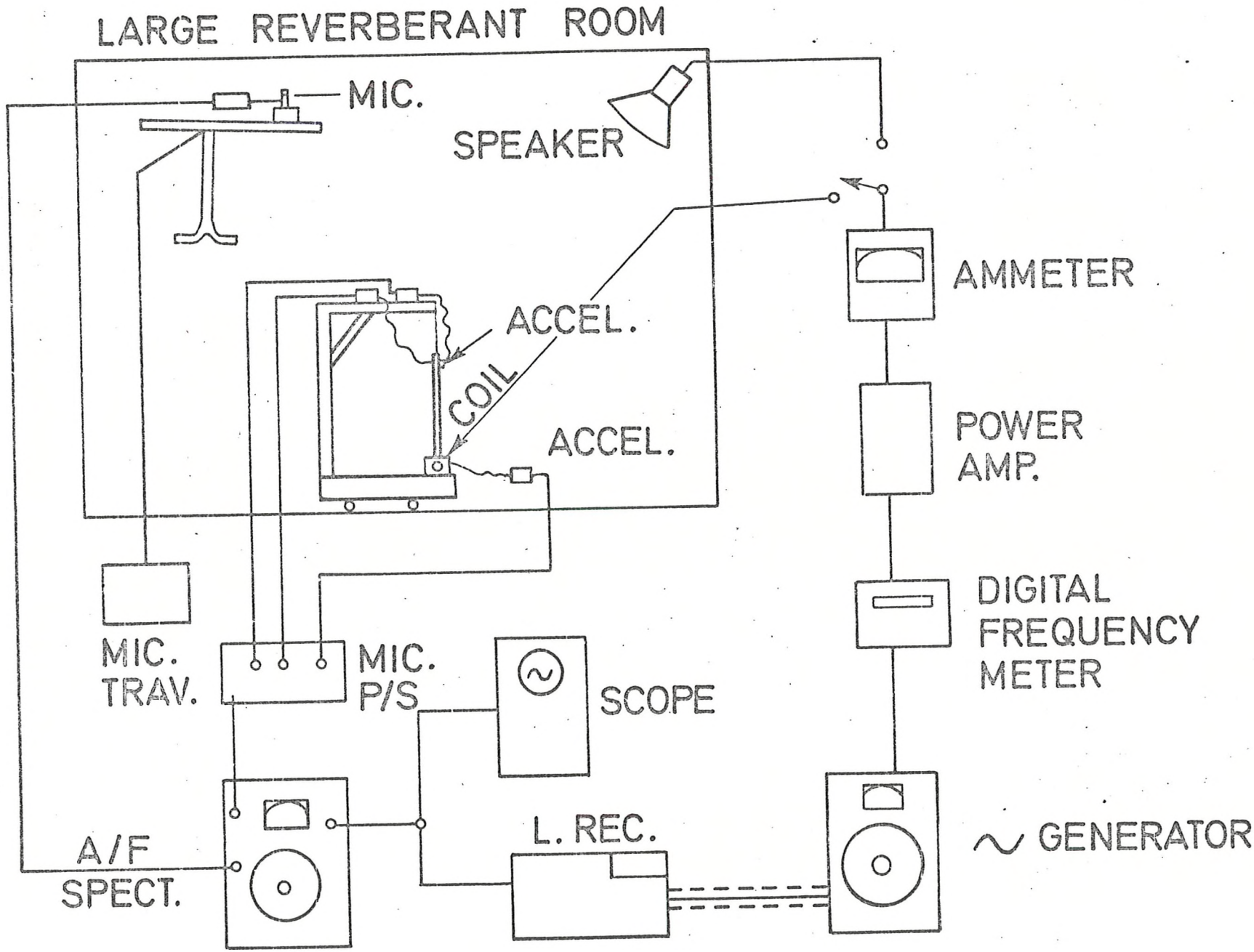

Fig. 7.1 The experimental apparatus.

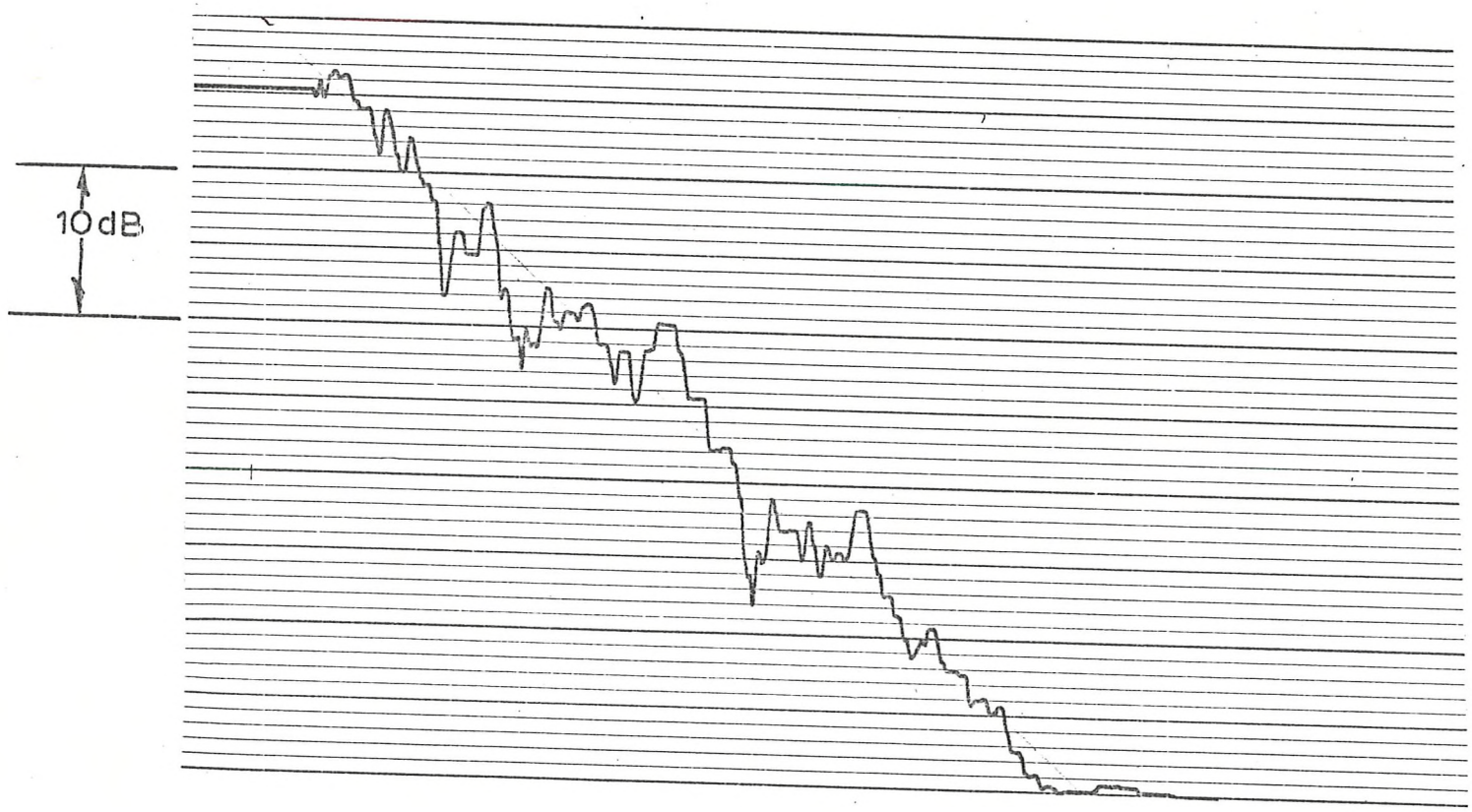

Fig. 7.2 Reverberation time decay trace.

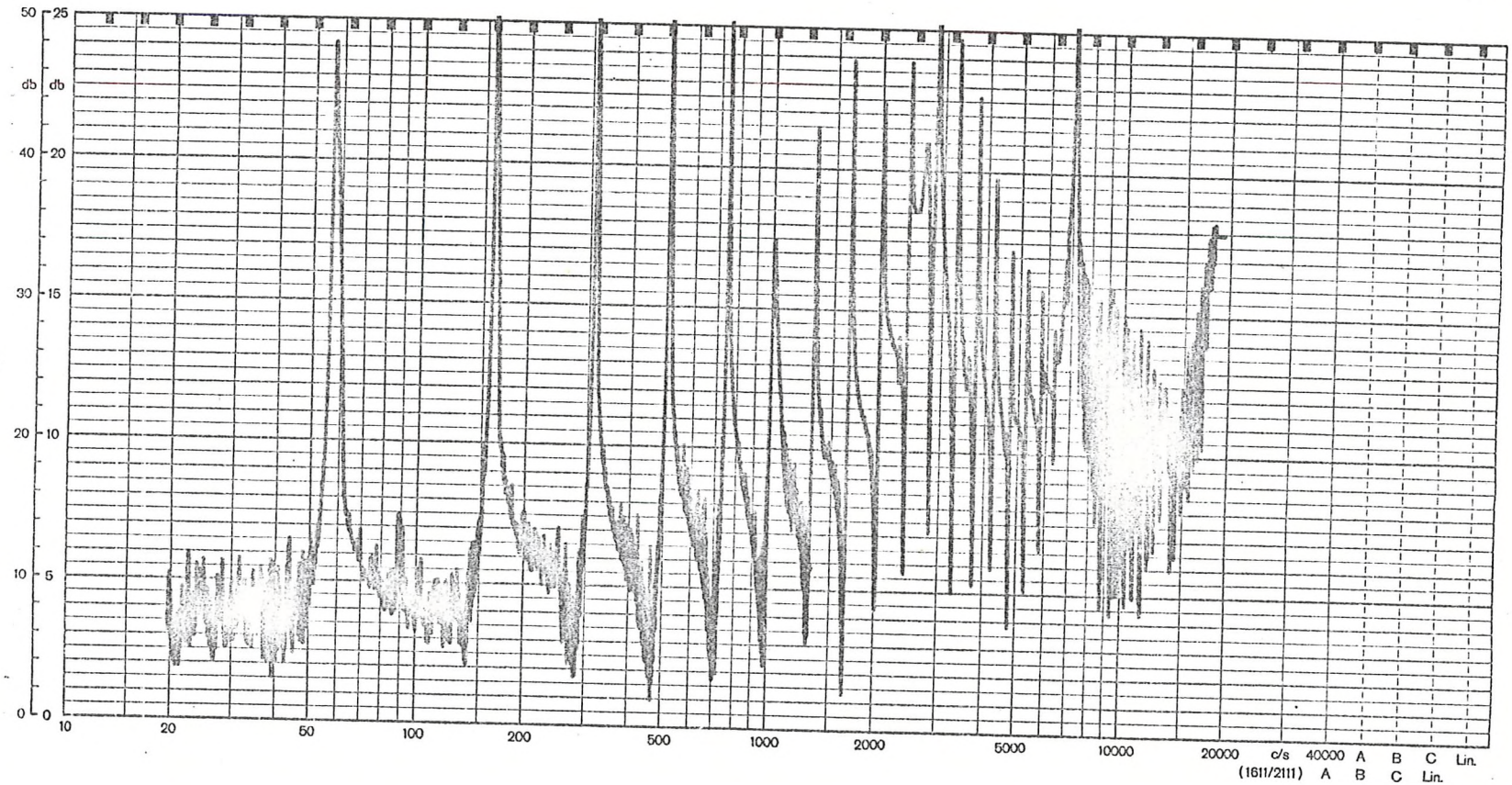

Fig. 7.3 Frequency response of beam III measured at the bottom opposite the coil.

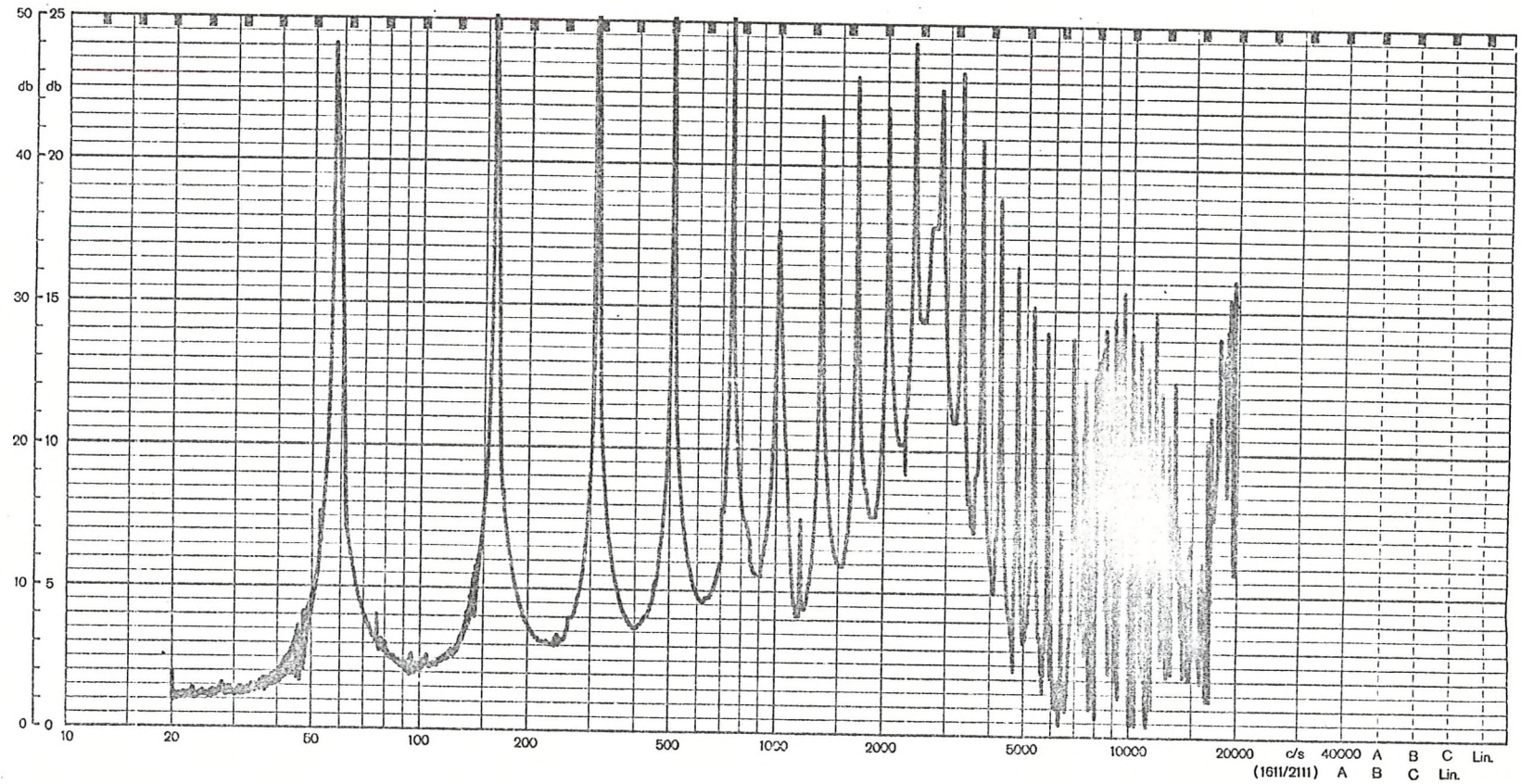

Fig. 7.4 Frequency response of beam III measured at the top end of the beam in plane with the coil.

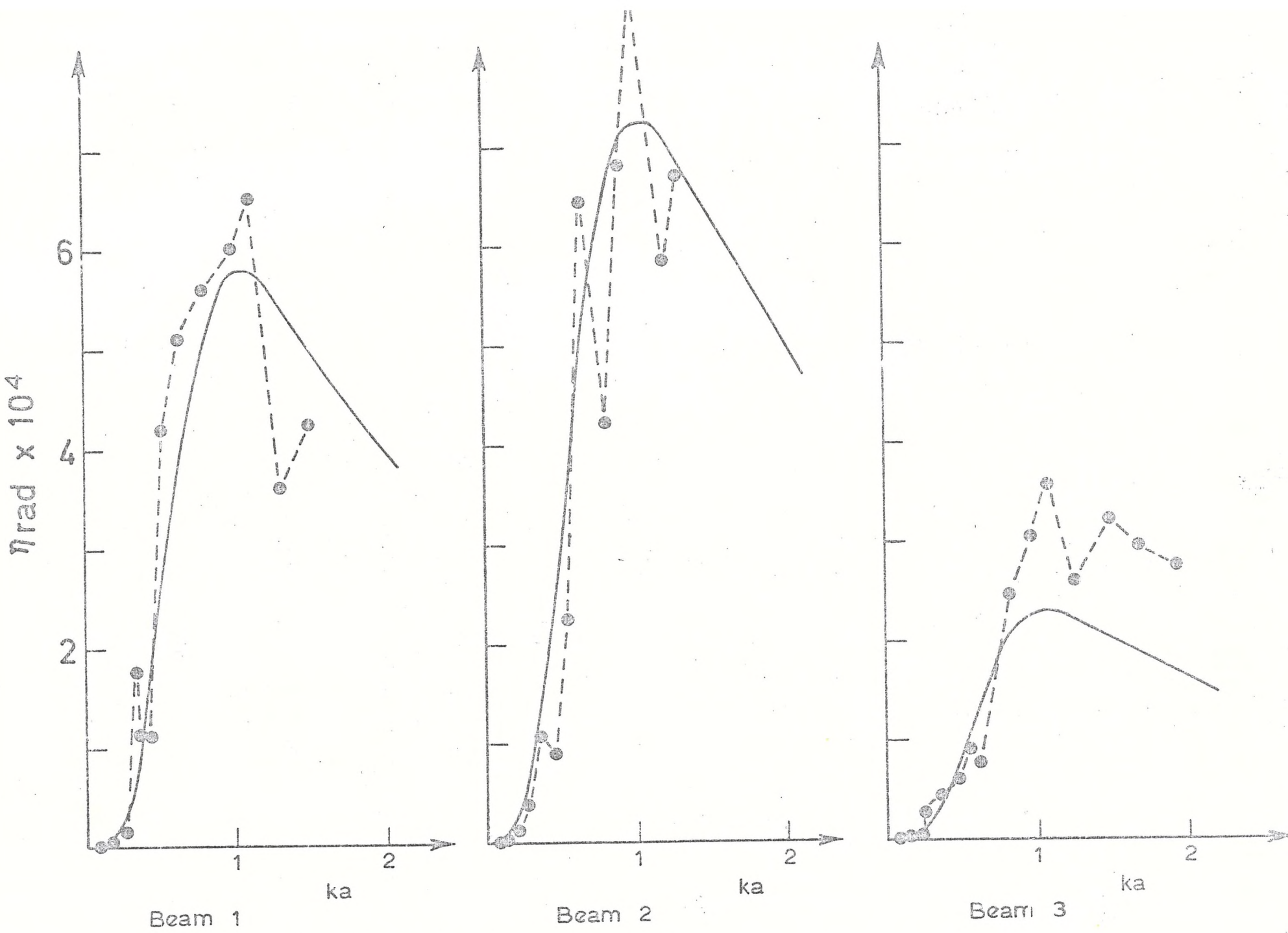

Fig. 7.5 Measured η_{rad}.

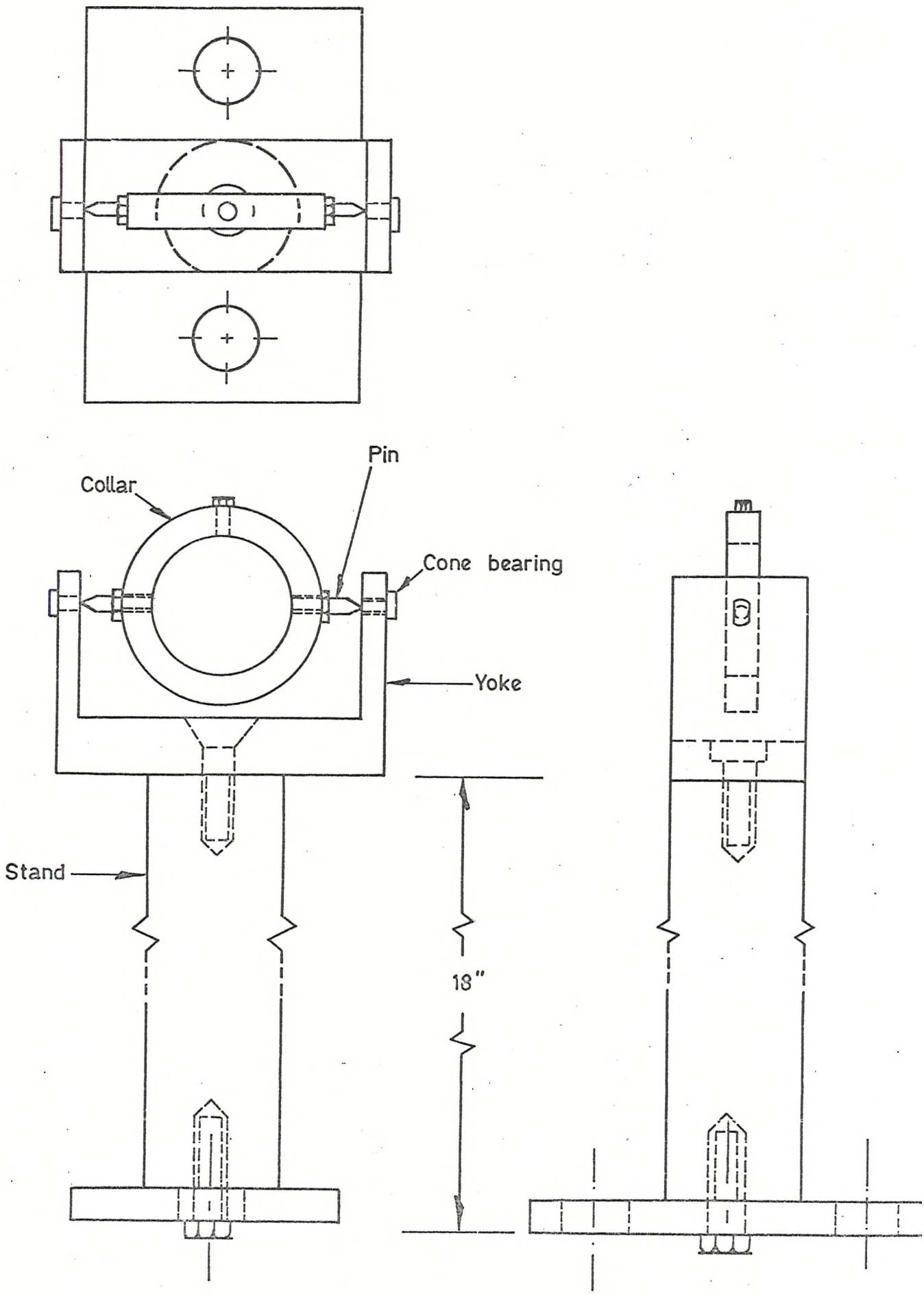

Fig. 7.6 Full scale drawing of simple support.

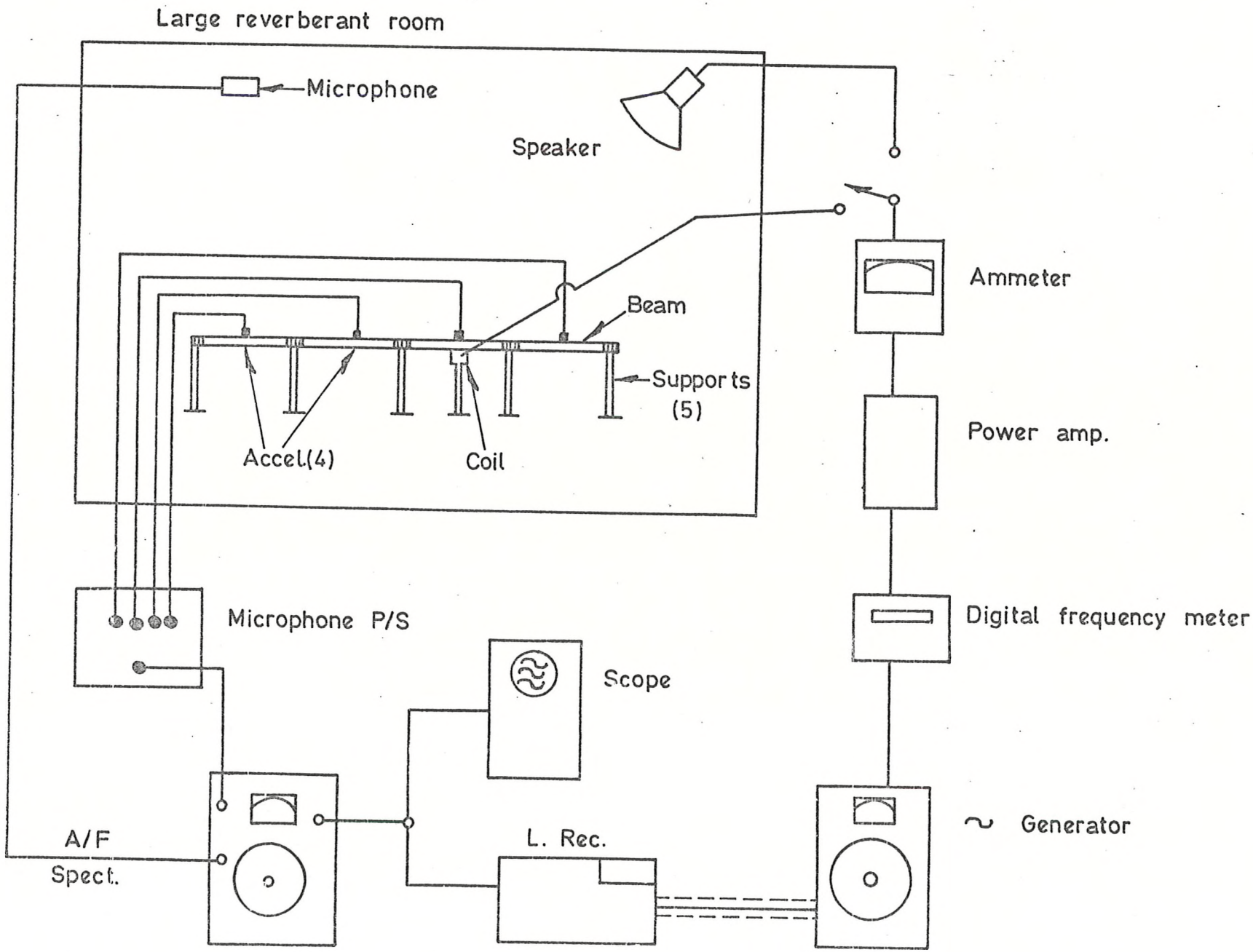

Fig.7.7 Experimental arrangement for periodically supported beam.

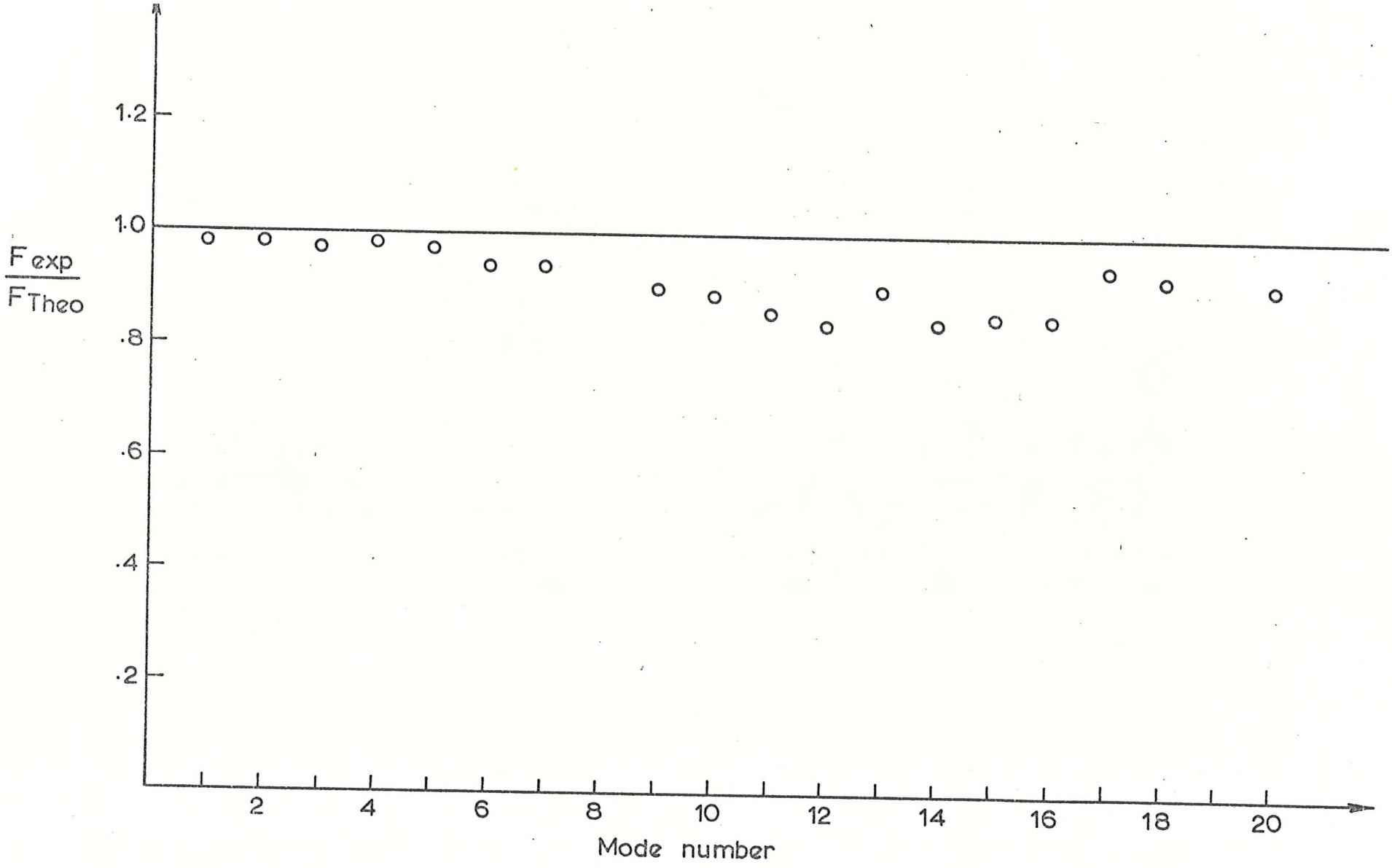

Fig. 7.8 Ratio of experimental to theoretical natural frequency with two supports

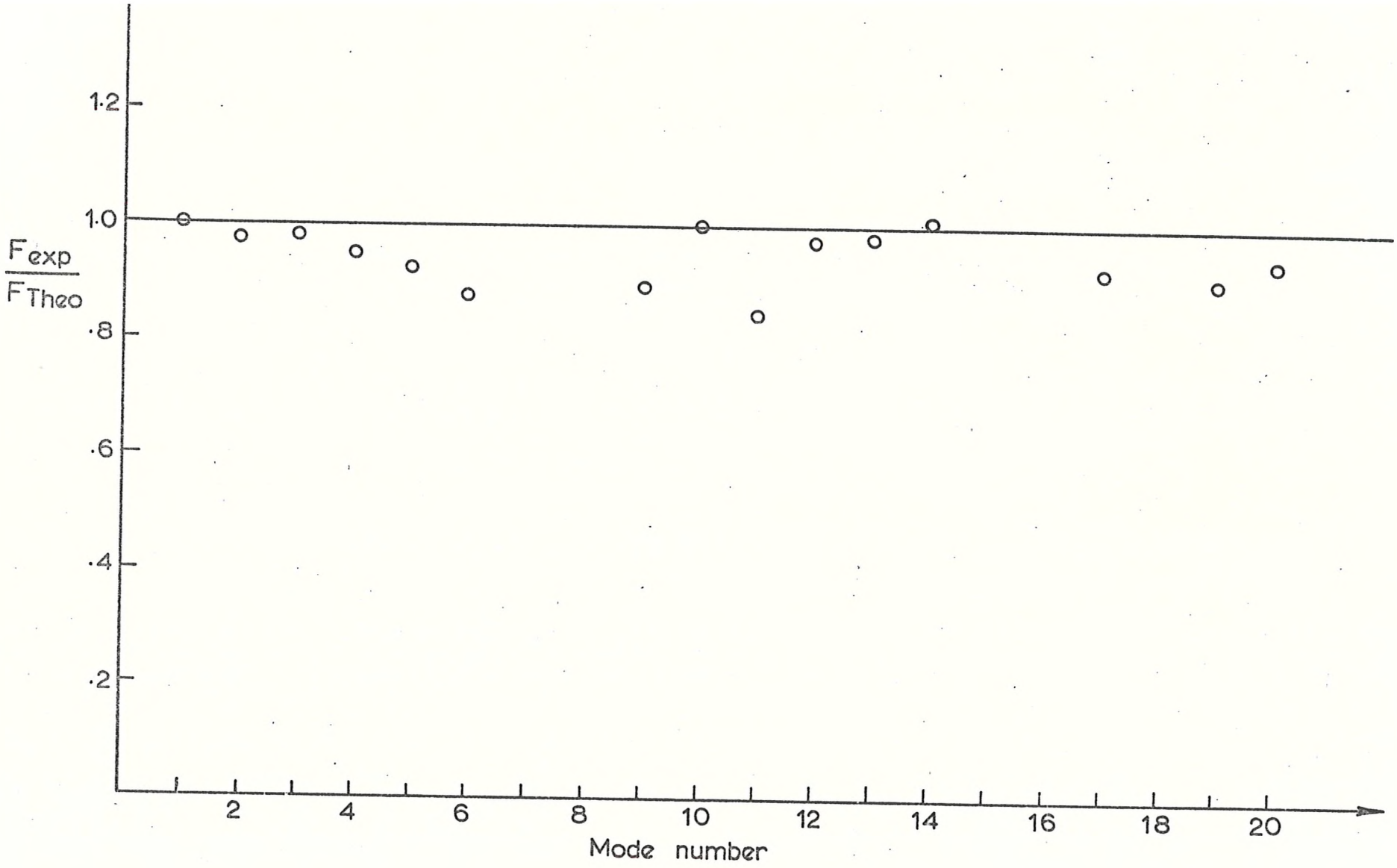

Fig. 7.9 Ratio of experimental to theoretical natural frequency with three supports

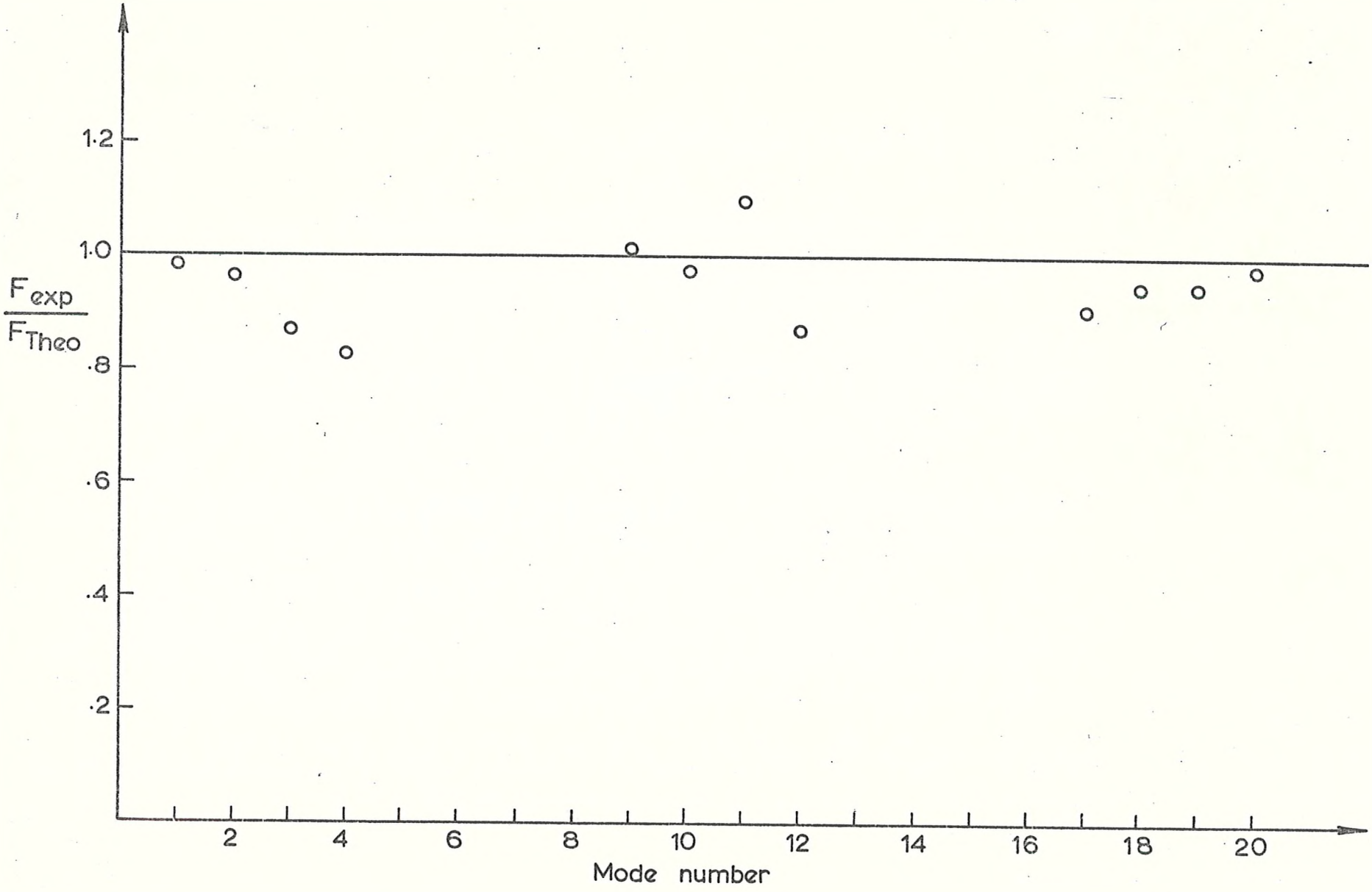

Fig. 7.10 Ratio of experimental to theorectical natural frequency with five supports

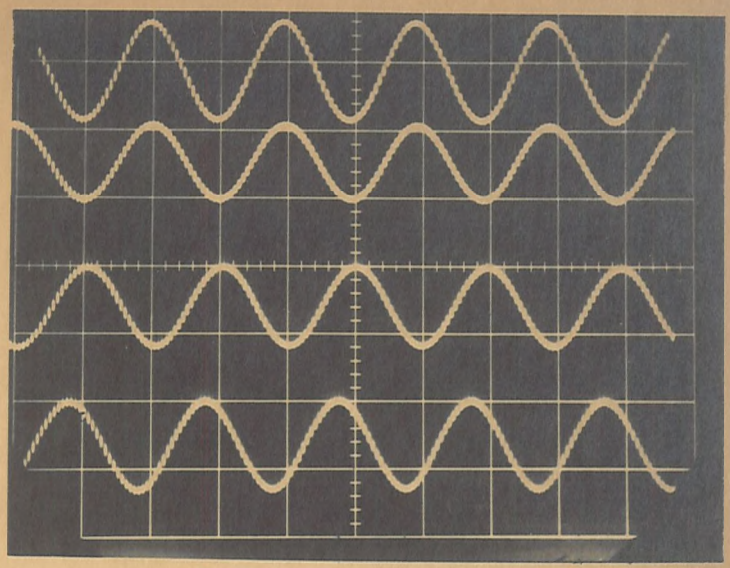

Fig. 7.11 Typical accelerometer outputs in each span.

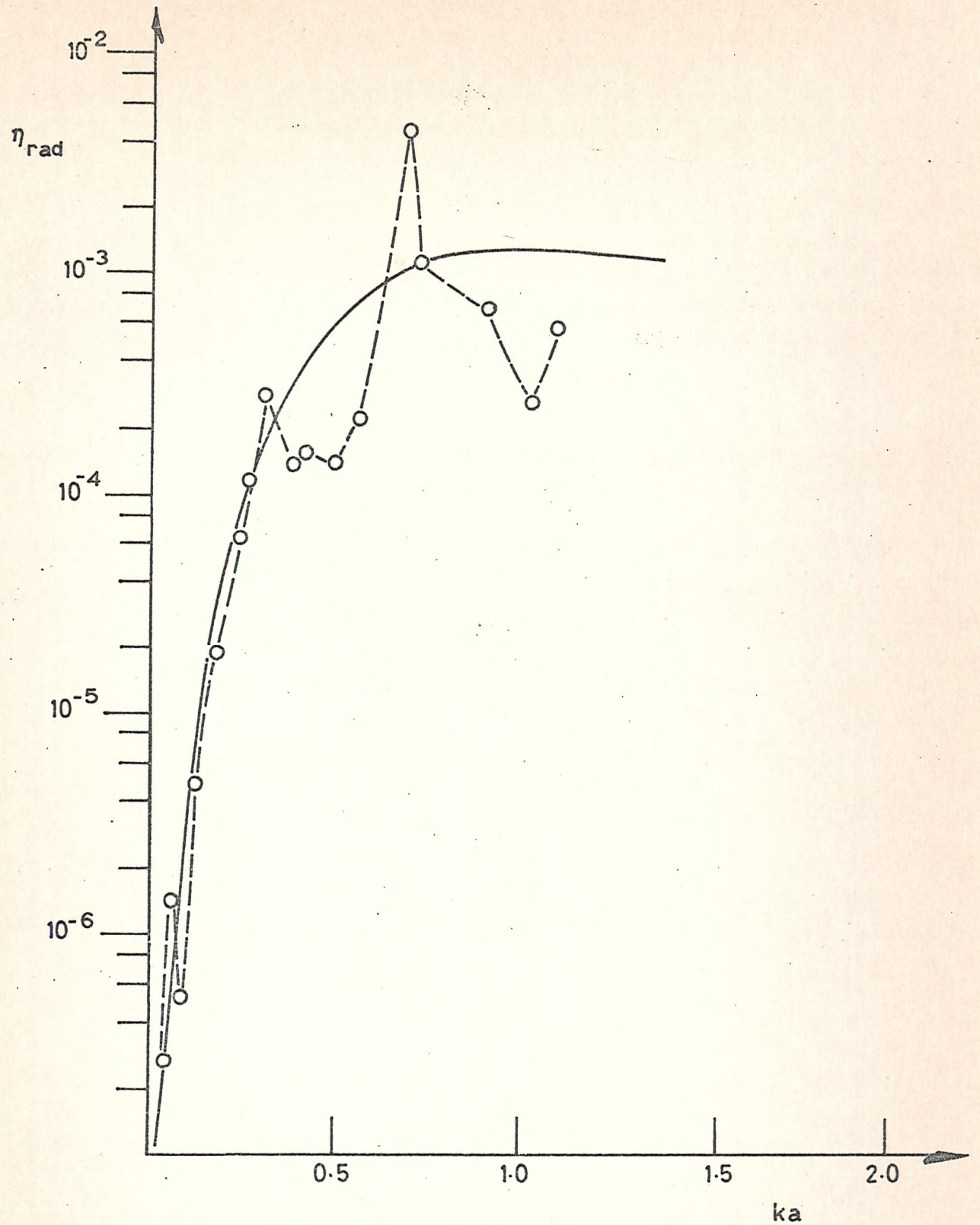

Fig.7.12 Radiation loss factor - 2 supports.

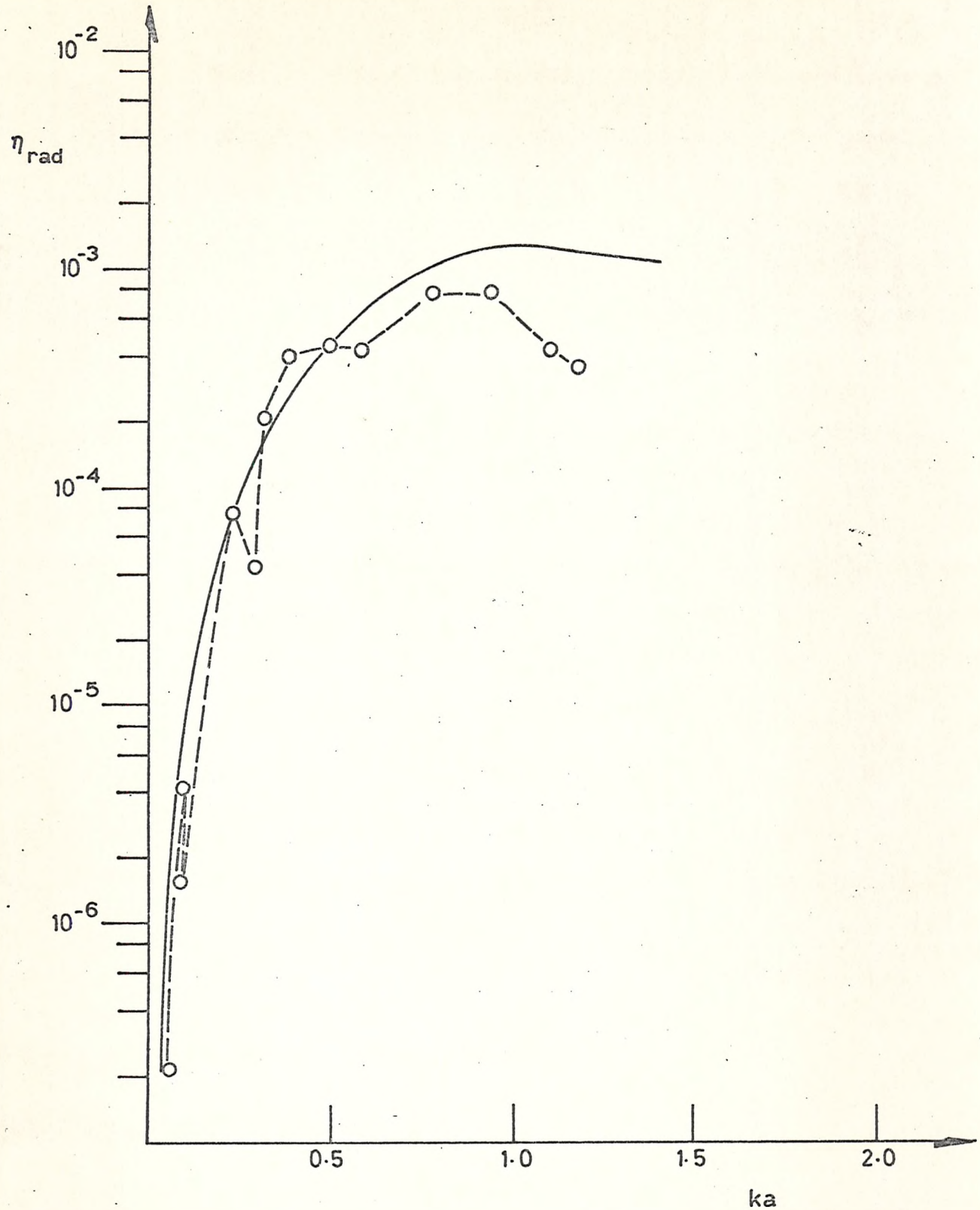

Fig. 7·13 Radiation loss factor - 3 supports.

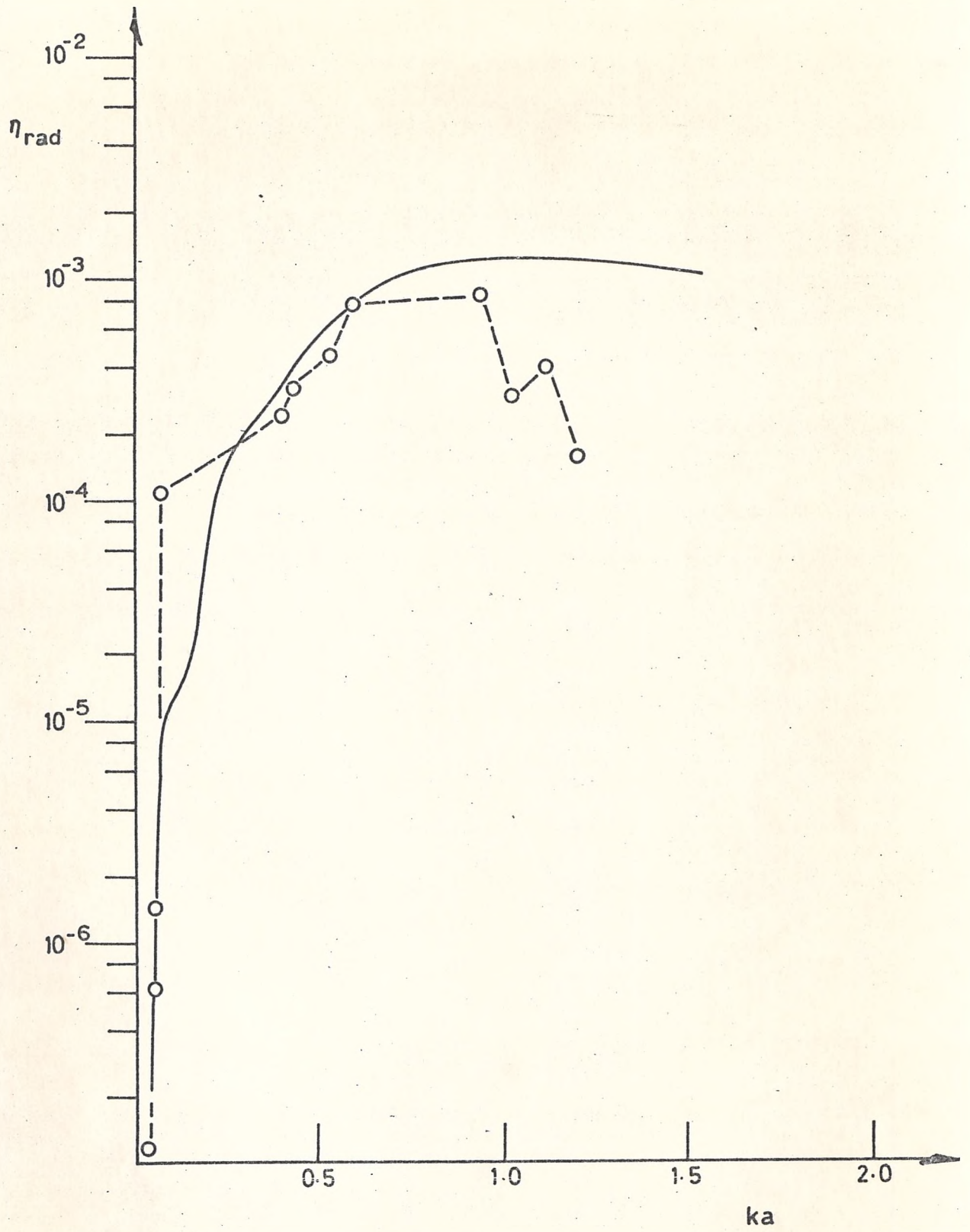

Fig 7.14 Radiation loss factor - 5 supports.

CHAPTER VIII

EXPERIMENTAL PROGRAMME FOR MEASURING THE RESONANT RESPONSE OF CYLINDRICAL BEAMS TO ACOUSTIC EXCITATION

Four experimental investigations are reported in the following chapter. The first experiment is concerned with measuring wavelength coincidence effects and polar directivity in a large anechoic room. The second study, conducted in a large reverberant room, deals with the resonant response of three freely-suspended beams to pure-tone acoustic excitation. The third experiment is directed toward measuring the response of a periodically supported beam to pure-tone sound and the fourth investigation is concerned with the acoustic response of a freely-suspended circular ring.

8.1 Anechoic Room Investigations

An attempt was made in Chapter IV to model a transversely vibrating beam as a line of coupled acoustic dipoles. One way to verify this theory would be to determine the acoustic directivity pattern by measuring the sound pressure radiated from a vibrating beam in an anechoic room. Since radiation and response are directly related by reciprocity, an equally good method of determining directivity is to measure the response of the beam to sound incident from a single direction. This approach was chosen because it requires considerably less effort.

8.1.2 Wavelength Coincidence Effects

The experimental arrangement for measuring wavelength coincidence effects is shown in Figure (8.1). The simply supported beam used in Chapter VII was mounted near one end of a large anechoic room. A 100 watt unbaffled loudspeaker was suspended from the ceiling so that it could be raised and lowered to vary the angle of incidence of the acoustic wave-

fronts with the beam. A microphone was positioned near the centre of the beam. The output of this microphone was fed into the compressor circuit of a beat frequency oscillator which was set to maintain a sound pressure level of 94 dB at the centre of the beam. The response of the beam was measured with four accelerometers equally spaced along the beam. With the speaker at nine different positions from zero to 90°, the outputs of the accelerometers were recorded as the frequency of the excitation from the oscillator was automatically swept from 150 to 3000 Hz. Typical results are shown in Figure (8.2) and (8.3) for zero and 35° angles of incidence. Directivity patterns were calculated by comparing the amplitudes of these recorded traces. The results for the sixth, seventh, ninth and tenth modes are plotted on a linear scale in Figures (8.4) through (8.7) for comparison with the theoretical patterns.

The sixth mode is particularly interesting because the acoustic wavelength is almost as long as the structural. The equivalent acoustic source model is a multipole radiator with each half wavelength of the beam acting as a dipole source. The dipoles are coupled together, resulting in destructive interference at certain angles. The measured results are in reasonably good agreement with theory, especially with regard to the major lobe in the directivity pattern. Unfortunately, measurements could not be made for angles from 60° to 90° because of physical limitations in positioning the speaker. The relatively large response at grazing incidence for this mode is probably due to ground effects since the acoustic wavelength is of the same order of magnitude as the depth of the absorbing wedges covering the floor of the anechoic room.

The seventh, ninth and tenth modes are supercritical with structural wavelength longer than the acoustic wavelength. Maximum response for each case occurs when the acoustic trace wavelength is equal to the structural wavelength.

Lower order modes were also excited in this experiment. However, the results are subject to uncertainty because the speaker could not be placed far enough from the beam to ensure a plane wavefront at the beam.

8.1.2 Polar Directivity

Sound pressure radiated from a beam vibrating in a plane is theoretically proportional to the cos θ, where $\theta = 0$ denotes the plane of vibration. The procedure used to measure this polar directivity is identical with that used the previous section. Results are shown in Figure (8.8) for comparison with cos θ.

Poorest agreement with theory is observed for the fourth mode. This is not surprising because the assumption of a plane wave for this low frequency mode would be doubtful. The sixth and ninth modes give considerably better agreement with theory. Again, the response for $\theta = 90^{\circ}$ is probably because of reflections from the floor of the anechoic room which would result in a net force on the beam.

8.2 Reverberant Room Experiments

8.2.1 Three Freely-Suspended Beams

The radiation loss factors of three freely-suspended beams were measured in ChapterVII. The resonant response of the beams to pure-tone sound in a reverberant room was also measured. The results are reported in the following section.

The apparatus used in this experiment is that shown in Figure (7.1) with the excitation provided by the loudspeaker. Typical frequency response traces are shown in Figures (8.9) and (8.10). It is interesting to compare these plots with Figures (7.3) and (7.4) which record the outputs of the same accelerometers with mechanical excitation. The first two modes are not excited acoustically. This is as expected since these modes did not radiate measurable sound.

Detailed analysis of the individual modes requires consideration of the total damping of the system. The main sources of damping are coulomb damping associated with the motion of the suspension wire, hysteresis damping due to the bending of the beam, and radiation damping. The total damping loss factor was measured by two methods. For the lower order modes it was found that the best method was to measure the decay of amplitude with the level recorder. A typical decay trace is shown in Figure (8.11). This plot is slightly concave up which implies that the damping is fundamentally viscous in nature with a slight dependance on amplitude. The damping of the higher order modes was measured by the half-power bandwidth or 3 dB-down method. The measured η_{TOT} ranged from 3.0×10^{-4} to 5.0×10^{-3}.

The procedure for measuring the response of the individual modes of the beam was to tune the oscillator to a resonant frequency of the beam with the excitation being provided by the coil; then switch the excitation to the loudspeaker thus ensuring that the speaker was tuned to the peak of the frequency response for that mode. Then the accelerometer outputs were recorded and the microphone was traversed to obtain an average sound pressure. The results are shown in Figure (8.12). Individual values are seen to differ from the theoretical by as much as a factor of two; but this is not unexpected since the experimental results depend on accurately measuring response, damping, and sound pressure level. Errors in accurately measuring the sound pressure level alone could result in scatter of 20% and it is extremely difficult to accurately measure the damping of a highly resonant structure. The degree of correspondence between the theoretical and experimental trends of frequency dependency is considered to be adequate to confirm the relationship between response and radiation which forms the basis of the response theory.

8.2.2 Periodically Supported Beams

The arrangement for measuring the resonant response of the periodically supported beam is shown in Figure (7.7) with the excitation supplied by the loudspeaker. Total damping loss factors, measured by the methods of the previous section, ranged from 5.0×10^{-4} to 1.0×10^{-2}. In general the lower frequency modes were more lightly damped. Part of the increased damping of the higher frequency modes is, of course, due to increased acoustic damping. The remainder is probably due to increased frictional losses at the supports.

Response to pure-tone acoustic excitation was measured by the procedure of the preceding section.

$< \bar{v} >$, the root mean square velocity averaged with respect to time and space, was calculated from the acceleration outputs by using the tables given in Bishop and Johnson (27). $< \bar{p} >$, the root mean square sound pressure averaged with respect to time and space, was calculated from the sound pressure levels recorded by the microphone transverse.

Measured results are plotted in Figures (8.13), (8.14) and (8.15) for two, three and five supports, respectively. In these Figures $< \bar{v} >$ is in ft/sec, $< \bar{p} >$ is in μ bars, and η_{TOT} is the measured total damping loss factor. The theoretical curves in these figures were calculated by the computer program listed in Chapter (V). Individual measured points differ from the theoretical by as much as a factor of 3. However, the degree of correspondence is adequate to justify the assumption of an effective structural wavelength, which is the main concern of this study.

As expected, only those modes which radiate sound could be excited acoustically. For the case with two supports the first mode to be excited acoustically was the fourth mode occurring at 172 Hz. The fundamental mode at 10 Hz and the second and third modes at 44 and 98 Hz could

not be excited acoustically. Obviously, the fundamental mode lies in the infrasound region. For the second and third modes, the acoustic wavelength is longer than the total length of the beam. These two modes are basically weak, multipole radiators with low acoustic coupling. With the standard loudspeaker used in these experiments, it was impossible to generate sound levels high enough to excite these modes.

8.2.3 A Freely-Suspended Circular Ring

This research has been mainly concerned with straight beams. There is considerable practical interest in the acoustic response of curved beams. For example, the boiler tubes in present nuclear power stations are wound in a helix about a solid central core. Intuitively, a section of a boiler tube having a relatively long radius of curvature and a structural wavelength longer than the acoustic wavelength should exhibit the same acoustic response characteristics as an equivalent straight beam.

A simple experiment was devised to test this hypothesis. A steel tube, having the same external dimensions as the periodically supported beam, was bent into a circular ring with the ends welded together. The ring, freely-suspended by a small wire, was excited with pure-tone sound in the reverberant room. The response of the ring was measured with two accelerometers attached with wax in the plane of curvature and two attached at 90° to the plane of curvature. Typical examples of response as the frequency was swept from 200 to 5000 Hz are shown in Figures (8.16) and (8.17). The general trend of acceleration response is seen to be similar to that of straight beams with response increasing with frequency to a maximum value and then decreasing.

From these results it can be concluded that the acoustic response of a curved beam would be very similar to that of the equivalent straight beam; especially at higher frequencies where the radius of curvature and the structural wavelength are longer than the acoustic wavelength.

8.3 Summary

Measured directivity patterns are in basic agreement with the theory derived in Chapter IV. These results confirm the multipole nature of sound radiation from transversely vibrating beams and demonstrate the principle of reciprocity which suggests that a structure which radiates strongly in one direction will also respond strongly to acoustic excitation from that direction.

Good agreement with theory has also been obtained in measuring the resonant response of freely-suspended and periodically supported beams to pure tone acoustic excitation in a reverberant, diffuse sound field.

Finally, experimental evidence has been presented to show that the response behaviour of curved beams is similar to that of straight beams.

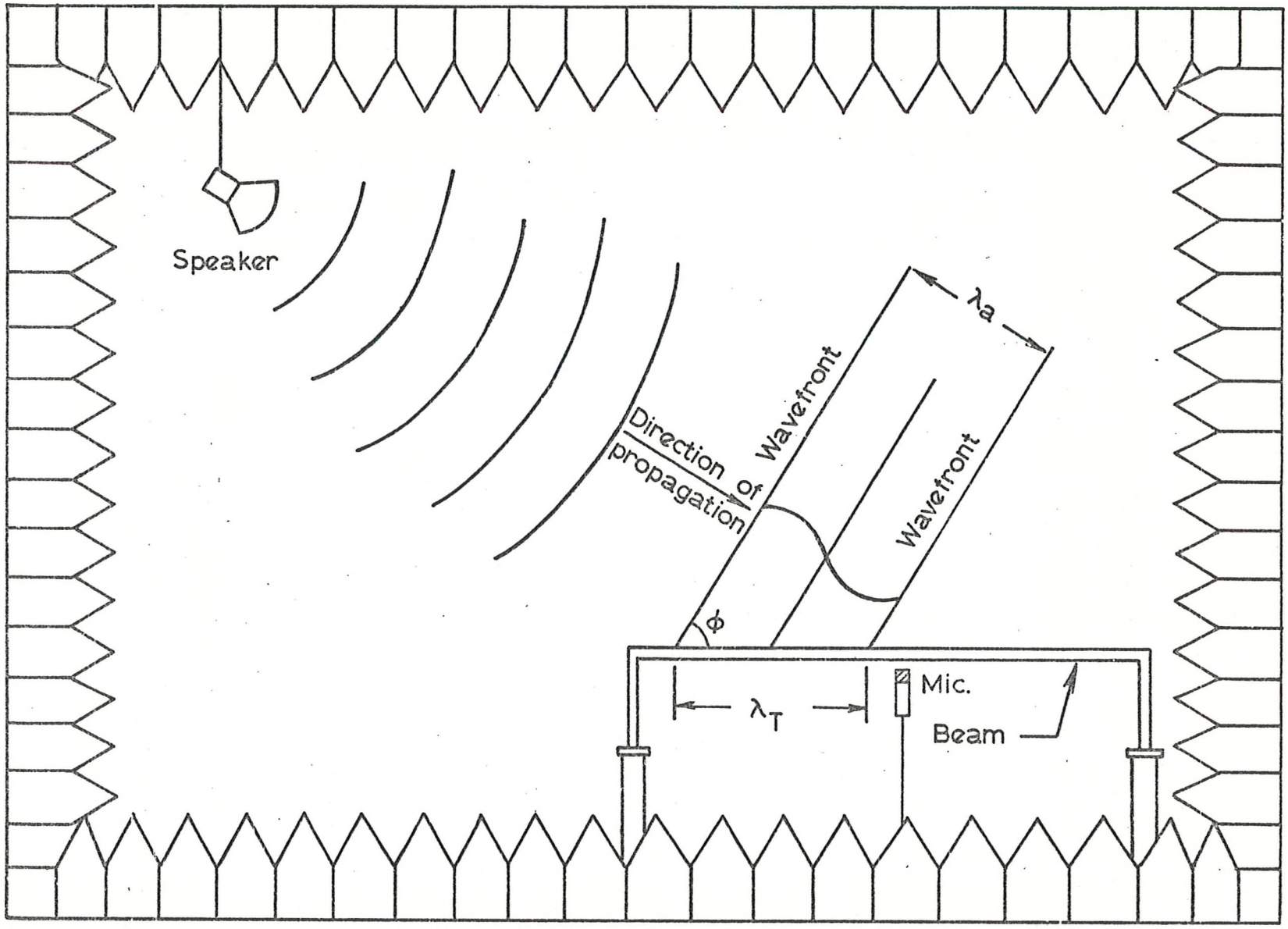

Fig.8.1 Experimental arrangement for measuring dual coincidence effect

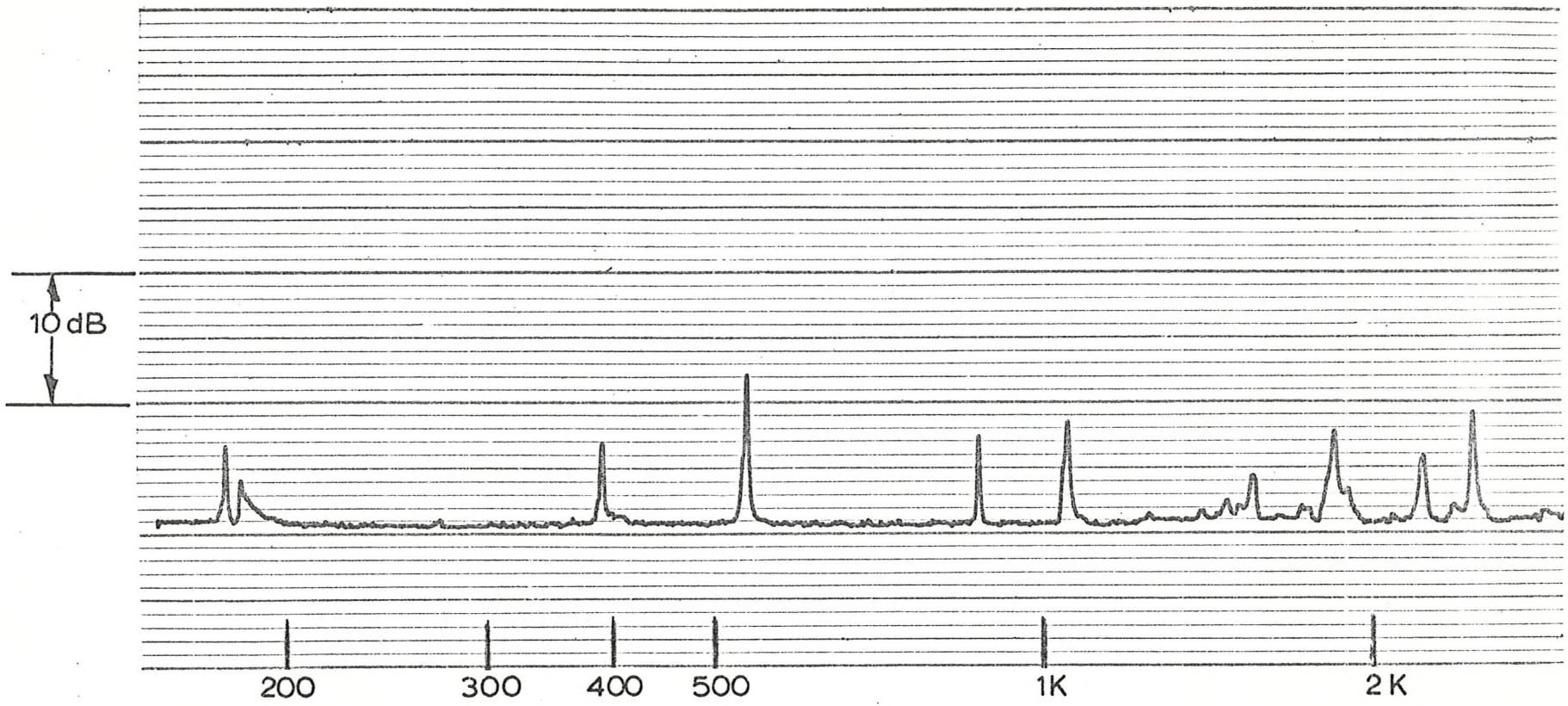

Fig. 8.2 Beam response to sound at grazing incidence.

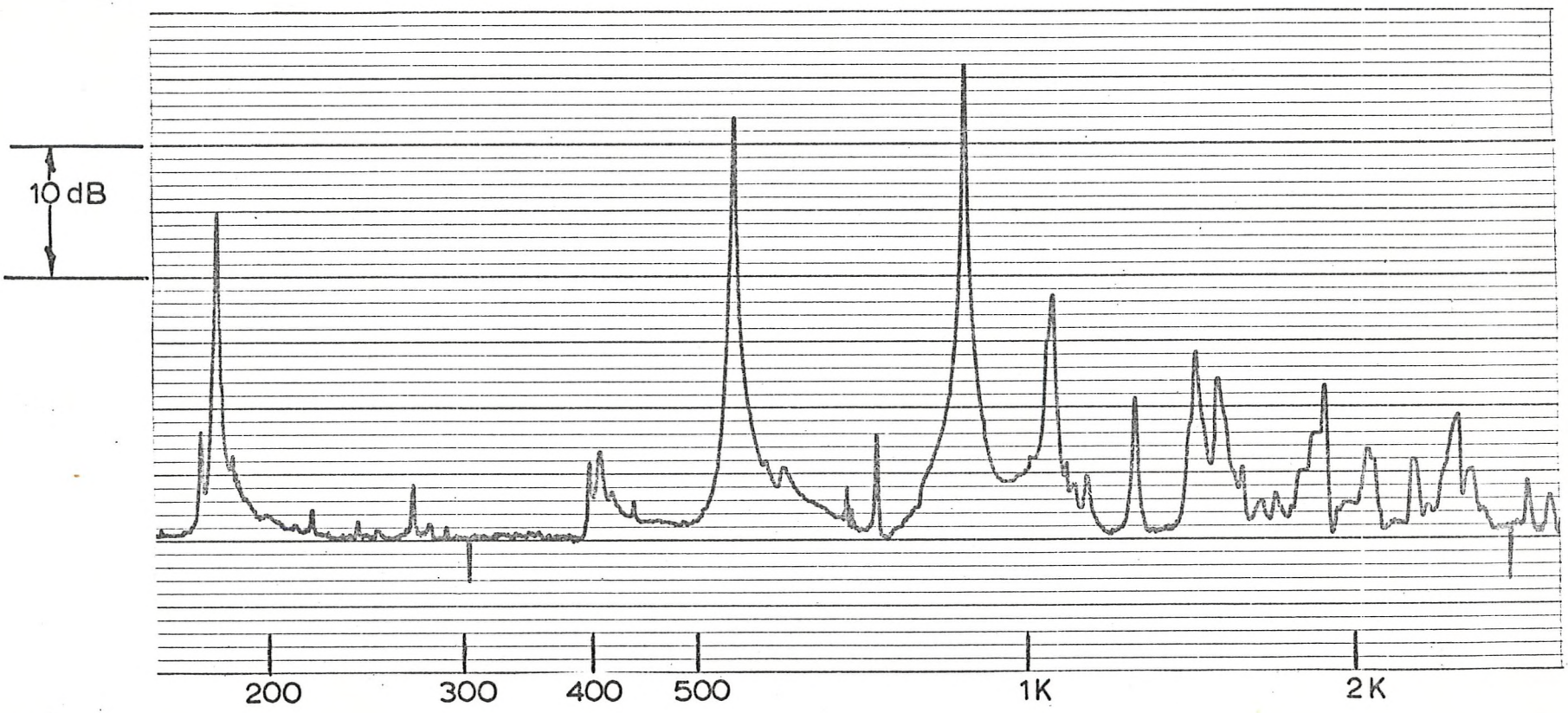

Fig. 8.3 Beam response to sound incident at 35°

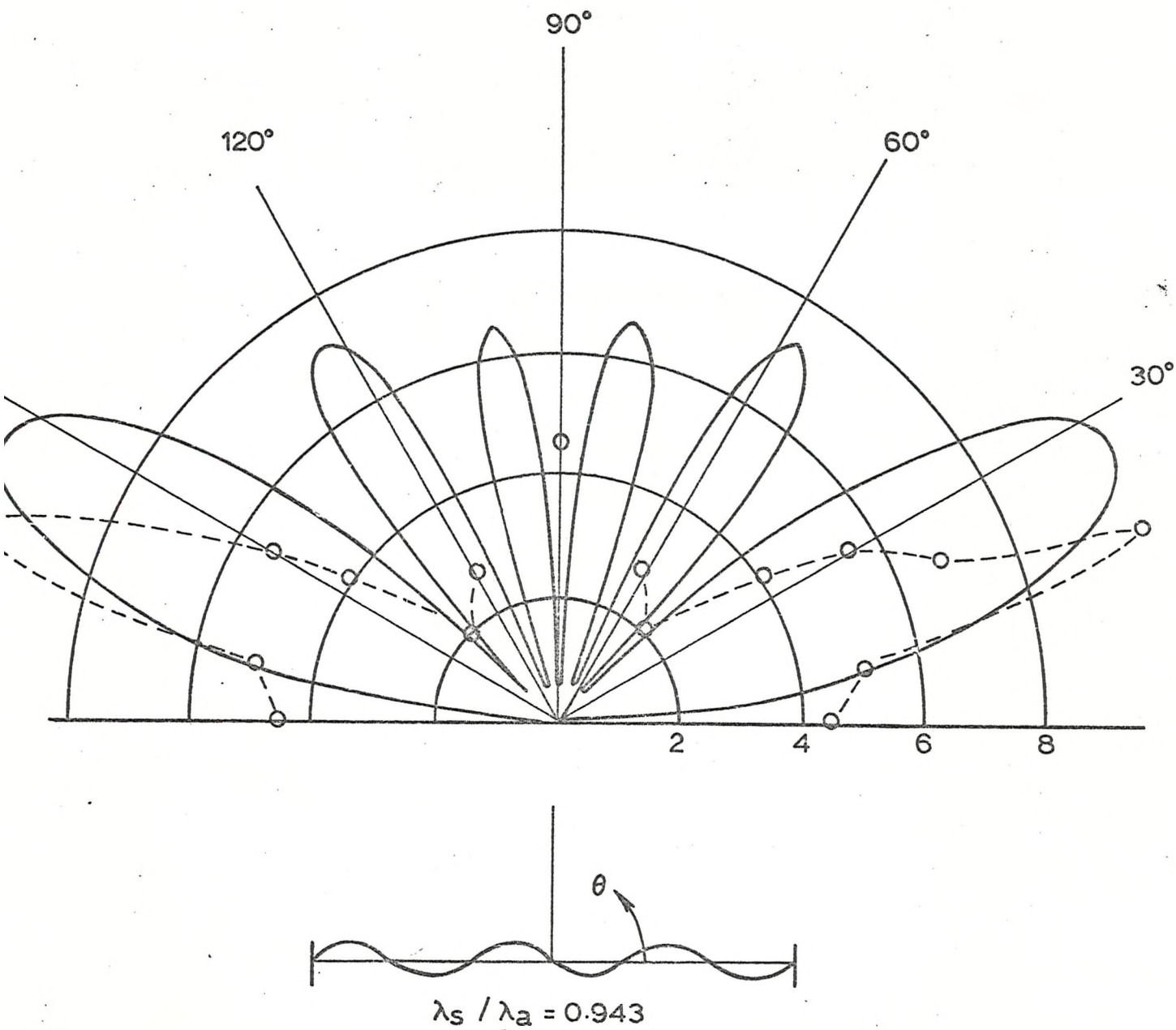

Fig.8.4 Subcritical directivity - 6th mode

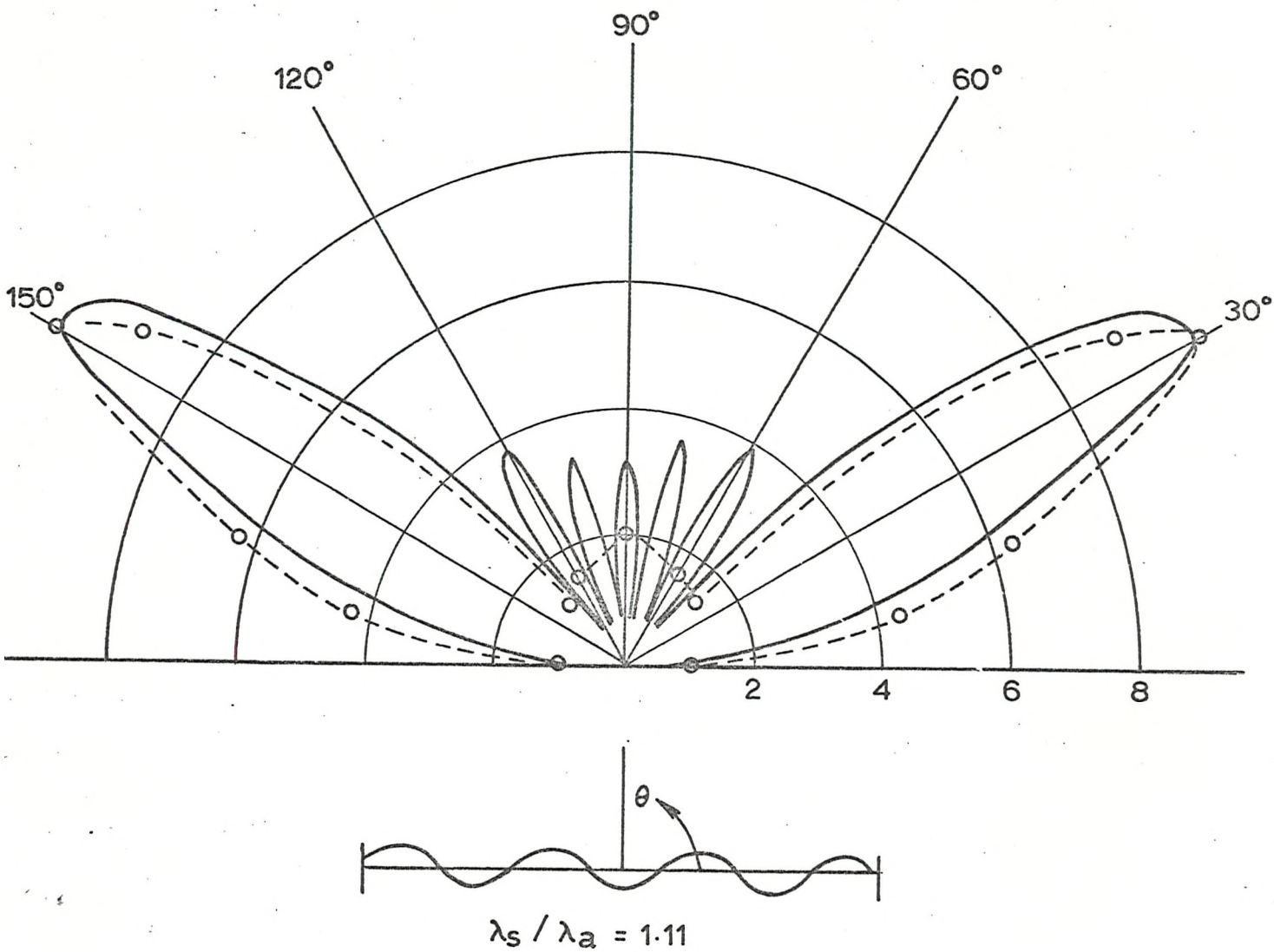

Fig.8.5 Supercritical directivity - 7th mode

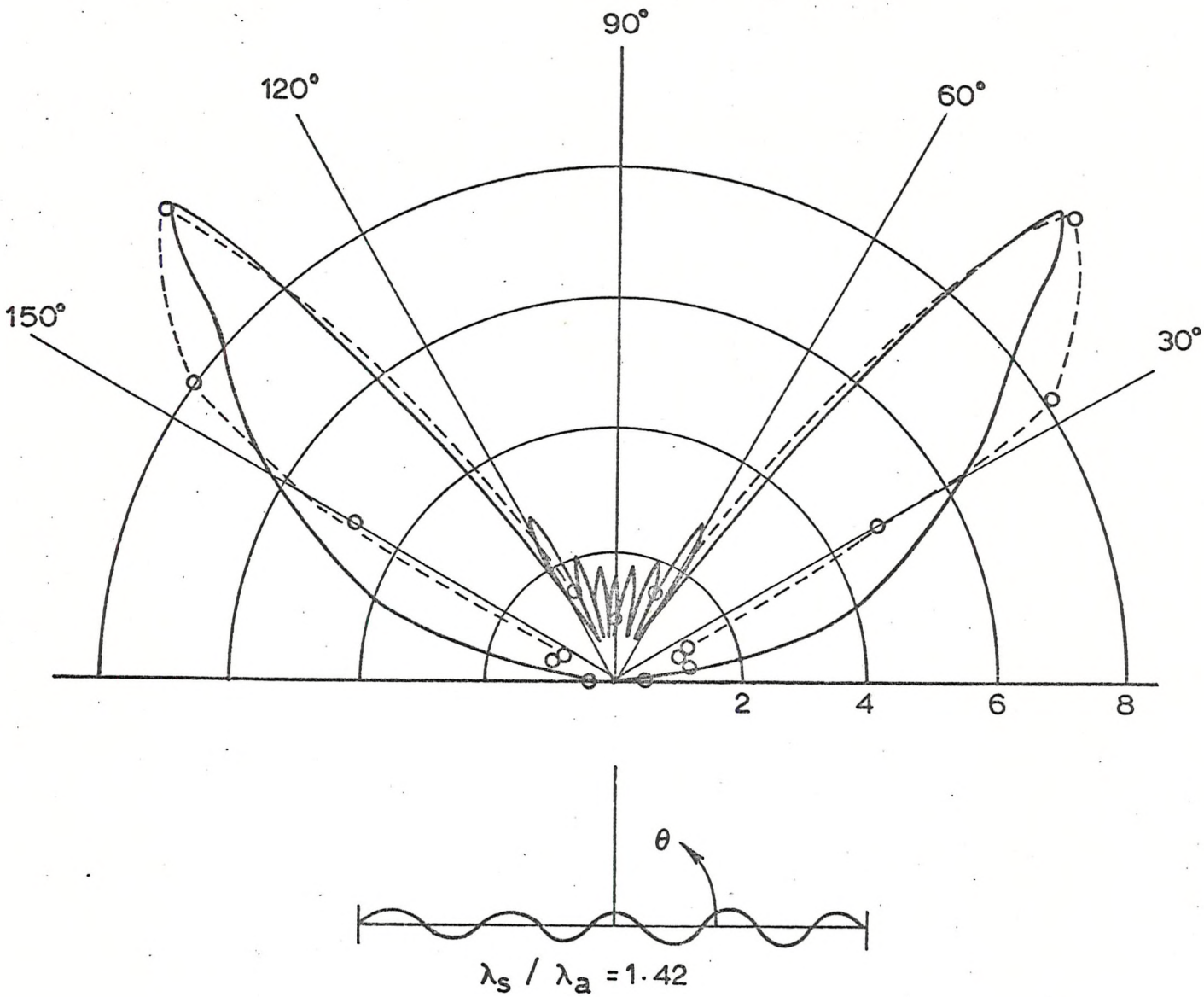

Fig. 8.6 Supercritical directivity - 9th mode

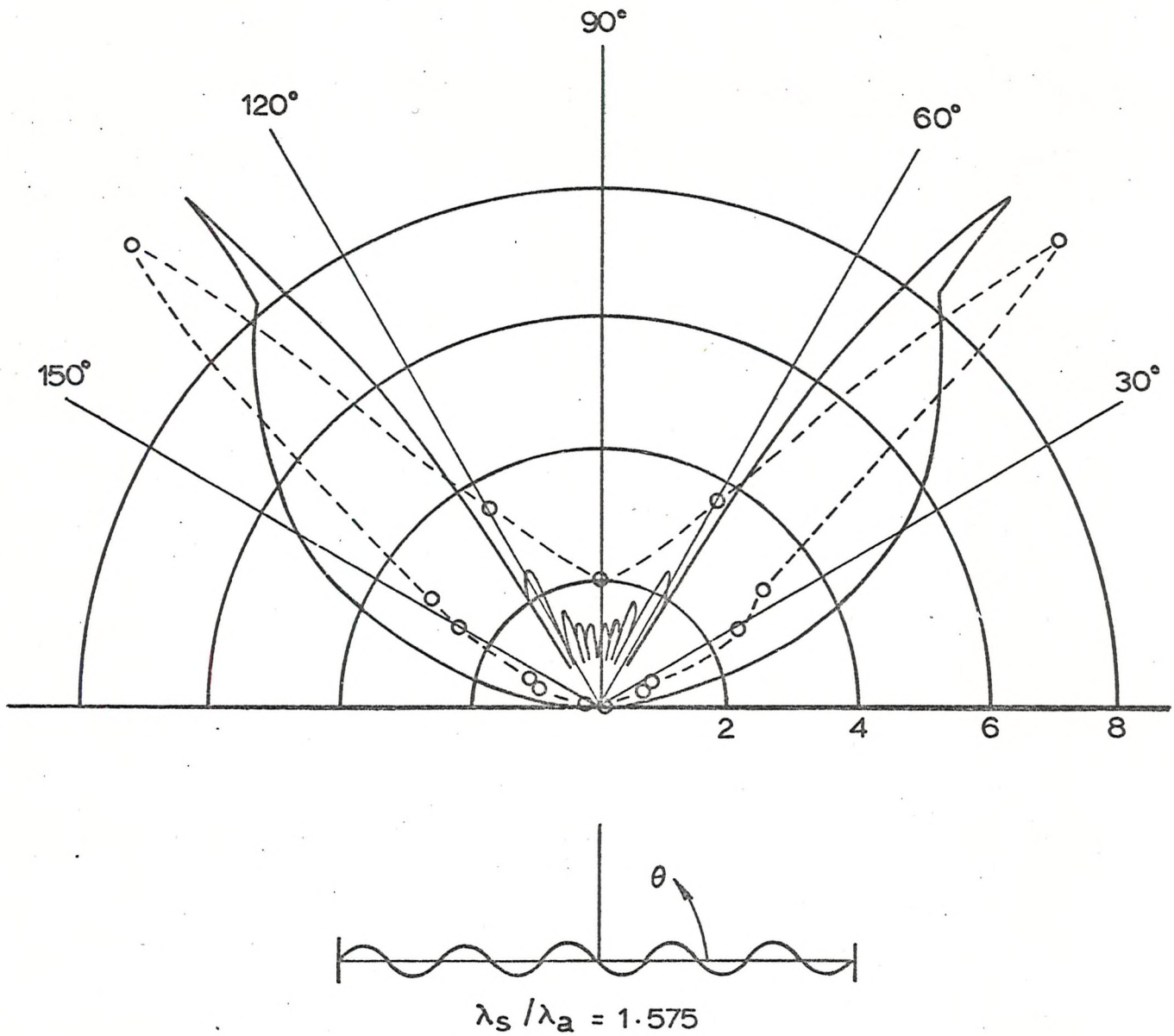

Fig.8.7 Supercritical directivity - 10th mode

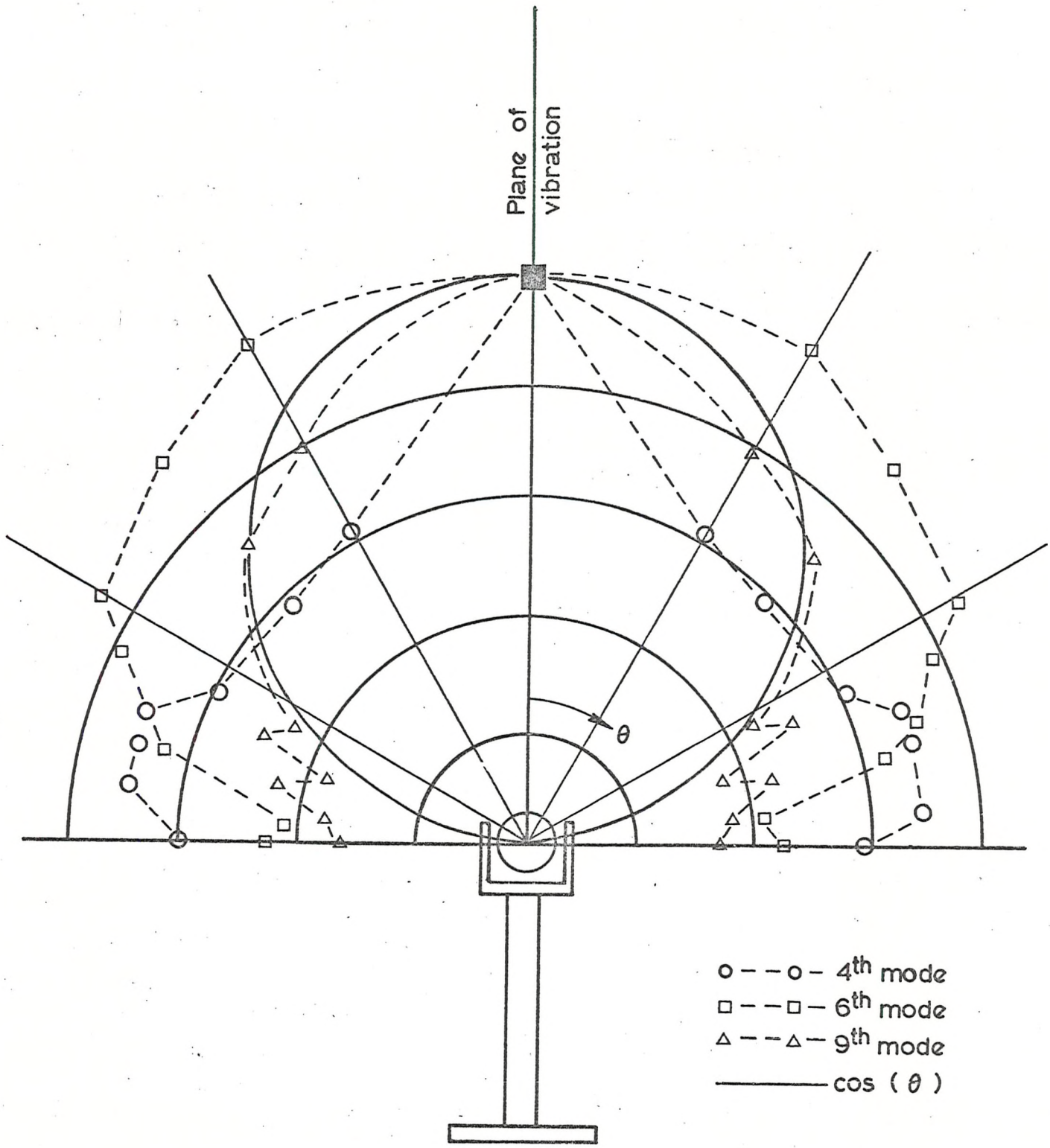

Fig.8.8 Polar directivity

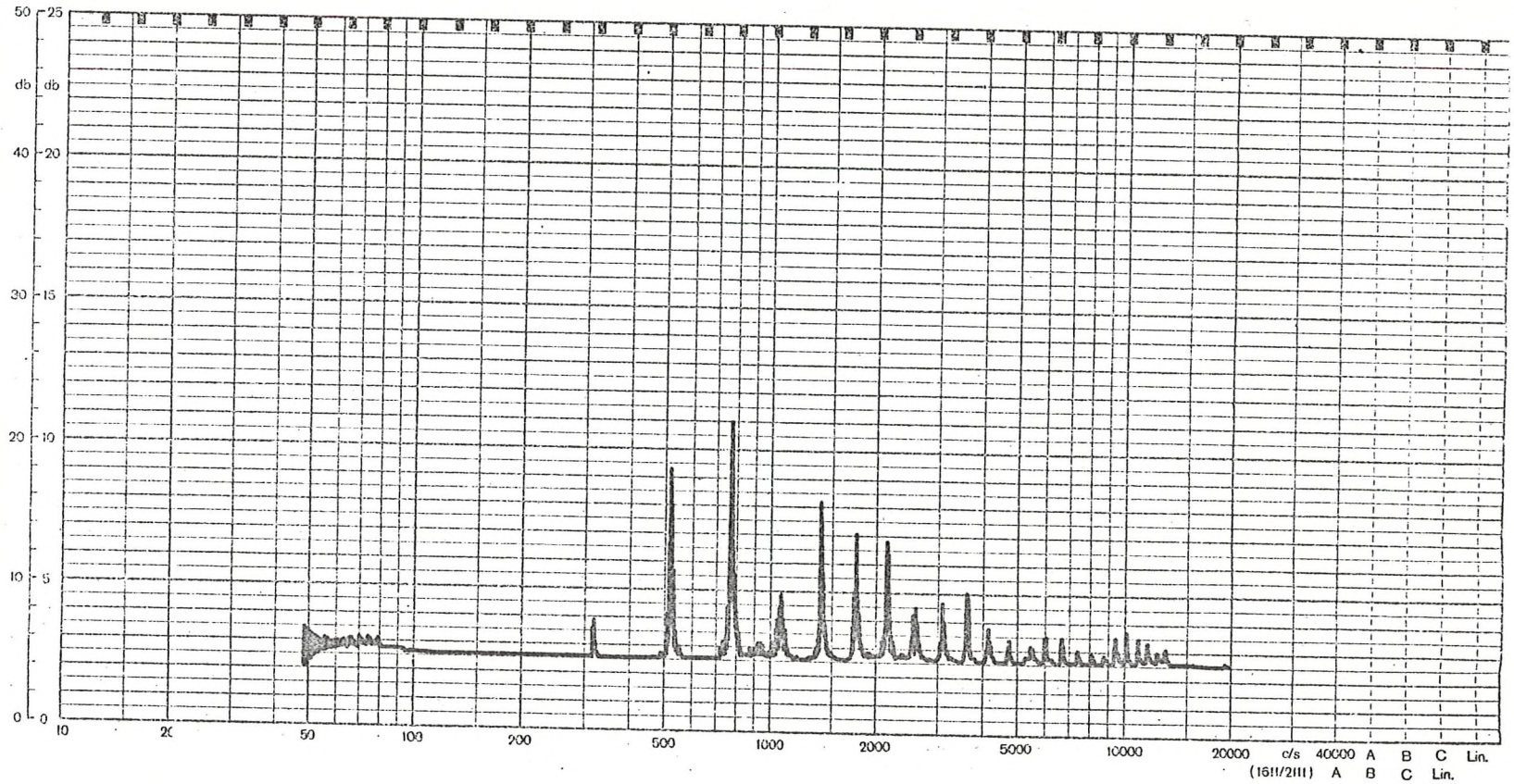

Fig. 8.9 Acoustic frequency response of beam III measured at the bottom opposite the coil.

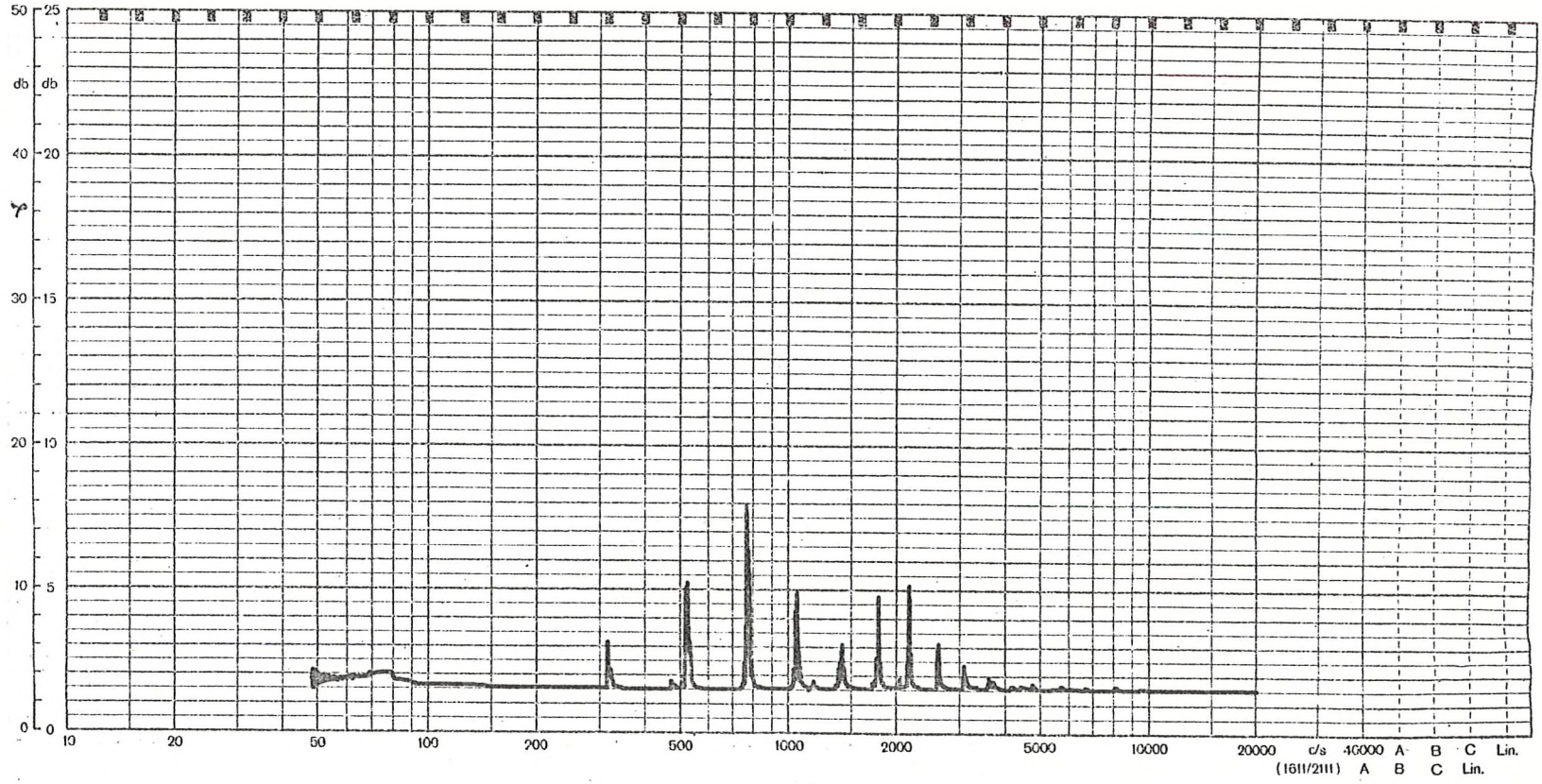

Fig. 8.10 Acoustic frequency response of beam III measured at the top of the beam in the plane of the coil.

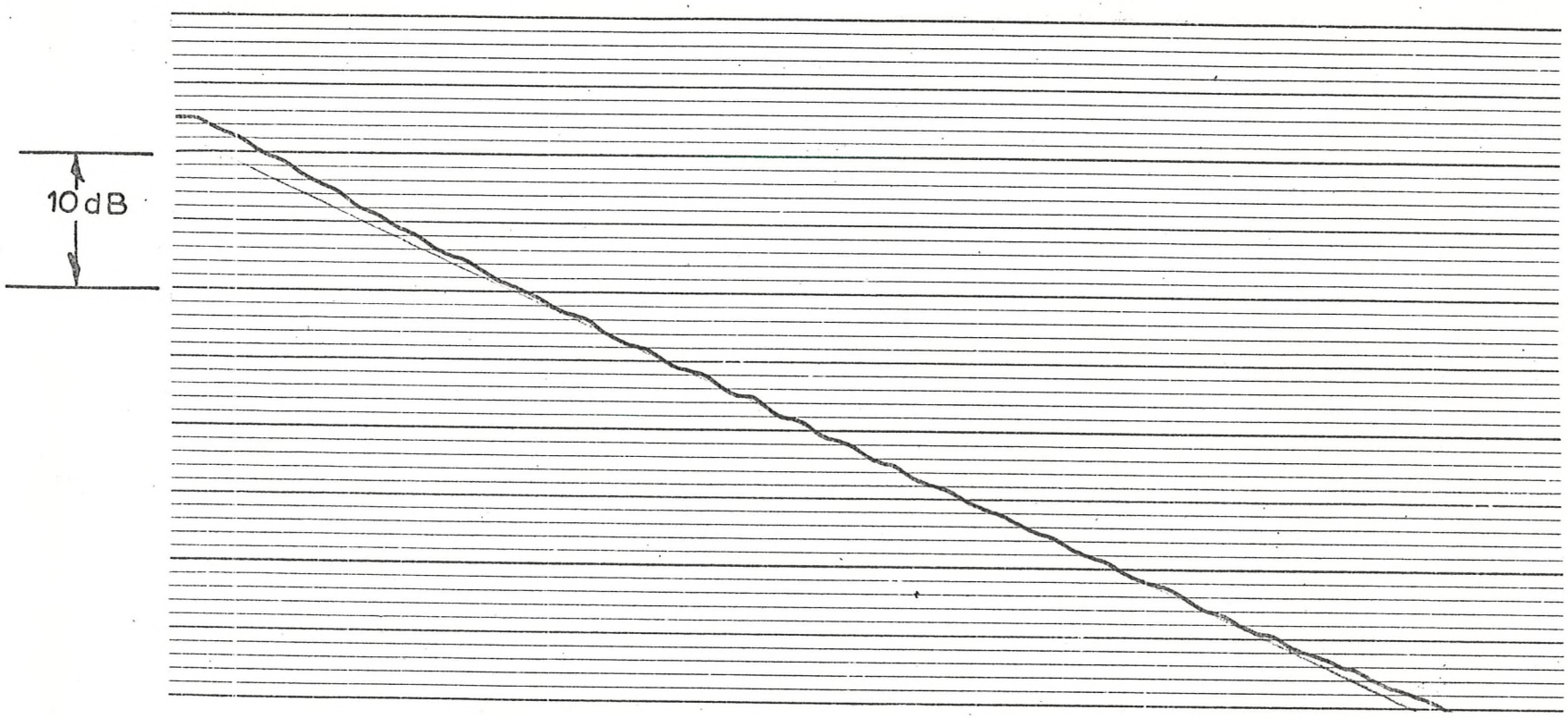

Fig. 8.11 Typical damping decay trace.

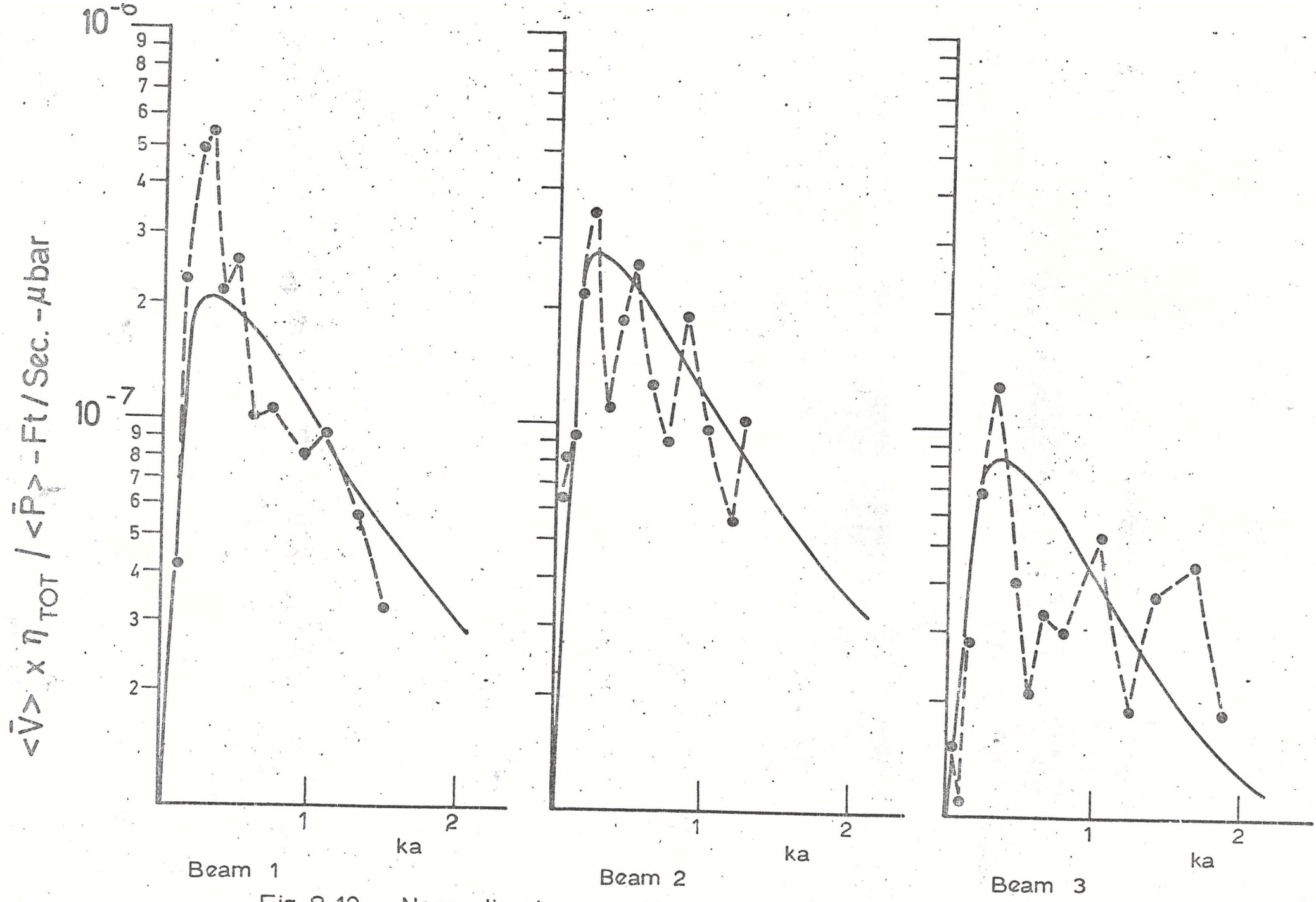

Fig. 8.12 Normalized acoustic response.

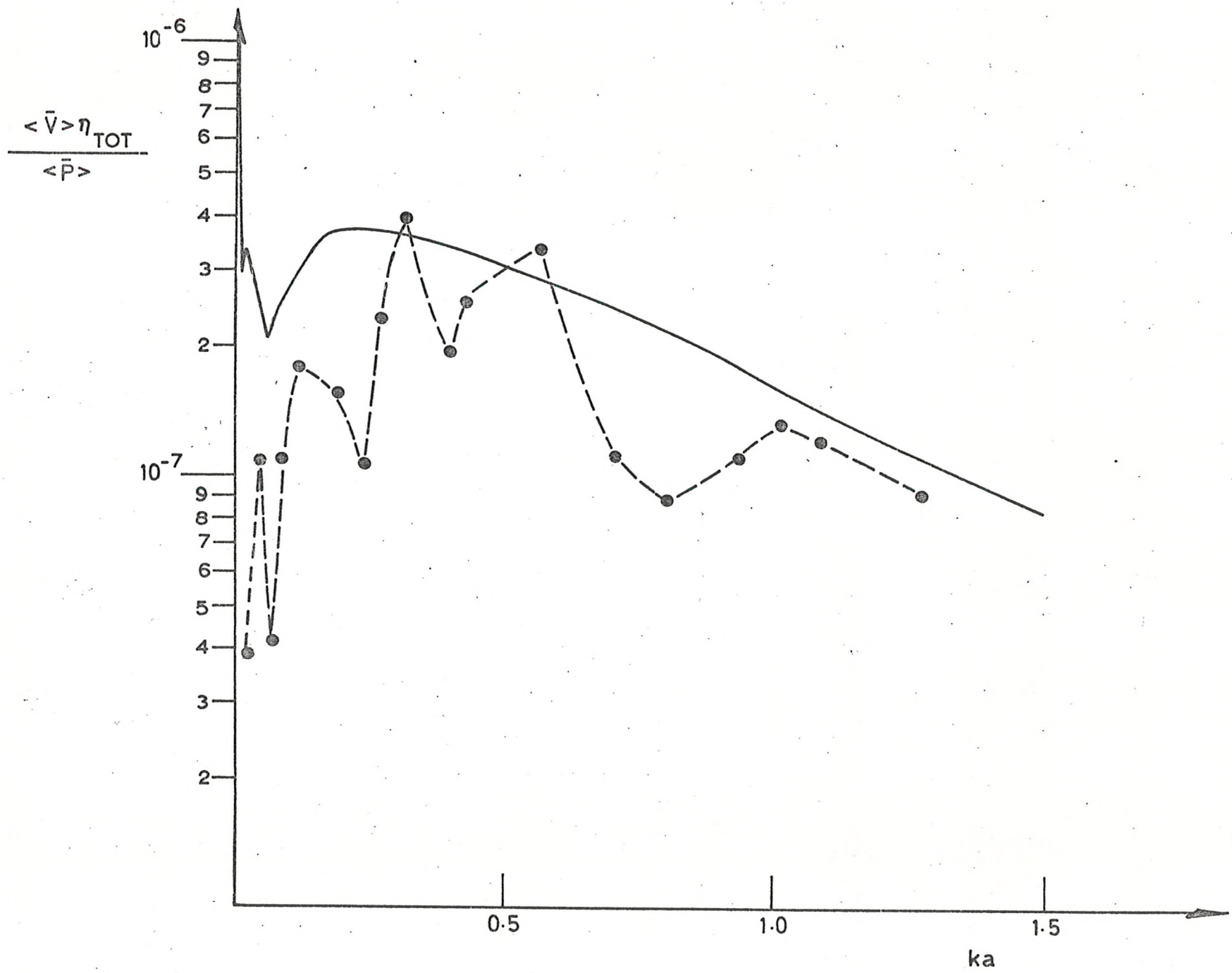

Fig.8·13 Pure-tone response - 2 supports.

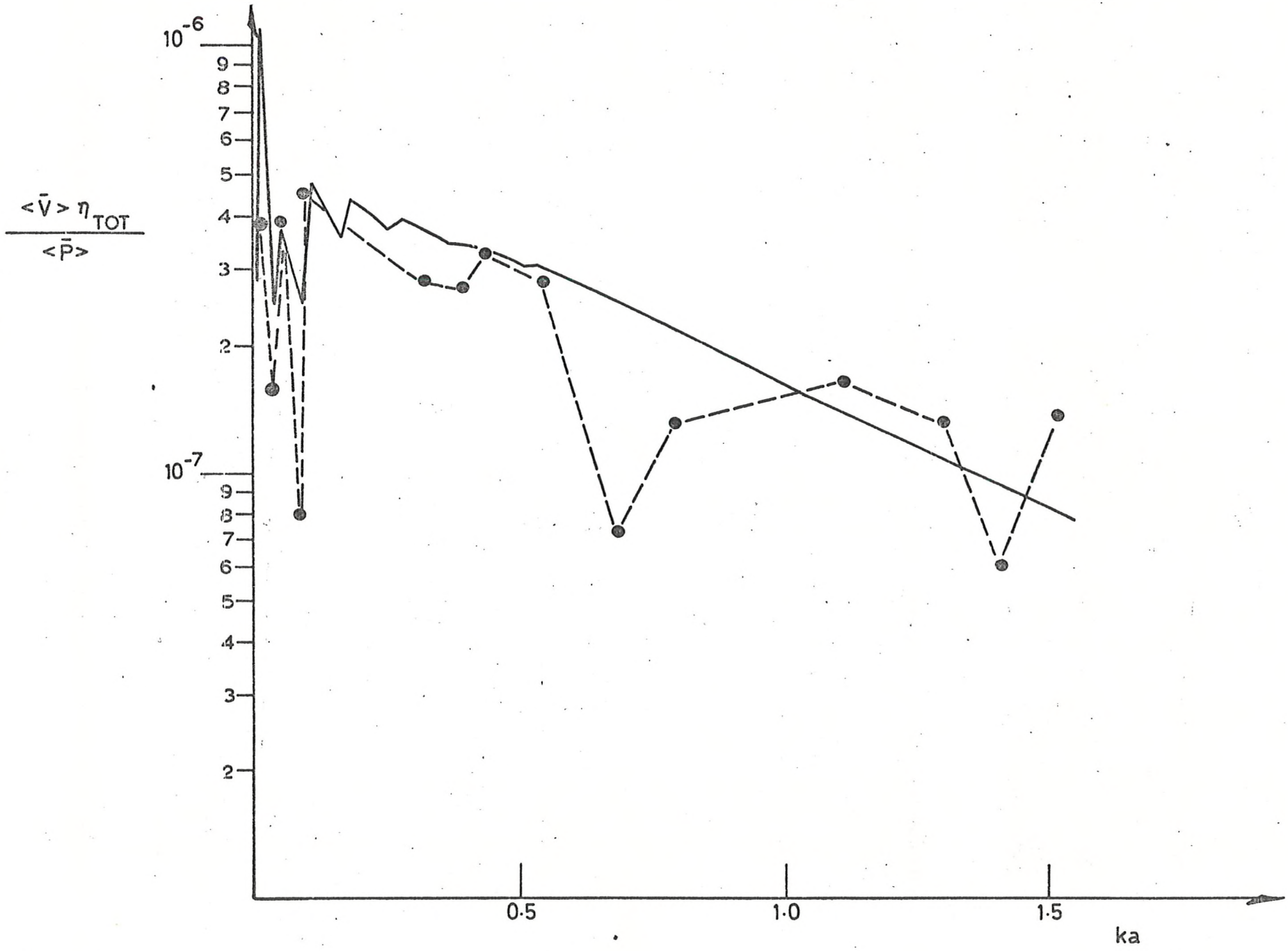

Fig. 8.14 Pure-tone response - 3 supports.

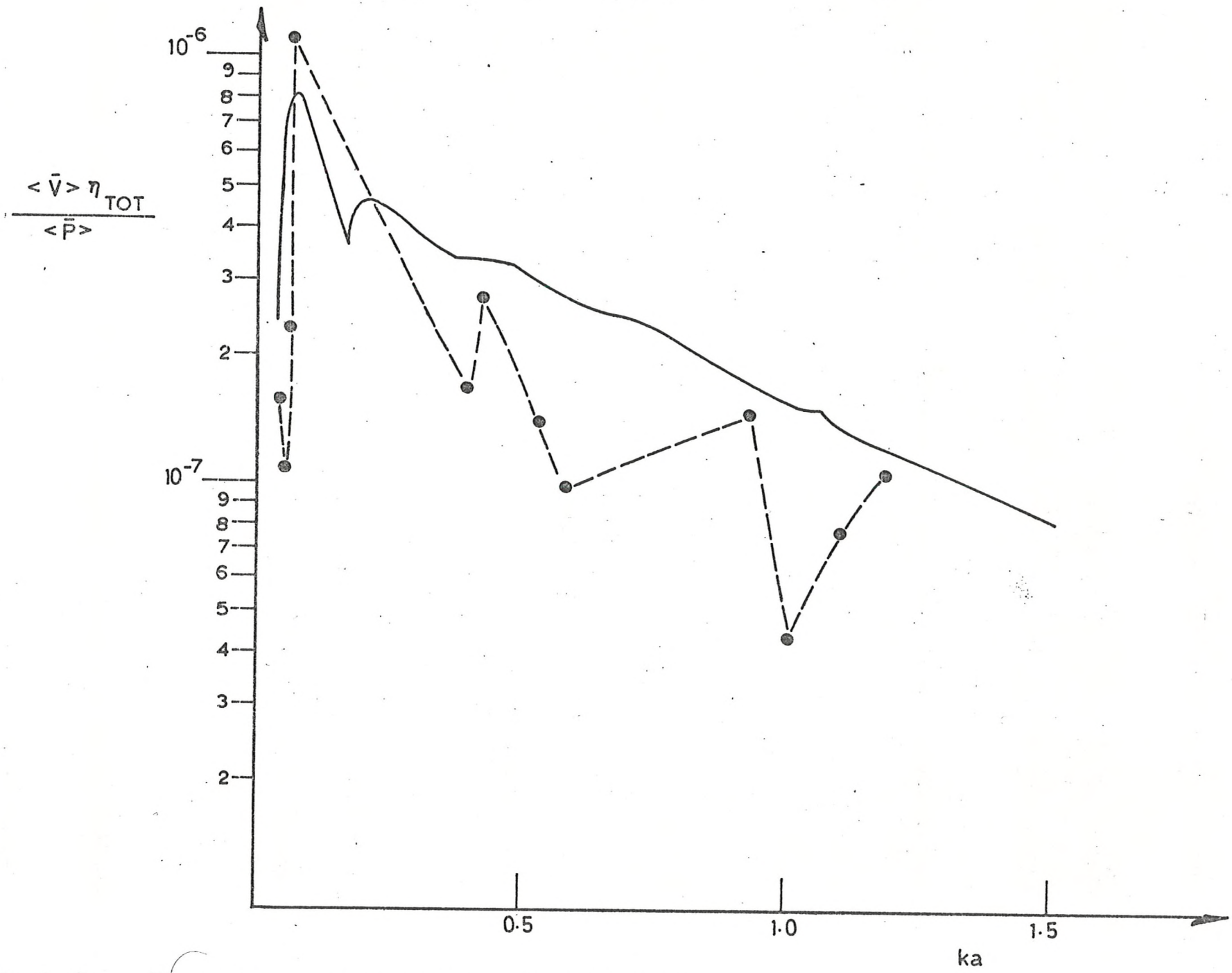

Fig. 8.15 Pure-tone response - 5 supports.

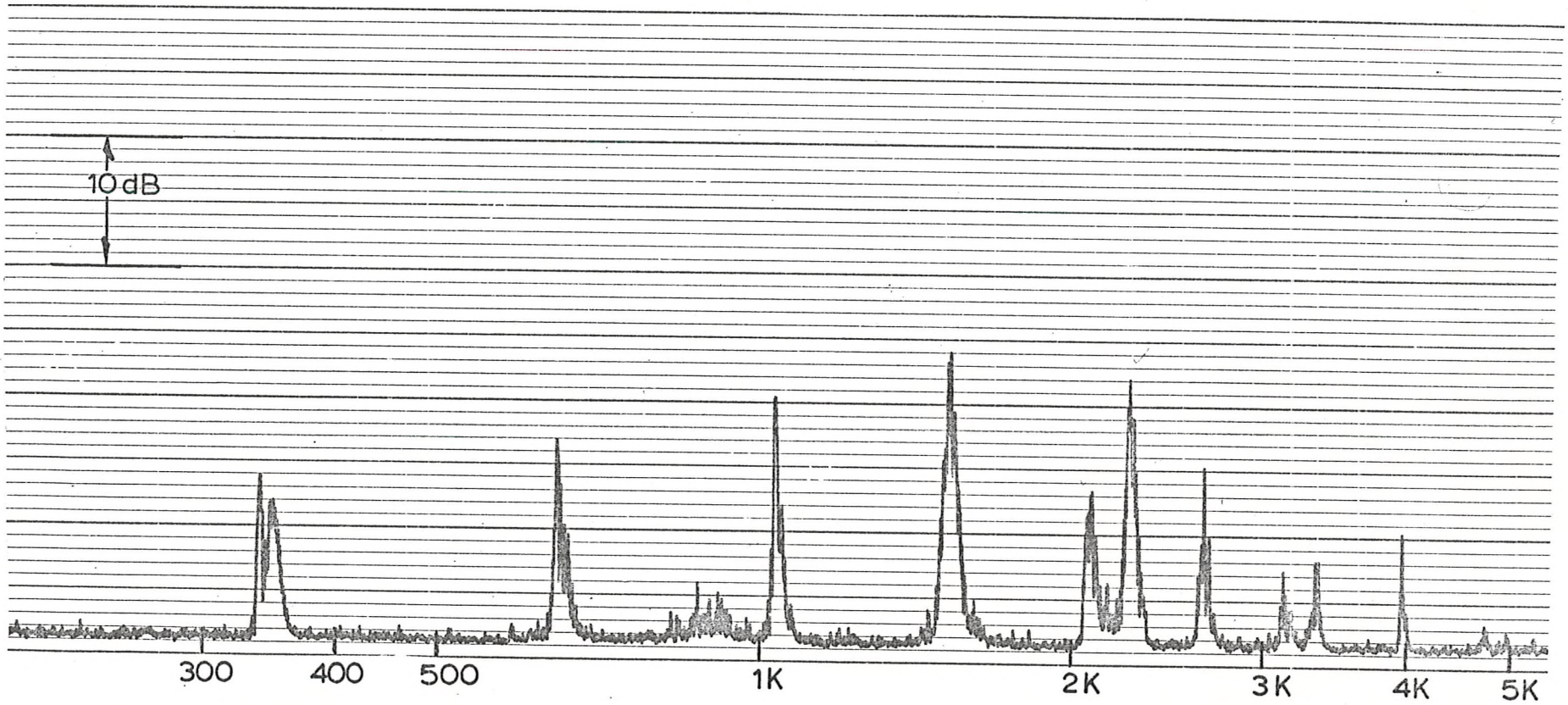

Fig.8.16 Frequency response of ring in the plane of curvature.

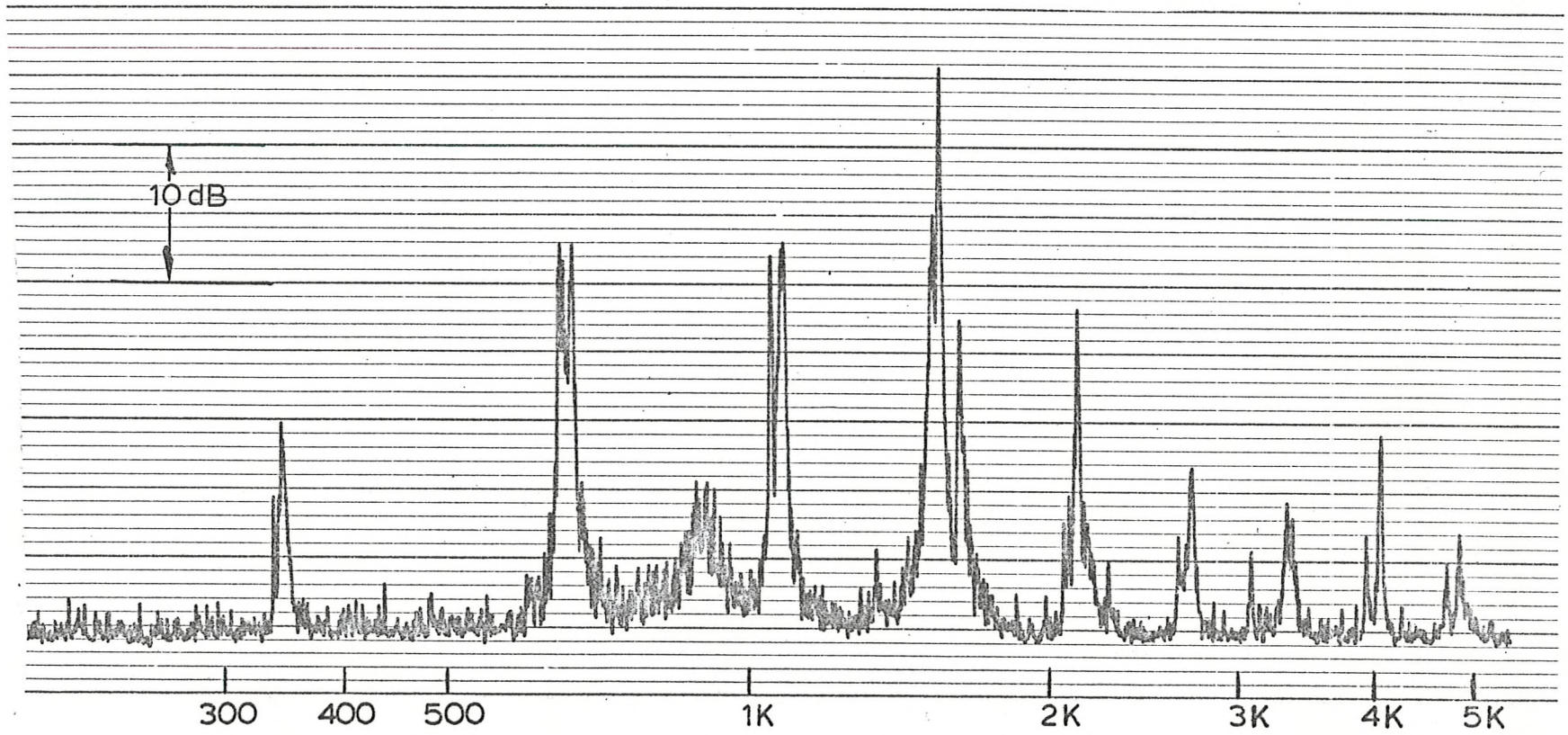

Fig. 8.17 Frequency response at 90° to plane of curvature.

CHAPTER IX

CONCLUSIONS

9.1 General Conclusions

The conclusions which are drawn from this research are listed below in the order of importance as they appear to the author.

It has been shown that a theory based on the principle of reciprocity can be used to predict the response of slender beams excited by sound.

A calculation of the sound radiation from a transversely vibrating, unbaffled cylindrical beam has shown that the radiation resistance is highly dependent on frequency. Radiation resistance increases with frequency to a maximum at ka = 1 where the radial component of the acoustic wavelength is equal to the circumference of the beam. At very high frequencies radiation resistance is independent of frequency and proportional to ρcS, where S is the surface area of the beam; i.e. the beam radiates as if it were a baffled piston radiating into an infinite acoustic medium. Physically, this means that acoustic short circuiting around the beam decreases as the dimensions of the beam become much larger than an acoustic wavelength.

The ratio of the acoustic wavelength to the structural wavelength (λ_a/λ_s) has been shown to be a very important parameter in controlling radiation and response. When $\lambda_a/\lambda_s > 1$, an infinitely long beam vibrating in a standing wave will not radiate sound and will not respond to acoustic excitation. The acoustic energy for this case is entirely reactive and no energy is radiated to the far field. Thus, the frequency corresponding to wavelength coincidence (ka = 0) may be defined as a lower 'cut-off' frequency for sound radiation and acoustic response

of infinitely long beams.

In contrast to the case of an infinitely long beam, it has been shown that a finite beam can radiate sound when $\lambda_a/\lambda_s > 1$. An understanding of the source of this radiation has been gained by showing that a line of coupled dipoles is an equivalent acoustic source model for a transversely vibrating beam. When λ_a is much longer than the total length of the beam, all odd beam modes radiate as dipole sources and all even modes radiate as quadrupole sources. When $\lambda_s/\lambda_a \simeq 1$, both odd and even modes radiate as relatively weak multipoles. In the limit as $\lambda_s \to \infty$, phase cancellation between adjacent quarter wavelengths decreases and the beam radiates as a dipole source until the acoustic wavelength becomes larger than the circumference of the beam. Above this frequency the dipole model breaks down and the radiation becomes line monopole in nature.

The acoustic source model also offers an explanation for the peculiar acoustic response behaviour of slender beams. At all frequencies the fundamental mode is a strong dipole source with relatively high acoustic response. If $\lambda_s/\lambda_a < 1$, the response of the second mode is greatly reduced because the equivalent acoustic source is a relatively weak quadrupole. Response increases for the third mode which once again exhibits dipole radiation, etc., until $\lambda_s/\lambda_a \simeq 1$. Above this frequency, response increases with frequency for all modes to a second maxima and then decreases as the dipole model breaks down. Experimental and theoretical results have shown that the acoustic response of a cylindrical beam is insignificant at these high frequencies if $ka > 2$. Therefore, the frequency corresponding to $ka = 2$ may be taken as a practical upper 'cut-off' frequency for design calculations.

It has been shown that the radiation resistance of a transversely

vibrating beam is relatively insensitive to the exact shape of the velocity distribution when $\lambda_s/\lambda_a > 1$. In fact, the radiation resistance of a finite beam is identical to that of an infinitely long beam when the structural wavelength is longer than the acoustic wavelength. This result is consistent with the basic principle that wave motions are insensitive to details smaller than a wavelength.

Approximate solutions for the radiation resistance of periodically supported beams have been obtained by defining an effective structural wavelength for sound radiation. The resulting radiation resistance is bounded by an upper limit corresponding to a rigid beam vibrating with uniform transverse velocity and a lower limit corresponding to a simply supported beam vibrating in a standing wave. A computer program has been developed to apply these results to the design of support systems. Computations have demonstrated the fact that increasing the number of supports can actually increase the response of a beam excited by sound.

An accurate method has been developed to measure pure-tone sound radiation from, and acoustic response of, transversely vibrating beams. Variations of room impedance have been investigated and it has been shown that the radiation resistance of an extended source can be accurately measured at a single source position if the length of the source is longer than an acoustic wavelength and many microphone positions are used to determine the average sound pressure level in the room. In comparison, previous theories (cf. 38, 40) have shown that the radiation resistance of simple acoustic sources can not be accurately measured at a single point, especially at low frequencies where the modal density of the room is low.

It has been shown that the maximum radiation loss factor of a solid steel beam vibrating in air is approximately 1.14×10^{-4} (see Figure (4.4)). Thus, the total damping of a slender beam would have to be

very light indeed for acoustic damping to be important in air. However, acoustic radiation can be an important damping mechanism in dense acoustic fluids.

9.2 Design Criteria

Various beam and acoustic medium parameters have been shown to be particularly important in controlling radiated sound power $\langle w \rangle$, radiation loss factor η_{rad}, and response to acoustic excitation $\langle \bar{v} \rangle$. A quick estimate of the importance of frequency, radius, beam length, material density, medium density, speed of sound, and (λ_a/λ_s) can be made by referring to the following table.

TABLE OF PARAMETERS

Frequency Range	$0 < ka < 1$			$ka \gg 1$		
	$\langle w \rangle$	η_{rad}	$\langle \bar{v} \rangle$	$\langle w \rangle$	η_{rad}	$\langle \bar{v} \rangle$
frequency	f^3	f^2	$f^{-1/2}$	-	f^{-1}	f^{-2}
radius of solid beam	a^4	a^2	-	a	a^{-1}	$a^{-3/2}$
length	ℓ	-	$\ell^{-1/2}$	ℓ	-	$\ell^{-1/2}$
mat'l density	-	ρ_m^{-1}	ρ_m^{-1}	-	ρ_m^{-1}	ρ_m^{-1}
medium density	ρ_o	ρ_o	-	ρ_o	ρ_o	-
speed of sound	c^{-2}	c^{-2}	$c^{-1/2}$	c	c	c
λ_a/λ_s	$[1-(\lambda_a/\lambda_s)^2]$	$[1-(\lambda_a/\lambda_s)^2]$	$\sqrt{1-(\lambda_a/\lambda_s)^2}$	-	-	-

9.3 Summary

In conclusion it may be said that all the objectives of this research have been successfully achieved. The principle of reciprocity has been demonstrated and a method for predicting the response of slender beams to acoustic excitation has been produced. The importance of beam and acoustic medium parameters has been established and a computer program has been written to aid in the design of periodically supported beams. Expressions have been derived for radiation damping and an equivalent acoustic source model for a transversely vibrating beam has been defined. The statistical problems of sound measurements in a reverberant room have been investigated and an accurate method for measuring pure-tone sound radiation from an extended source has been developed.

REFERENCES

1. Putnam, A.A. 1964. ASME WA/HT-21, Paper No. 21. Flow-Induced Noise and Vibration in Heat Exchangers.

2. Chen, Y.N. 1968. Journal of Engineering for Industry, Trans. of ASME. pp. 134-156. Flow-Induced Vibration and Noise in Tube-Bank Heat Exchangers due to von Karman Streets.

3. Rizk, W. and Seymour, D.F. 1965. Proc. Inst. Mech. Engrs. 179, part 1 (No. 21). Investigations into the failure of gas circulators and circuit components at Hinkley Point Nuclear Power Station.

4. Yeh, L. Beaney, E.M. and Smith B. 1967. Inst. Mech. Engrs. Conference on High Pressure Gas as a Heat Transport Medium. Paper No. 9, Acoustically Induced Stresses in Nuclear Structures.

5. Lyon, R.H. and Maidanik, G. 1962. J. Acoust. Soc. Am. 34, (5), 623. Power Flow between Linearly Coupled Oscillators.

6. Leehey, P. and Hanson, C.E. 1969. Acoustics and Vibration Laboratory Tech. Rpt. No. 76234-4. Mass. Inst. Tech. Aeolian Tones Associated with Resonant Vibration.

7. Attenborough, K. 1970. Proceedings of the British Acoustical Society. Conference on Building Acoustics, Newcastle Upon Tyne. A Prediction of Oblique Incidence Behaviour of Porous, Fibrous Absorbents.

8. Lyon, R.H. 1967. SVM-1. Random Noise and Vibration in Space Vehicles. The Shock and Vibration Centre. United States Department of Defense.

9. Smith, P.W., Jr. and Lyon, R.H. 1965. NASA CR-160. Sound and Structural Vibration.

10. Smith, P.W., Jr. 1962. J. Acoust. Soc. Am. 34, (5), 640. Response and Radiation of Structural Modes Excited by Sound.

11. Powell, A. 1958. J. Acoust. Soc. Am. 30, 1130. On the Fatigue Failure of Structures due to Vibrations Excited by Random Pressure Fields.

12. Mercer, C. 1965. Journal of Sound and Vibration 2, (3), 293. Response of a Multi-Supported Beam to a Random Pressure Field.

13. Lin, Y.K. 1967. Probabalistic Theory of Structural Dynamics. McGraw-Hill Book Co. N.Y.

14. Morse, P.W. 1948. Theory of Sound. McGraw-Hill Book Co. N.Y.

15. Reschevkin, S.N. 1963. A Course of Lectures on the Theory of Sound. Translated from the Russian by O.M. Blum. The MacMillan Company, N.Y.

16. Morse, P.M. and Feshbach, H. 1953. Methods of Theoretical Physics. McGraw-Hill Book Co. N.Y.

17. Kinsler, L.E. and Frey, A.R. 1962. Fundamentals of Acoustics, John Wiley and Sons, Inc. N.Y.

18. Morse, P.M. and Ingard, K.O. 1968. Theoretical Acoustics, McGraw-Hill Book Co. N.Y.

19. Skudrzyk, E. 1968. Fundamentals of Acoustics. Pennsylvania State University Press, State College, Pennsylvania.

20. Maidanik, G. 1962. J. Acoust. Soc. Am. 34, (6), 809. Response of Ribbed Panels to Reverberant Acoustic Fields.

21. Junger, M.C. 1953. J. Acoust. Soc. Am. 25 (1), 40. The Physical Interpretation of the Expression for an Outgoing Wave in Cylindrical Co-ordinates.

22. Junger, M.C. 1953. J. Acoust. Soc. Am. 25, (5), 899. The Concept of Radiation Scattering and It's Application to Reinforced Cylindrical Shells.

23. Greenspon, J.E. 1961. J. Acoust. Soc. Am. 33, (10), 1321. Vibrations of Thick and Thin Cylindrical Shells surrounded by Water.

24. Laird, D.T. and Cohen, H. 1952. J. Acoust. Soc. Am. 24, (1), 46. Directionality Patterns for Acoustic Radiation from a Source on a Rigid Cylinder.

25. Manning, J.E. and Maidanik, G. 1964. J. Acoust. Soc. Am. 36, (9), 1691. Radiation Properties of Cylindrical Shells.

26. Runkle, C.J. and Hart, F.D. 1969. NASA CR-1437. The Radiation Resistance of Cylindrical Shells.

27. Bishop, R.E.D. and Johnson, D.C. 1960. The Mechanics of Vibration, Cambridge University Press.

28. Timoshenko, S. 1955. Vibration Problems in Engineering. 3rd Edition. D. Von Nostrand Co. N.Y.

29. Chertock, G. 1964. J. Acoust. Soc. Am. 36, (8), 1305. Sound Radiation from Vibrating Surfaces.

30. Erdelyi, A., 1956. Asymptotic Expansions. Dover Publications, Inc.

31. Ayre, R.S. and Jacobson, L.S. 1950. Journal of Applied Mechanics. Natural frequencies of Continuous Beams of Uniform Span Length.

32. Schroder. 1962. J. Acoust. Soc. Am. 34, (12), 1819. Frequency-Correlation Functions of Frequency Response in Rooms.

33. Doak, P.E. 1959. Acoustica. 9, 1-9. Fluctuations of Sound Pressure Levels in Rooms when the Receiver Position is Varied.

34. Baade, P. 1970. Proceedings of the British Acoustical Society Conference on Building Acoustics, Newcastle Upon Tyne. Equipment Sound Power Measurement in Reverberant Rooms.

35. Lubman, D. 1969. J. Acoust. Soc. Am. 46, (3) Part 1, 532. Spacial Averaging in a Diffuse Sound Field.

36. Schroder, M.R. 1969. J. Acoust. Soc. Am. 46, (a), Part 1, 277. Effect of Frequency and Space Averaging on the Transmission Responses of Multimode Media.

37. Schroder, M.R. 1969. J. Acoust. Soc. Am. 46, (3), Part 1, 534. Spatial Averaging in a Diffuse Sound Field and the Equivalent Number of Independent Measurements.

38. Lyon, R.H. 1969. J. Acoust. Soc. Am. 45, (3), 545. Statistical Analysis of Power Injection and Response in Structures and Rooms.

39. Suggestion of P.E. Doak of The Institute of Sound and Vibration Researc The University, Southampton.

40. Beaney, E.M. and Yeh, L. 1969. Mechanical Engineering Laboratory Report No. W/M(IC) p. 1598. Acoustically Induced Stresses in Boiler Tubes: Part III.

41. Doak, P.E. 1966. ISAV Memorandum No. 154. An Introduction to Sound Radiation and It's Sources. Institute of Sound and Vibration Research. The University, Southampton.

42. Kells, L.M. 1960. Elementary Differential Equations. 5th Edition. McGraw-Hill Book Co. N.Y.

APPENDIX I

Acoustic Point Sources

In this section we will consider several examples of simple acoustic sources. The results obtained here are useful in the discussions on sound radiation and acoustic response of slender beams. These examples are presented in detail in standard acoustic textbooks such as References (14) through (19).

A.1.1 The Monopole

Consider a small sphere of radius a which pulsates periodically with uniform radial velocity given by $V_o e^{-i\omega t}$. The radiated sound pressure is given by Doak (41) as

$$p = \frac{\rho c V_o a(ika) e^{-i\omega t + ikr}}{r(1 + ika)} \qquad (A.1.1)$$

At large distances from the source, the radiated wave is essentially a plane wave with the particle velocity strictly in phase with the pressure. For this case the mean intensity can be written as

$$\langle I \rangle = \frac{\rho c V_o^2 a^2 (ka)^2}{2 r^2 [(ka)^2 + 1]} \qquad (A.1.2)$$

The total mean radiated power can be calculated by integrating the intensity over the surface of a sphere of radius r.

$$\langle w \rangle = \int_0^{\pi} \int_0^{2\pi} \langle I \rangle r^2 \sin\theta \, d\theta \, d\phi \qquad (A.1.3)$$

$$\langle W \rangle = \frac{\rho c V_o^2 (4\pi a^2)}{2} \quad \frac{(ka)^2}{(ka)^2 + 1} \tag{A.1.4}$$

The mean square velocity averaged with respect to time and space will be

$$\langle \bar{v}^2 \rangle = V_o^2/2. \tag{A.1.5}$$

Substituting this into equation (3.8) and utilizing (2.6) yields

$$R_{rad} = \rho c(4\pi a^2) \frac{(ka)^2}{(ka)^2 + 1} \quad . \tag{A.1.6}$$

Limiting values for ka<<1 and ka >>1 are therefore given by

$$R_{rad} = \begin{cases} \rho c(4\pi a^2) (ka)^2 & , \quad ka<<1; \\ \rho c(4\pi a^2) & , \quad ka>>1. \end{cases} \tag{A.1.7}$$

A.1.2 The Dipole

Sound can also be generated by simply moving a fluid back and forth along an axis. Consider the case of a small sphere of radius a which oscillates harmonically with normal velocity $V_o \cos\theta\, e^{-i\omega t}$. The radiated pressure is given by Doak (41) as,

$$p = \frac{-\rho c V_o k^2 a^3 \cos\theta (1 + 1/ikr) e^{-i\omega t + ikr}}{\left[(ka)^2 + 2(1 + ika)\right] r} \tag{A.1.8}$$

Following the procedure of section (A.1.1), the mean intensity at large distances from the source can be written as

$$\langle I \rangle = \frac{\rho c V_o^2 a^2 \cos^2\theta (ka)^4}{2r \left[(ka)^4 + 4\right]} \quad . \tag{A.1.9}$$

Substitution into equation (A.1.3) yields

$$\langle w \rangle = \frac{\rho c \, V_o^2 \, a^2 \, (ka)^4}{2[(ka)^4 + 4]} \int_0^{\pi} \int_0^{2\pi} \cos^2 \theta \sin\theta \, d\theta \, d\phi \, . \quad \text{(A.1.10)}$$

The result of evaluating the above integral is

$$\langle w \rangle = \frac{\rho c (4\pi a^2) \, V_o^2 \, (ka)^4}{6 \, [(ka)^4 + 4 \,]} \, . \quad \text{(A.1.11)}$$

Again, the mean square velocity averaged with respect to time and space is $\langle \overline{v^2} \rangle = V_o^2/2$. Substituting this together with equation (A.1.11) into equation (2.6) yields

$$R_{rad} = \frac{\rho c (4\pi a^2) \, (ka)^4}{3[(ka)^4 + 4 \,]} \, . \quad \text{(A.1.12)}$$

Limiting values for large and small ka are therefore given by

$$R_{rad} \approx \begin{cases} \dfrac{\rho c (4\pi a^2) \, (ka)^4}{12} \, , & ka \ll 1; \\ \dfrac{\rho c (4\pi a^2)}{3} \, , & ka \gg 1. \end{cases} \quad \text{(A.1.13)}$$

The above approximation when $ka \ll 1$ can also be obtained by placing close together two simple sources of equal magnitude and opposite sign (e.g. (18)).

A.1.3 The Quadrupole

A third well known type of acoustic source is the quadrupole, which can be represented by two dipoles; one orientated in the positive direction, the other pointing in the negative direction. Of course, this is equivalent to an ensemble of four simple sources with appropriate signs. When the distance between the simple sources is small compared with the wavelength (i.e. $ka \ll 1$), the radiation resistance can be written as (18)

$$R_{rad} = \frac{\rho c(4\pi a^2)\,(ka)^6}{1,\,215} \quad . \qquad \text{(A.1.14)}$$

At higher frequencies (ka>>1), the pressure radiated from each individual source will not be disturbed by the radiation from the other sources. Hence, if the two dipoles which combine to make the quadrupole are far enough apart, the total radiated power will be the sum of the power radiated from each dipole. Similarly, if the simple sources which make the two dipoles are widely separated, the total power will be the sum of that radiated from the four simple sources individually. The previous two sections are applicable for these cases.

A.1.4 Multipoles

The simplest example of a multipole source is the dipole which results from bringing close together two monopoles of opposite sign. Because of constructive and destructive interference, the dipole has a figure eight directivity pattern with sound intensity proportional to $\cos^2\theta$. A multipole of order m is made up of 2^m simple sources. Thus, a dipole is a multipole of the first order.

A quadrupole is a second example of a simple multipole radiator. The directivity pattern for this case has a four leaved rose shape with sound intensity proportional to $\cos(2\theta)$. Since four simple sources are required, the quadrupole is said to be of the second order.

Expressions for the radiation resistances of monopoles, dipoles, and quadrupoles have been given in the three preceding sections. A general expression for the radiation resistance of a multipole is given by (18) as

$$R_{rad} = \frac{\rho c(4\pi a^2)\,(ka)^{2m}}{(m+1)1.3.5\ \ldots(2m+1)} \quad . \qquad \text{(A.1.15)}$$

A summary of the results of this Appendix is given in the following Table of radiation resistances. It is interesting to compare the radiation resistances of a pulsating and an oscillating sphere. For equal areas and velocities, a pulsating sphere will radiate three times as much acoustic energy.

TABLE OF RADIATION RESISTANCES

TYPE OF SOURCE	Radiation Resistance		
	General Expression	$ka<<1$	$ka>>1$
Pulsating sphere (monopole).	$\frac{\rho c(4\pi a^2)(ka)^2}{(ka)^2 + 1.}$	$\rho c(4\pi a^2(ka)^2$	$\rho c(4\pi a^2)$
Oscillating sphere (dipole)	$\frac{\rho c(4\pi a^2)(ka)^4}{3\,[(ka)^4 + 4]}$	$\frac{\rho c(4\pi a^2)(ka)^4}{12}$	$\frac{\rho c(4\pi a^2)}{3}$
Quadrupole	$\frac{\rho c(4\pi a^2)(ka)^6}{1,215}$	-	-
Multipole of order m	$\frac{\rho c(4\pi a^2)(ka)^{2m}}{(m+1)1.3.5...(2m+1)}$	-	-
Infinitely long, pulsating cylinder (per unit length)	$\frac{16\rho c\ell}{K E_o^2}$	$\rho c(\pi^2 a\ell)(ka)$	$\rho c(2\pi a\ell)$

APPENDIX II

The Hankel Function

The following properties and approximations are given by Morse and Ingard (18):

$$\frac{\partial H(kr)}{\partial r} = \frac{\partial H(kr)}{\partial (kr)} \cdot \frac{\partial (kr)}{\partial r} = k \frac{\partial H(kr)}{\partial (kr)} \qquad (A.2.1)$$

$$\frac{\partial H_o(kr)}{\partial r}\Big|_{r=a} = \frac{ki\, E_o}{2}\, e^{i\gamma_o} \qquad (A.2.2)$$

$$\frac{\partial H_m(kr)}{\partial r}\Big|_{r=a} = ki\, E_m\, e^{i\gamma_m}, \quad m \neq 0. \qquad (A.2.3)$$

Values of E_m are tabulated in Reference (18). Limiting values of amplitude and phase are given by the following:

For $ka \ll m + \frac{1}{2}$;

$$E_o \simeq \frac{4}{\pi ka}, \quad \gamma_o \simeq \pi \left(\frac{ka}{2}\right)^2, \qquad (A.2.4)$$

$$E_m \simeq \frac{m!}{2}\left(\frac{2}{ka}\right)^{m+1}, \quad \gamma_m \simeq -\frac{\pi m}{(m!)^2}\left(\frac{ka}{2}\right)^{2m}, \quad m > 0. \qquad (A.2.5)$$

For $ka \gg m + \frac{1}{2}$;

$$E_o \simeq \sqrt{\frac{8}{\pi ka}}, \quad \gamma_o = ka - \frac{\pi}{4}, \qquad (A.2.6)$$

$$E_m \simeq \sqrt{\frac{2}{\pi ka}}, \quad \gamma_m = ka - \frac{1}{2\pi}(m + \tfrac{1}{2}) \quad m > 0. \qquad (A.2.7)$$

At the surface r = a, the Hankel function of order one can be written as

$$H_1(ka) = J_1(ka) + iN_1(ka) = \frac{-iE_o e^{i\gamma_o}}{2}. \qquad (A.2.8)$$

At large distance from the surface,

$$H_m(kr) \simeq \sqrt{\frac{2}{\pi kr}}\; e^{i\left[kr - \frac{\pi}{4}(2m+1)\right]} \qquad (A.2.9)$$

When $ka \ll 1.5$, the following expansion can be used for the case $k_o > K$.

$$\frac{H_1(ka)}{aH_1'(ka)} \simeq -1 + a^2(k_o^2 - K^2)\left[\ell_n\left(Ca\sqrt{k_o^2 - K^2}\right) - \frac{i\pi}{2}\right] \qquad (A.2.10)$$

For $k_o < K$, the expansion is

$$\frac{H_1(ka)}{aH_1'(ka)} \simeq -1 - a^2(K^2 - k_o^2)\,\ell_n\left(Ca\sqrt{K^2 - k_o^2}\right) \qquad (A.2.11)$$

where $C = 0.8905$.